PhD Thesis

School of Chemistry

Cardiff University

Disposable Nappies to Fine Chemicals

Thesis submitted in accordance with the requirements of Cardiff University for the degree of Doctor of Philosophy by

Rhodri John Maunder

January 2022

Acknowledgements

First and foremost, I would like to thank my project supervisors, Dr Jennifer Edwards & Dr Jonathan Bartley, for their expert guidance and support as I have worked on getting this PhD together. My gratitude goes out to Dr Sankar Meenakshisundaram, whose knowledge and experience in the field of biomass conversion were invaluable.

Thanks to Rob and Simon from NappiCycle Ltd. for giving me a fascinating insight into the research and development that has gone into their ground-breaking recycling concept.

To everyone at the CCI, thank you for sharing your knowledge, your experience, and most importantly, your kindness and friendship. A special thank you to Dr Alex Howe, who made sure that I hit the ground running; to my lab partners, Alex Barnes, Ashley, David, and so many others, we made it together through these strange times!

To my mother, father, brother, and my partner, I can't express how much your support has meant to me. Thank you for being there for me through it all.

Publications

A. G. R. Howe, R. Maunder, D. J. Morgan and J. K. Edwards, *Catalysts*, 2019, **9**, 748.

Abstract

Chapter 1 introduces the general principles of catalysis, along with the scope and objectives of this study. This is followed in Chapter 2 by a literature review of previous catalysis-focussed research in the fields of biomass conversion and the direct synthesis of reactive oxygen species.

Chapter 3 details the experimental procedures that were undertaken to fulfil this study's objectives. Firstly, the catalyst synthesis and testing methods used are described, followed the analytical methods that were used to characterise the catalysts and to identify and quantify their post-reaction products.

Chapter 4 describes the efforts to characterize NappiCycle's 'recycled nappy fibre' (RNF) material. It was found from thermogravimetric analysis that cellulose was the most abundant component of the material by weight, at $\approx$ 40 wt.%. Both the RNF and Avicel PH-101, a reference microcrystalline cellulose, were subjected to cellulose hydrolysis reactions in a pressure reactor to determine the RNF's response. Both materials were pre-treated by a mechanical and chemical method to establish whether such treatments would decrease RNF's recalcitrance to hydrolysis. It was found, using a relatively mild cellulose hydrolysis reaction, that glucose was produced by the RNF in a comparable, albeit low yield when compared to Avicel. However, neither of the pre-treatments were effective at increasing glucose yield from RNF; a 0.5% increase was the most pronounced when ball-milling was used. When the time, energy, and additional pre- and post-treatment reagents required are considered, it was determined that neither treatment would be viable for scaled-up processes involving RNF's conversion into value-added commodities.

Chapter 5 investigates an alternative pathway for cellulose conversion to hydrolysis; a one-pot hydrogenolysis/hydrogenation to sorbitol. It was hoped that such a reaction would minimise the formation of undesirable by-products (namely, humins) that typically arise in hydrolysis reactions. RNF was found to produce a very low yield of sorbitol when compared to Avicel (0.2% for RNF versus 32.7% using Avicel), which

was attributed in part to the presence of residual chlorides arising from NappiCycle's recycling process; when $CaCl_2$ was added in incremental concentrations to a model glucose hydrogenation reaction, the yield of sorbitol obtained decreased from 50.4% to 1.9%. Focus shifted to the synthesis of Ru/C catalysts for glucose hydrogenation using a microwave-assisted solvothermal method. Screening experiments were conducted that investigated the effect of modifying catalyst synthesis parameters on the yield of sorbitol produced. Here, it was found that the choice of ruthenium precursor and activated carbon support type had the greatest influence upon catalytic activity. A selected series of Ru/C catalysts were characterised to determine if differences in their performance could be attributed to surface and bulk characteristics. All XC72R-based catalysts had a close agreement between their actual and expected metal loading, however much greater discrepancies were observed with the Black Pearls-based catalysts. No differences could be found in ruthenium's oxidation state across the catalysts that were analysed by XPS; ruthenium was present as RuO_2 in all instances. In the case of Ru/TiO_2 catalysts, a mixture of metallic ruthenium and RuO_2 was found on the surfaces. In a similar manner to the Ru/C catalysts, it is likely that the presence of RuO_2 was a consequence of air oxidation between catalyst preparation and analysis.

Chapter 6 investigates the direct synthesis of H_2O_2 from gaseous H_2 and O_2, by applying the same microwave-assisted solvothermal method as that used in Chapter 5 to produce series of mono- and bi-metallic 1 wt.% x/TiO2 catalysts (x = Au, Pd, Ni, AuPd, NiPd). The 1 wt.% NiPd catalyst with a nominal molar ratio of metals of 1:1 had a H_2O_2 synthesis activity of 77 mol_{H2O2} kg_{cat} h^{-1}, performing well against the most active AuPd catalyst (also with a 1:1 nominal molar ratio of metals), producing 85 mol_{H2O2} kg_{cat} h^{-1}. It was found that the Au, Pd and AuPd catalysts had a good agreement with their nominal metal loadings, however in the case of the Ni and NiPd catalysts, it was found that there was an inadequate attachment of Ni to the TiO_2 support, likely due to an inadequate catalyst preparation temperature.

Table of Contents

List of Abbreviations

AHP	Absorbent Hygiene Product
Avicel	Avicel PH-101 Microcrystalline Cellulose
BE	Binding Energy
BSE	Backscattered Electrons
BP	Vulcan Black Pearls 2000 activated carbon
CrI	Crystallinity Index
FEG	Field Emission Gun
GC	Gas Chromatography
HPLC	High-Performance Liquid Chromatography
ICP-MS	Inductively Coupled Plasma – Mass Spectrometry
MP-AES	Microwave-Plasma Atomic Emission Spectroscopy
RNF	Recycled Nappy Fibre(s)
SE	Secondary Electron(s)
SEM	Scanning Electron Microscopy
TEM	Transmission Electron Microscopy
TGA	Thermogravimetric Analysis
XC72R	Vulcan XC72R activated carbon
XRD	X-Ray Diffraction
XPS	X-Ray Photoelectron Spectroscopy

1: Introduction

1.1: Scope and Objectives

This project was funded by the second round of Knowledge Economy Skills Scholarships (abbreviated as KESS2). This pan-Wales initiative is a collaboration between the European Social Fund, the Welsh Government, and several higher education institutions within Wales. In this case, the Cardiff Catalysis Institute collaborated with NappiCycle Ltd., a single-use nappy and sanitary products recycling service based in Ammanford, South Wales. This collaboration's primary objective is a determination as to how viable it would be for their recycled product to become a value-added commodity. Following this, the objectives are to develop, test, and characterise a series of heterogeneous supported-metal catalysts for cellulosic biomass conversion and for the direct synthesis of reactive oxygen species (namely, hydrogen peroxide).

1.2: The Fundamental Principles of Catalysis

The concept of chemical catalysis was defined in 1835 by the Swedish chemist Jöns Jacob Berzelius, who described the phenomenon as:

> "...the property of exerting on other bodies an action which is very different from chemical affinity. By means of this action, they [catalysts] produce decomposition in bodies, and form new compounds into the composition of which they do not enter...". [1]

The above is a concise definition of a catalyst, in that they produce decomposition without becoming a structural part of the new compounds formed. However, it does not explain what 'decomposition' entails or why it occurs. Subsequent investigations shed more light on these phenomena.

In 1889, Savante Arrhenius proposed a formula that describes the relationship between temperature and reaction rate.[2] The Arrhenius equation can be used to explain the

kinetic effect of a catalyst; that is, how the addition of a catalyst can reduce the amount of energy that needs to be provided to a given system.

$$k = A \cdot e^{-\frac{E_a}{RT}}$$

Where:

k	is the rate constant
A	is the Arrhenius constant
E_a	is activation energy (J.mol)
R	is the gas constant (8.31 $J.K^{-1}.mol^{-1}$)
T	is temperature (K)

Equation 1-1

The rate (k) of a reaction can be increased by increasing T or by reducing E_a. It is the latter that a catalyst does, not by reducing the activation energy *per se*, but by providing an alternative route for a reaction to take place that has a lower overall activation energy. This is illustrated in Figure 1-1.

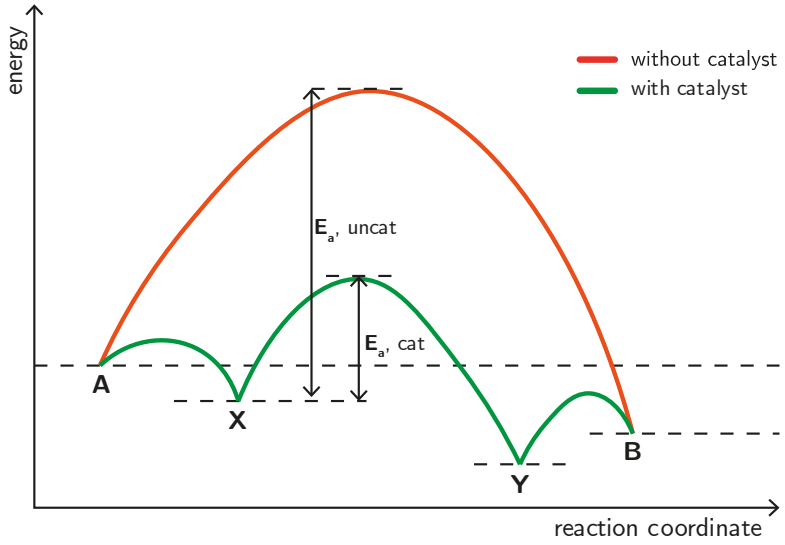

Figure 1-1: Illustrated energy diagram of a reaction with and without a catalyst. A and B denote the unreacted substrate(s) and final product, respectively. X denotes the formation of an intermediate substrate-catalyst complex. Y denotes the formation of the product, adsorbed onto the catalyst surface. Adapted from work by C. Beeker.[3]

Some insight is provided by the knowledge that a catalyst does not form any part of the reactants or products in a chemical reaction, and that it provides an alternative pathway for such reactions to take place. However, this does not explain how these are achieved. It is pertinent to discuss in further detail the mechanisms by which catalysts operate. The way that a catalyst operates can be immensely complex, and there are

many reaction mechanisms that are applied to catalysed reactions of various types. However, there are two primary mechanisms of surface interaction that are often applied to the study of heterogeneous catalytic systems.

Irving Langmuir and Cyril Hinshelwood proposed and refined, respectively, the Langmuir-Hinshelwood mechanism in 1929. In this mechanism, both of the reactants are chemisorbed onto the surface of the catalyst prior to their reaction and desorption.[3,4]

(1)	$A + * \rightleftharpoons A*$	adsorption of A
(2)	$B + * \rightleftharpoons B*$	adsorption of B
(3)	$A* + B* \rightleftharpoons P_{ad}$	reaction to products (P_{ad})
(4)	$P_{ad} \rightarrow P_{des} + 2*$	desorption of products (P_{des})

$*$ denotes an adsorption site on the surface of a catalyst

A second mechanism was later proposed by Eley and Rideal in 1938. In this mechanism, only one of the reactants adsorbs onto the surface, which then reacts with the other, unbound reactant.

(1)	$A + * \rightleftharpoons A*$	adsorption of A
(2)	$A* + B \rightleftharpoons P_{ad}$	reaction to products (P_{ad})
(3)	$P_{ad} \rightarrow P_{des} + *$	desorption of products (P_{des})

$*$ denotes an adsorption site on the surface of a catalyst

The Langmuir-Hinshelwood and Eley-Rideal mechanisms are the foundation of modern surface chemistry theory. The two mechanisms appear to be similar. However, differences in the adsorption, desorption and interactions of the substrates result in measurable differences in their properties. The rate of a reaction that is catalysed via the L-H mechanism is highly dependent on the availability of adsorption sites for both reactants ($A*$ and $B*$). Conversely, a reaction that proceeds via the E-R mechanism does not require there to be adsorption sites for both reactants. The rate of reaction would remain significant at total surface coverage of $A*$, whereas a total surface coverage of $A*$ would result in a reaction rate of zero for a L-H catalysed reaction. It has been reported that despite the reaction barrier for L-H catalysed reactions tending

to be greater than those that proceed by an E-R mechanism, L-H is the preferred mechanism for the vast majority of applicable catalytic reactions; the precise reason for this is not as of yet fully understood.[5] Other mechanisms are used in more specific circumstances, such as the Mars-van Krevelen mechanism for selective oxidations over metal oxide catalysts.[6]

The Boltzmann distribution equation (Equation 1-2) provides more detail into the effect that a catalyst has.

$$\frac{p_i}{p_j} = e^{\left(\frac{(-\mathrm{E}_i - \mathrm{E}_j)}{kT}\right)}$$

Where:

p_i and p_j are the populations of species in their respective states, i and j

$\mathbf{E}_i$ and $\mathbf{E}_j$ are the energies of the two states

k is the Boltzmann constant

T is the temperature constant (K)

Equation 1-2

The number of species with a sufficient energy to react increases with the addition of a catalyst (p_i / p_j decreases), as the overall activation energy requirement is decreased. This can be represented in a simplified manner by a Maxwell-Boltzmann distribution curve, as in Figure 1-2.

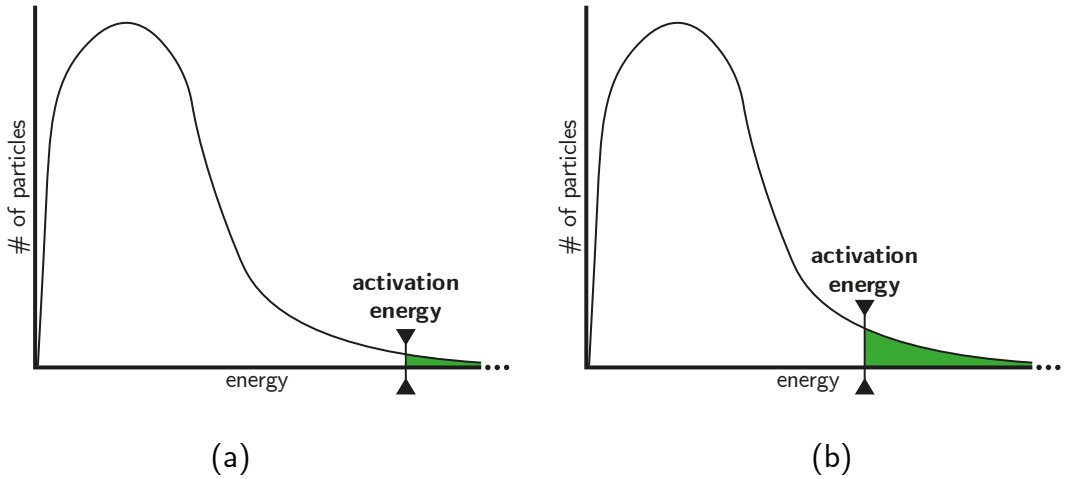

Figure 1-2: Boltzmann distribution curves of an uncatalyzed reaction (a) and the equivalent catalysed reaction (b). More species have sufficient energy to react upon addition of a catalyst as the overall activation energy requirement is reduced by the catalyst.

Catalysts are usually described as either heterogeneous or homogeneous. Heterogeneous catalysts are in a different phase of matter to the reactants and/or products. Homogeneous catalysts are in the same phase as these. Each type has its own set of characteristic properties that may be advantages or disadvantages, based upon the desired reaction to catalyse. The choice of which type to use for a given reaction depends on many factors, including the nature of the reaction itself and the nature of

its reactants and products. The scale of production, operating costs, catalyst durability and environmental regulations are some of the considerations.

Despite heterogeneous catalysts often having limited activity and selectivity when compared with homogeneous counterparts, catalyst design and testing within this study is exclusively focused on heterogeneous catalysts due to their low cost, ability to withstand wide ranges of operating conditions, durability, and the ease of their synthesis, use, and re-use.[7]

The primary advantage of heterogeneous catalysts are their ease of separation from the reaction mixture and their ability to be easily re-used.[8] Homogeneous catalysts can achieve very high reaction rates along with very high selectivities, however they are difficult to separate and recover for re-use, and methods for doing so are often complex.[9] A third, distinct category of catalyst exists, that is biological catalysts, or enzymes. These are a highly specialised class of catalyst that can achieve incredible rates of reaction. An example of this speed is carbonic anhydrase, the enzyme responsible for converting carbon dioxide to carbonic acid and vice-versa in the blood. Carbonic anhydrase achieves a CO_2 hydration turnover of 10^6 s^{-1} in optimum conditions,[10] and with perfect selectivity. Enzymes are also enantioselective, allowing for production of a specific enantiomer rather than racemic mixtures, something that is very difficult or impossible to achieve with manufactured chemical catalysts. Despite these attributes, there are crucial drawbacks which make them unsuitable in many instances. They are very sensitive to pH, temperature, and pressure; significant deviations of these irreversibly alter the active site of an enzyme and can therefore render them permanently inactive.[11] Because of this, they are considered only when it is technologically and economically feasible.

1.3: The Principles of Green Chemistry

Green chemistry is defined as the reduction or elimination of hazardous substances from a chemical process.[12] The principles of green chemistry were considered in all aspects of material testing, catalyst synthesis, testing and characterisation. The twelve

principles of green chemistry were laid out in a publication by P. Anastas and J. C. Warner in 1998.[13] These are listed in Table 1-1.

Table 1-1: The Twelve Principles of Green Chemistry

Term	Definition
Prevention	Preventing waste is better than treating or cleaning up waste after it is created.
Atom economy	Synthetic methods should try to maximise the incorporation of all materials used in the process into the final product. This means that less waste will be generated as a result.
Less hazardous chemical syntheses	Synthetic methods should avoid using or generating substances toxic to humans and/or the environment.
Designing safer chemicals	Chemical products should be designed to achieve their desired function while being as non-toxic as possible.
Safer solvents and auxiliaries	Auxiliary substances should be avoided wherever possible, and as non-hazardous as possible when they must be used.
Design for energy efficiency	Energy requirements should be minimised, and processes should be conducted at ambient temperature and pressure whenever possible.
Use of renewable feedstocks	Whenever it is practical to do so, renewable feedstocks or raw materials are preferable to non-renewable ones.
Reduce derivatives	Unnecessary generation of derivatives—such as the use of protecting groups—should be minimised or avoided if possible; such steps require additional reagents and may generate additional waste.
Catalysis	Catalytic reagents that can be used in small quantities to repeat a reaction are superior to stoichiometric reagents (ones that are consumed in a reaction).
Design for degradation	Chemical products should be designed so that they do not pollute the environment; when their function is complete, they should break down into non-harmful products.
Real-time analysis for pollution prevention	Analytical methodologies need to be further developed to permit real-time, in-process monitoring and control before hazardous substances form.
Inherently safer chemistry for accident prevention	Whenever possible, the substances in a process, and the forms of those substances, should be chosen to minimise risks such as explosions, fires, and accidental releases.

As well as being a distinct entry within the twelve principles themselves, the use of catalysts allows for an effective execution of many of the other principles. A well-optimised catalyst increases the efficiency and environmental sustainability of the reaction that it catalyses and reduces the number of derivatives and the need for stoichiometric reagents. Also, a process can be made safer than its uncatalyzed equivalent, due to a lesser or eliminated need for hazardous stoichiometric reagents.

An example of the benefits of developing and utilising catalysts in a chemical process is highlighted in a comparative study by Tian *et al.*[14,15] Existing commercial methods to produce disodium iminoacetate, a key intermediate in the production of the herbicide glyphosate, either relied on the use of hazardous materials, or produced them as part of the process. These include hydrogen cyanide, hydrochloric acid, and ammonium chloride. An alternative process was developed in 1996 which includes a copper-catalysed dehydration that forgoes the need for a synthesis step involving stoichiometric amounts of cyanohydrin and HCN, demonstrating a clear advantage from a process efficiency and green chemistry perspective. There are several methods of quantifying the environmental impact and efficiency of chemical processes, though the most well-known is the concept of Environmental factor, or the "*E*-factor", that was introduced by Roger A. Sheldon in 1992. It has been the driving concept for optimising efficiency and sustainability of chemical processes in recent decades.[16] A process' *E*-factor is calculated by dividing the mass of its waste products by the mass of its desired products; therefore, a process that produces no waste has an *E*-factor of zero, with greater inefficiency producing a higher *E*-factor value. The *E*-factor provides a straightforward way to assess the efficiency and environmental impact of a given process.

1.4: The Role of Catalysts in Recycling Waste Materials

Freshly-manufactured, virgin materials are preferred over their recycled equivalents in manufacturing industries, a notable example of this being plastics.[17] Recycled materials are usually of a lower quality and purity,[18] and recycling processes tend to be energy intensive and uneconomical. There is a drive to improve the efficiency and economic viability of existing recycling processes and to develop new ones, so that manufacturing becomes more sustainable in the long-term. The efficiency of a given recycling process and the rate of recovery of the material is dependent on its type, with some performing better than others. For example, 74% of waste paper and cardboard was recycled in the UK in 2018, whereas this was only 43% for plastics.[19]

In general, recycling involves physical separation and purification, with chemical processes playing a minor role. When chemistry is used, it is usually in aid of the physical processes, such as bleaching pulp for paper or cardboard production. Due to the low value of recycled materials, the use of catalysts for recycling waste is not common. In the case of some plastics, zeolite catalysts are used to break polymer chains down to low molecular weight compounds or to their constituent monomers,[20] but aside from this, no reported uses for catalysts in municipal waste recycling could be found in previous literature.

1.5: The Production of Single-Use Nappies

There is some variation between manufacturers, however the production of single-use nappies generally involves of the construction and shaping of multiple layers of fabrics that are bonded to each other, each having a distinct purpose. The inner layer is what contacts the wearer's skin and is usually made from a thin film of polypropylene. There may also be an applied layer of emollient to ease friction between the garment and the wearer.[21] The 'core' layer consists of a mixture of cellulose and a superabsorbent polymer (SAP), most commonly sodium polyacrylate (the mechanism of their action is discussed further in section 1.6). The outer layer consists of a waterproof plastic, typically polypropylene.

1.6: NappiCycle, Their Recycling Process and the Constituents of Single-use Nappies and Absorbent Hygiene Products

Single-use nappies and absorbent hygiene products (AHPs) are the preferred choice by parents/guardians and care professionals; over 90% of parents opt to use single-use nappies over their re-usable counterparts.[22] They are effective, hygienic, and convenient. Perhaps unsurprisingly, used examples are disposed of in landfill or are incinerated, as with other waste streams without an established recycling pathway. In the United Kingdom alone, almost 3 billion nappies are thrown away annually, representing approximately 4% of all solid waste sent to landfills by volume.[23] The materials present in single-use nappies and AHPs can take hundreds of years to degrade in landfill conditions, and their bulk makes them a significant contributor to the overall volume of landfill waste. Incineration relieves this, however. Not only does doing so contribute to the already excessive levels of anthropogenic greenhouse gas emissions, but it is also a waste of potentially valuable materials.

Alternative routes to landfill or incineration have been proposed in patented processes. A 1981 patent filed by B. Steffens acknowledges that the production of hygiene products for single-use purposes is wasteful as it results in the loss of ultimately valuable material.[24] This is not the only issue. The leachates generated by their decomposition in landfill conditions have the potential to pose a threat to underground water supplies.[25] Aside from a small number of patents between the early eighties and late nineties, there is little to no mention of nappy and AHP recycling in academic or commercial literature prior to NappiCycle's process, which was conceptualised in 2009, and in 2014 began operating.

A flow chart of the process can be viewed in appendix A. In essence, used nappies and AHPs are placed through a series of washing and shredding steps, yielding a partially homogenised mixture comprised of the constituent parts of the input material. This is then dried to a moisture content of <= 10 wt. %. Its visual appearance is shown in Figure 1-3.

Figure 1-3: The appearance of NappiCycle's 'recycled nappy fibre' as received (<=10wt%

Some uses for this material have been proposed and implemented by NappiCycle. These are based on using the material as-is, without any physical separation or chemical conversion steps, such as an additive in the production of paper-based products, for example, in the production of pin boards. There have been no studies that investigate a chemical or catalytic conversion of this specific material type into value-added products.

The composition of the material, henceforth referred to as "recycled nappy fibres" or "RNF", can be approximated prior to any quantitative analysis, based on the input feedstock of the recycling process. Cotton, superabsorbent polymers, and plastic films were assumed to be its primary constituents. It was also known that the superabsorbent polymers (SAPs) were 'deactivated' during recycling. That is, by adding calcium chloride to the mixture during the washing steps of the recycling process, the SAPs are rendered incapable of absorbing water to any significant degree.

This is done to prevent uncontrolled expansion of the volume of the input material as it goes through the recycling process. To explain the reason why this occurs, the mechanism of their action will be discussed.

Many different materials are classified as "superabsorbent" polymers. Early examples were made by modifying starches, cellulose, polyvinyl alcohol or polyethylene oxide by cross-linking them, either chemically or physically.[26] These were significant improvements from using cotton or cloths alone as they were able to absorb many times their weight in water whilst, crucially, being able to retain this water when put under pressure.

Today's choice of superabsorbent polymer for use in single-use absorbent hygiene products is cross-linked sodium polyacrylate; the cross-linking agent being acrylic acid.[27] Various forms of this material are manufactured that have varying degrees of cross-linking within the polymer's structure, however the mechanism of their action remains the same.

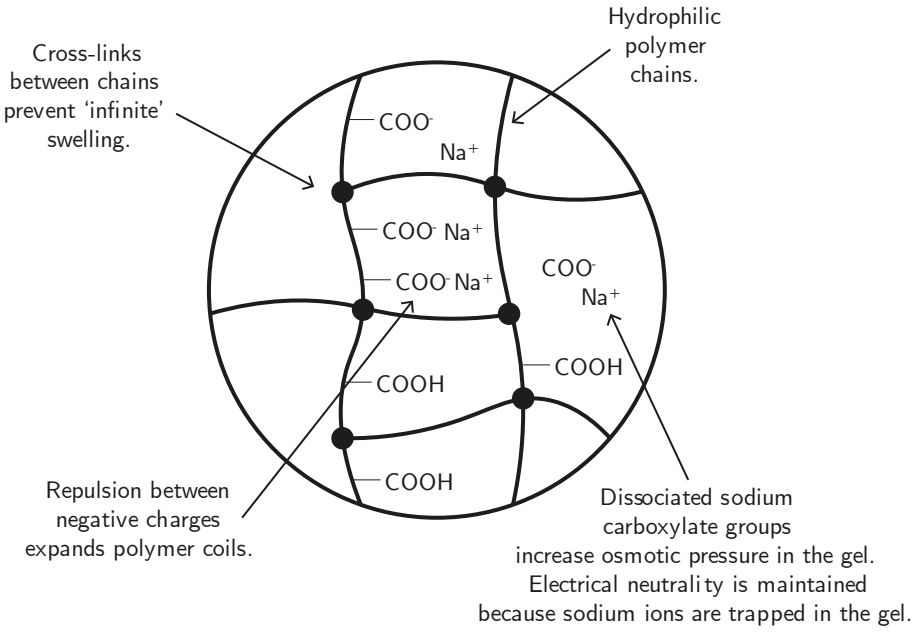

Figure 1-4: Illustration of a part of a SAP network. Adapted from work by M.Elliott.[26]

In the presence of water or water-based solutions, SAPs undergo a process known as osmotic swelling. The cross-linking within their structure prevents 'infinite' swelling, which would destroy the material. Sodium ions that are associated with functional

groups on the polymer network are trapped within the structure and promote the osmotic swelling effect. There are a number of monovalent ions that can be used for this purpose other than sodium,[26] a notable example of an alternative being potassium polyacrylate. The selection of ion modifies the properties of the SAP as a whole, mainly its ability to retain water and the degree of salinization of the surrounding solution.

If SAPs are placed in a solution of a divalent salt, such as calcium chloride, their osmotic swelling capability is impacted by a phenomenon known as 'ion-bridging', whereby the association of each M^{2+} ion with two of the polymer's functional groups rather than just one tightens the overall structure and significantly reduces their swelling ability.[28] This process has been reported to be reversible.[29] This gives potential to a method of recycling used SAPs from recycled nappies and AHPs rather than their disposal, in applications such as improving the water retention ability of degraded soils for agricultre.[27]

Whilst recycled and re-generated sodium polyacrylate presents itself as a material with real-world applications, it is the other major constituent of single use nappies and AHPs that has the greatest potential for upgrading to value-added products: cellulose. For this reason, it is the cellulose within the recycled nappy fibres that was targeted as the primary conversion candidate in this work. Separation of the constituents of recycled nappies may be achieved mechanically,[30] however this study will investigate the merits of using the material as-is.

1.7: References

1 J. Wisniak, *Educ. Química*, 2010, **21**, 60–69.

2 S. Arrhenius, *Zeitschrift für Phys. Chemie*, 1889, **4U**, 96–116.

3 C. Becker, in *Encyclopedia of Interfacial Chemistry: Surface Science and Electrochemistry*, Elsevier, 2018, pp. 99–106.

4 I. Langmuir, in *Transactions of the Faraday Society*, 1921, vol. 17, pp. 607–620.

5 R. J. Baxter and P. Hu, *J. Chem. Phys.*, 2002, **116**, 4379–4381.

6 A. Hagemeyer and A. Volpe, in *Encyclopedia of Condensed Matter Physics*, Elsevier, 2005, pp. 158–165.

7 A. Z. Fadhel, P. Pollet, C. L. Liotta and C. A. Eckert, *Combining the benefits of homogeneous and heterogeneous catalysis with tunable solvents and nearcritical water*, 2010, vol. 15.

8 I. Bertini, *Inorganic and Bio-Inorganic Chemistry - Volume II*, EOLSS Publishers Company Limited, 2009.

9 A. Behr, G. Henze and R. Schomäcker, *Adv. Synth. Catal.*, 2006, **348**, 1485–1495.

10 S. Lindskog, *Pharmacol. Ther.*, 1997, **74**, 1–20.

11 A. Dev, A. K. Srivastava and S. Karmakar, *New generation hybrid nanobiocatalysts: The catalysis redefined*, Elsevier Inc., 2018.

12 M. Doble and A. K. Kruthiventi, *Green Chemistry and Engineering*, 2007.

13 P. T. Anastas and J. C. Warner, *Green Chem. Theory Pract. Oxford Univ. Press. New York,* 1998.

14 J. Tian, H. Shi, X. Li, Y. Yin and L. Chen, *Green Chem.*, 2012, **14**, 1990–2000.

15 I. Delidovich and R. Palkovits, *Green Chem.*, 2016, **18**, 590–593.

16 R. A. Sheldon, *Green Chem.*, 2017, **19**, 18–43.

17 S. Ali, A. A. Garforth, D. H. Harris, D. J. Rawlence and Y. Uemichi, *Catal. Today*, 2002, **75**, 247–255.

18 L. Shen and E. Worrell, *Plastic Recycling*, Elsevier Inc., 2014.

19 DEFRA, UK Statistics on Waste *Gov. Stat. Serv.*, 2021, 1–25, https://www.gov.uk/government/collections/waste-and-recycling-statistics (Accessed 18 July 2022)

20 N. Rudolph, R. Kiesel and C. Aumnate, in *Understanding Plastics Recycling*, eds. N. Rudolph, R. Kiesel and C. Aumnate, Carl Hanser Verlag GmbH & Co. KG, München, 2020, pp. 15–46.

21 R. Marcus, What are your baby's disposable nappies made from? – Which? News, https://www.which.co.uk/news/article/whats-in-your-babys-disposable-nappies-ayNtN5r7wsb4, (accessed 16 July 2022).

22 K. S. Kim and H. S. Cho, *Waste Manag.*, 2017, **67**, 11–19.

23 J. R. Ajmeri and C. J. Ajmeri, *Developments in the use of nonwovens for disposable hygiene products*, Elsevier Ltd, 2016.

24 B.Steffens, PROCESS FOR THE CONTINUOUS SEPARATION OF DISCARDED HYGENE ARTICLES INTO THEIR COMPONENTS, US Patent No. 4,303,501, 1981.

25 B. Bartlett, Disposable Diaper Recycling Process, US Patent No. 4990244, 1991.

26 M. Elliott, *Superaborbent Polymers*, BASF Aktiengesellschaft, 2004, 1-13.

27 A. Hüttermann, L. J. B. Orikiriza and H. Agaba, *Clean - Soil, Air, Water*, 2009, **37**, 517–526.

28 W. Siriwatwechakul, J. Siramanont and W. Vichit-Vadakan, *J. Mater. Civ. Eng.*, 2012, **24**, 976–980.

29 F. Horkay, P. J. Basser, A.-M. Hecht and E. Geissler, *Spec. Issue Artic. Proc IMechE Part H J Eng. Med.*, 2015, **229**, 895–904.

30 R. B. Chowdhury and M. Wijayasundara, *Sci. Total Environ.*, 2021, **799**, 149339.

2: Literature Review

2.1: Fine Chemicals and Fuels Production: Crude-Oil Versus Biomass

Crude oil is a brown to black-coloured liquid of varying viscosity that is found within geological formations within the Earth's crust. It is a physical mixture of many compounds, predominantly of hydrocarbons of various structures and chain lengths. Once extracted, its constituents are physically separated and refined by their boiling points in a process known as fractional distillation.[1] This property of crude oil makes it a versatile feedstock for an immense number of valuable products, including fuels, plastics, lubricants, and pharmaceutical drugs. In short, it has become, and will continue to be, an essential ingredient to our way of life. Crude oil refinement and conversion chemistry is well-established and highly optimised. Fractional distillation, combined with catalytic reforming and cracking, can selectively and efficiently produce useful compounds from most weight fractions.[2] Crude-oil conversions are either physical, catalytic, or thermal, and a given source of oil and its distillates go through a combination of these to achieve the desired product.

The processes by which biomass is converted and refined into value-added products is inherently different to those that use crude oil, due to the significant difference in chemical composition between the two types of feedstocks. Biomass that is earmarked for processing into fuels and chemicals is classified by its generation. Biofuels such as bioethanol and biodiesel are derived from "first-generation" energy-dense, edible plants and oils such as rapeseed, sugarcane, or corn. Their high content of sugars and oils makes them ideal as feedstocks, however, there are significant drawbacks. As well as inflating the price of the chosen crop due to increased demand, arable land that would otherwise be used to grow food for human and animal consumption is rendered unavailable. "Second-generation" biomass encompasses a much wider variety of plant and animal matter. It may be derived from a high-quality homogeneous source, such

as wood chippings or grass, or it may be a solid waste stream, such as agricultural waste or the recycled nappy fibres used in this study.[3]

In contrast to crude oil, which is composed of many relatively low molecular weight compounds, biomass of either generation is composed of polymers that are highly functionalised, chemically complex, and which contain extensive networks of inter- and intramolecular bonds. Second-generation biomass is typically composed of a varying ratio of three biopolymers: each having a distinct structural role in plants. These are cellulose, hemicellulose, and lignin.

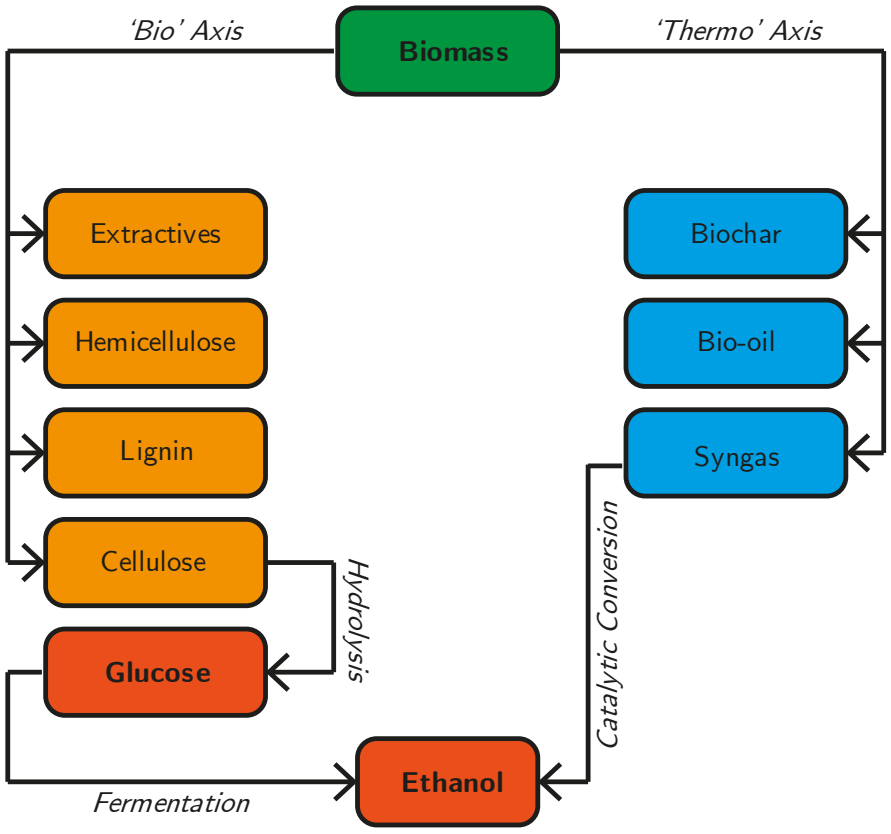

Figure 2-1: A simplified pathway for the conversion of second-generation lignocellulosic biomass into bioethanol. Adapted from Lee and Lavoie (2013).[3]

No two sources of biomass are the same. Each will have its own ratio of cellulose, hemicellulose, and lignin, as well as varying amounts and types of impurities.

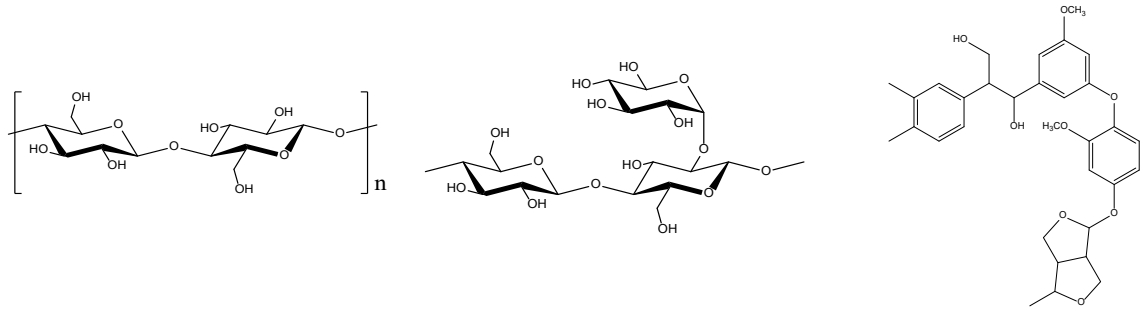

cellulose hemicellulose lignin

Figure 2-2: Molecular structures of the three fractions of lignocellulosic biomass.

The molecular structure of each biopolymer within lignocellulosic biomass is shown in Figure 2-2. Each possesses distinct chemical and physical properties. Cellulose is typically the most abundant of these, and has a highly crystalline, unbranched structure, forming an integral part of plant cell walls. It is comprised of many repeating glucose units, joined together by β-1,4-glycosidic bonds. Cellulose forms its highly crystalline structures by hydrogen bonding interactions between its hydroxyl groups. This makes it highly resistant to physical or chemical degradation, properties which are integral in its primary use as a woven fabric for clothing and various textiles.

Like cellulose, hemicellulose is composed primarily of (anhydro)glucose sub-units bonded by glycosidic bonds. However, it is a branched polymer, and contains additional functionality, making it chemically more complex. Its branching prevents it from taking on the same highly crystalline forms, therefore, it is much more susceptible to degradation.

Lignin is an umbrella term for a poorly characterised set of cross-linked aromatic biopolymers, found as a structural component in many plants; useful due to its resistance to rotting and hydrophobicity.[4] Its heterogeneity makes it a difficult feedstock for conversion. Research that has focussed on processes for its conversion was summarised in a review by Upton and Kakso in 2016.[5] They conclude that for lignin to be a viable feedstock for the production of valuable and fine chemicals, less-complex and more efficient processes will need to be developed, and significant progress needs to be made in 'many areas'.

Despite the difficulties associated with its use, lignocellulosic biomass conversion has been the subject of intense research interest for many decades. It has long been acknowledged that for fuels and key platform chemicals production to continue sustainably, processes that are based on renewable sources must be developed. In 1925, Henry Ford commented:

> "The fuel of the future is going to come from fruit like that sumac out by the road, or from apples, weeds, sawdust - almost anything. There is fuel in every bit of vegetable matter that can be fermented."[6]

A discussion of the viability of biorefineries that make use of second-generation biomass by Clark concludes that it is 'inevitable' that crude-oil will be replaced,[7] however, significant challenges remain. To selectively produce a desired compound from lignocellulosic biomass requires more steps and more energy than is economically viable in many instances, due to the complex nature of the input feedstock. Despite this, efforts are ongoing to allow biomass to become a viable and renewable feedstock for replacing fossil fuels in many applications.

2.2: Catalytic Cellulose Conversion

The synthesis of fine chemicals and fuels from crude-oil and cellulosic biomass fall into two methodologies: 'bottom-up' and 'top-down', respectively. This is illustrated by Deuss *et al.*, shown in Figure 2-3.[8]

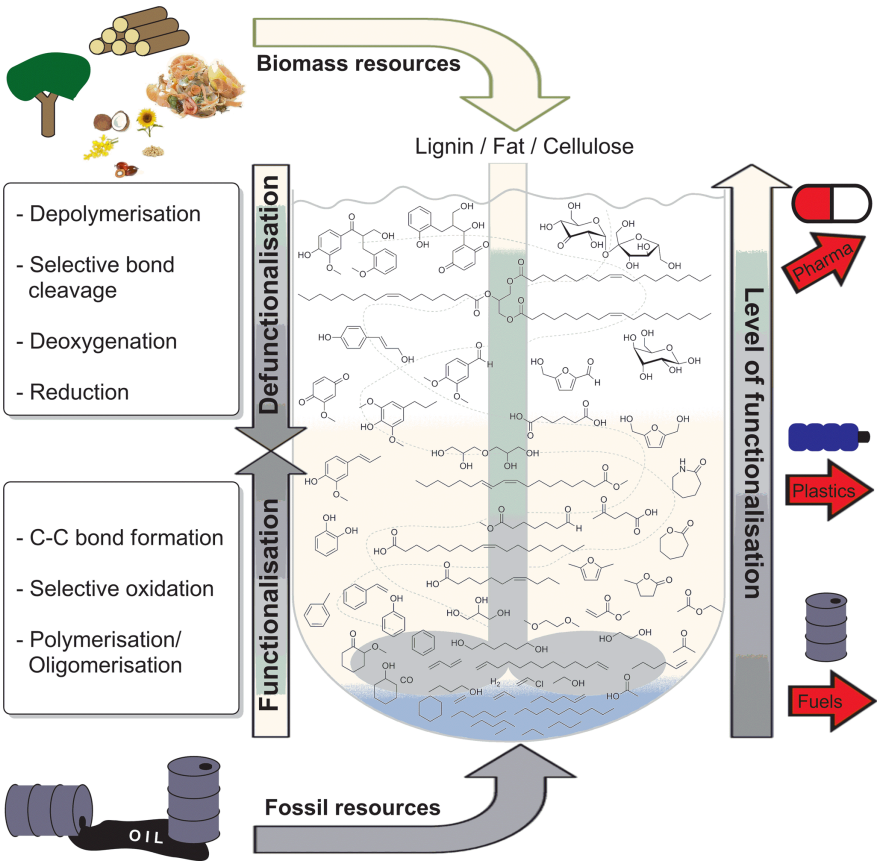

Figure 2-3: Deuss et al.'s illustration of the 'top-down' and 'bottom-up' approaches to fine chemicals and fuels synthesis from both crude oil and biomass.[8]

Fine chemicals synthesis from crude oil often requires the addition of functionality, with desired molecules built up from distilled hydrocarbon precursors. In contrast, the conversion of biomass, and by extension, cellulose, into value-added products relies on reducing its functionality, through depolymerisation and selective bond cleavage. Due to its complexity, a biomass-conversion catalyst design and testing study will usually target a specific fraction of biomass and its hydrolysates rather than the source material, for example, the conversion of cellulose exclusively.

The primary product of cellulose conversion is its monomeric constituent, glucose. In the same way that cellulose is the most abundant biopolymer, glucose is the most abundant simple sugar, or monosaccharide.[9] It is an aldohexose, that is, a carbohydrate with a carbon chain of six atoms, containing an aldehyde group. In solution, it exists in either its open-chain form or its closed-ring form, as shown in Figure 2-4.

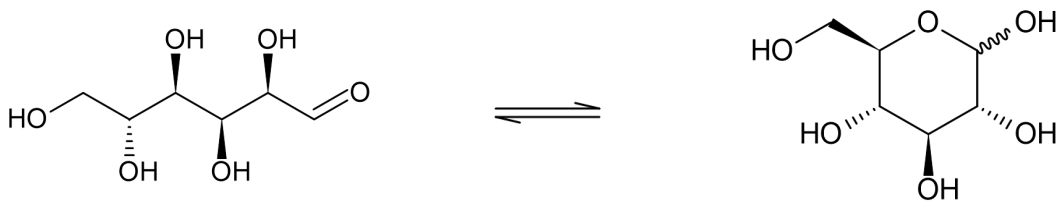

D-glucose *D-glucopyranose*

Figure 2-4: The tautomers of D-glucose. D-glucopyranose is the most thermodynamically stable form in an aqueous solution.

Due to its reactive functional groups, in particular its terminal aldehyde group, glucose can be converted into a wide variety of products. Sugars that react in this fashion are known collectively as reducing sugars. Kobayashi *et al.*'s comprehensive schematic illustrates the large number of products and intermediates that are possible *via* various transformations, shown in Figure 2-5.

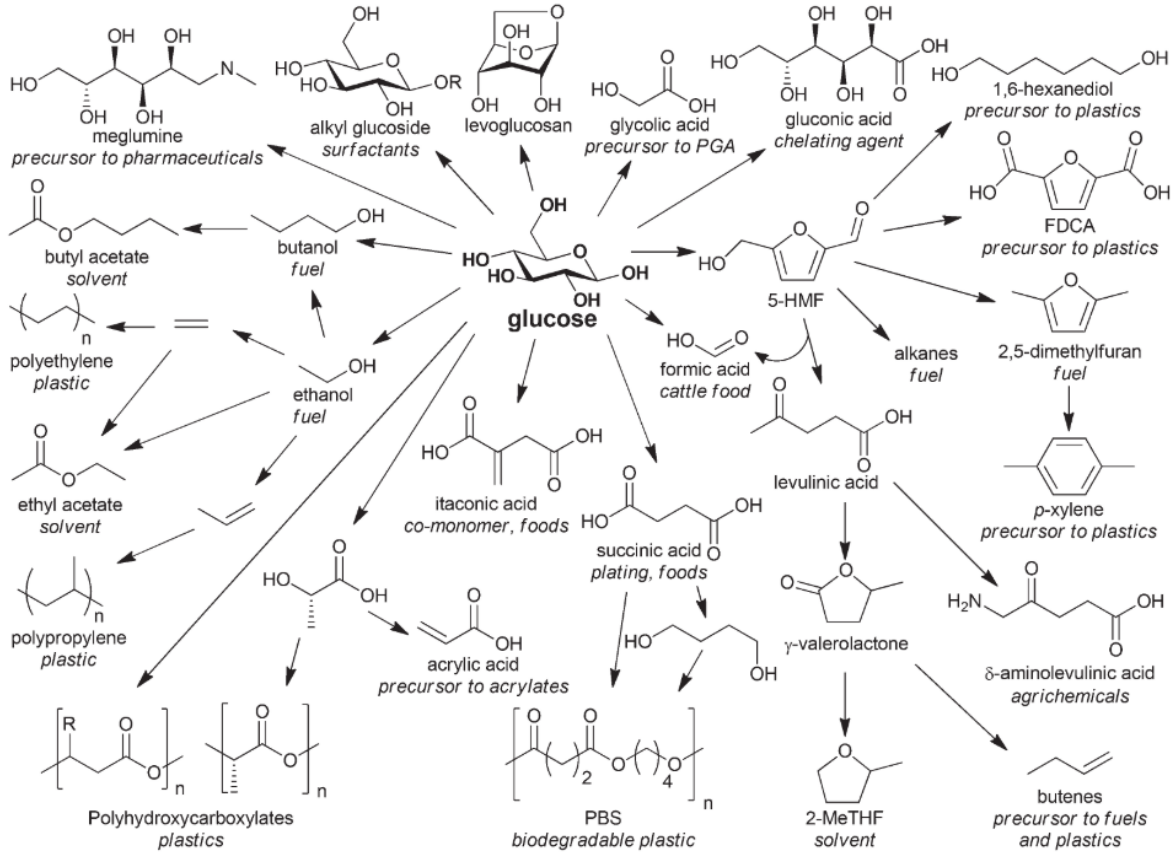

Figure 2-5: Kobayashi and Fukuoka's illustrated schematic of the possible derivatives from the catalytic conversion of cellulose-derived glucose.[10]

Notable reactions from Figure 2-5 that are relevant to this study are the conversion of glucose to form 5-HMF and levulinic acid, which takes place using bifunctional

Lewis/Brönsted acid catalysts,[11] and its hydrodeoxygenation to various hydrocarbons such as ethanol and butanol using various supported metal catalysts such as Ru/C.[12]

2.2.1: Cellulose Hydrolysis

Recent research efforts into cellulose hydrolysis are focussed on developing solid acid catalysts to produce glucose and other hydrolysates as a viable alternative to using liquid acids such as sulphuric acid.[13,14] Solid acids have several key advantages. They are easy to separate from their products in an aqueous solution, can be re-used effectively, and the need for extensive post-processing and waste clean-up processes are reduced or eliminated. Activated carbon-supported sulphonic acid catalysts have been reported to be able to achieve comparable rates of hydrolysis to sulphuric acid. Seminal work by Onda *et al.* details the production of a sulphonated activated carbon catalyst which achieved a 40.5% yield of glucose from pre-treated microcrystalline cellulose.[15] The catalyst was shown to be highly re-usable, achieving a consistent yield of glucose on its second and third use. However, there were drawbacks. A high concentration of SO_4^{2-} ions were detected in the post-reaction solution, which would require a degree of post-processing in a similar manner to if sulphuric acid was used. Leaching of sulphonic acid groups from their activated carbon supports is reported elsewhere,[16] which has prompted research efforts into investigating whether modifying the surface properties or type of activated carbon that's used as the support can have a beneficial effect in this regard. Sulphonic acid-functionalised carbons have been shown to be the most active and selective catalysts in later research efforts when compared to other sulphonated materials such as TiO_2-SO_3H or plastic resins. The reason why activated carbon offers this advantage in biomass hydrolysis reactions has been investigated by Lam and Luong, amongst others, who state that interactions between the reactants and activated carbon's surface -OH groups promotes reactivity when compared to the hydrophobic surfaces of many other solid acids.[17] Forgoing the need for sulphonic acid functionalisation altogether has also become the target for some research efforts, such as Kobayashi *et al.*'s Ru/CMK-3 catalyst, which was shown to be an effective and reusable cellulose hydrolysis catalyst, albeit with a comparably lower level of activity.[16]

Kobayashi *et al.*'s research highlights one of the most significant challenges associated with cellulose conversion: striking a balance in reaction conditions that are harsh enough to facilitate the effective hydrolysis of cellulose, yet delicate enough to prevent excessive and uncontrolled onward reactions of the resultant hydrolysates into undesirable side products, known as humins.

The issue with trying to suppress humin formation arises since the products of cellulose's hydrolysis are more reactive than cellulose itself. The mechanism of humin formation is dependent on several factors, including the type of catalyst present, the reaction solvent, temperature and pressure.[18,19] It has been proposed that they primarily form through condensation reactions between glucose (and its derivatives) and the α and β positions of the furan ring of 5-HMF.[20] A certain level of humin formation is inevitable, however, and attempts to mitigate it have been the subject of research efforts. Many of these were comprehensively reviewed in a highly cited publication by Van Zandvoort *et al.*, who concluded that the formation of humins is highly dependent on the reaction conditions that are employed, but in particular the reaction temperature and strength of the acid groups in the reaction environment.[21] A strategy that is commonly employed to minimise humin formation, as well as to enable a milder set of reaction conditions to be used along with a higher rate of conversion into desired products, is to pre-treat the cellulose. This decreases its resistance to chemical attack by increasing its solubility and reducing the number of intramolecular hydrogen bonding interactions.[22] Ball-milled cellulose is used as a feedstock in a large number of studies on its hydrolysis.[10] The procedure by which ball-milling is carried out for this study is detailed in chapter 2. Briefly, it is a treatment where cellulose is subjected to pulverising mechanical forces due to its interaction with solid spherical balls in a closed, rotating chamber. Kobayashi *et al.* reported that conversion increased from 66% using untreated cellulose to 82% when ball-milled, with a corresponding increase in the yield of and selectivity towards desired products, highlighting the significant benefit that this relatively simple and low-cost pre-treatment method can have.[23]

Extensive cellulose pre-treatment has drawbacks however, as whilst the rate of cellulose conversion and the yield of desired products needs to be maximised for a given process to be viable, speed and energy efficiency is also crucial if such a process is to become feasible on a large scale. Rather than extensive pre-treatments or modifications, some research efforts have investigated the benefit of dissolving cellulose completely prior to its hydrolysis with the use of uncommon solvents such as ionic liquids. This has shown to be highly effective, mainly because it significantly reduces the mass transfer limitations associated with using solid catalysts along with a solid reactant, however ionic liquids are hazardous, costly, and difficult to separate from desired products post-reaction.

2.2.2: Cellulose Hydrogenolysis

One of the major pathways for upgrading cellulose is the hydrogenation of the products of its hydrolysis. In the study of this process, in particular the conversion of cellulose and its monomer, glucose, into sorbitol, one-pot reactions have been touted as an efficient alternative to having distinct reactions for cellulose hydrolysis and glucose hydrogenation. The primary advantage of a one-pot process is that it facilitates the rapid removal of unstable and reactive cellulose hydrolysis intermediates, which in turn suppresses humin formation and increases the overall conversion of cellulose into valuable products.[24] The presence of H_2 or the inclusion of a solvent that can act as a transfer-hydrogenation agent is required, along with a catalyst that is capable of hydrolysing cellulose under such conditions, whilst also containing active sites for the hydrogenation reaction.

It is possible to produce a variety of alcohols, acids and ketones from cellulose, such as ethylene glycol, propylene glycol, acetic acid, and hydroxy acetone, as Fabičovicová *et al* demonstrated in their catalytic conversion of cellulose over their activated carbon-supported nickel and tungsten catalysts at a high H_2 pressure (65 bar).[25] Kusserow *et al.*'s illustrated schematic of the products of glucose/cellulose's hydrogenation shows that despite the high selectivity to sorbitol that can be achieved, there are a number

of products that can arise from the hydrogenation/hydrogenolysis process, as shown in Figure 2-6.[26].

Hydrogenation catalysts based on supported ruthenium have been found to be highly active in both one-pot cellulose hydrogenolysis reactions and for the hydrogenation of glucose alone.[26–28] Geboers *et al.* reported a $< 90\%$ yield of hexitols when ball-milled cellulose was reacted with their zeolite-supported ruthenium catalysts in a reducing/acidic environment. They state that not only does the reducing environment allow for the rapid conversion of cellulose hydrolysates, but that the products of the hydrogenations themselves are more thermally stable, allowing for harsher reaction conditions to be used that further facilitates the hydrolysis of cellulose.

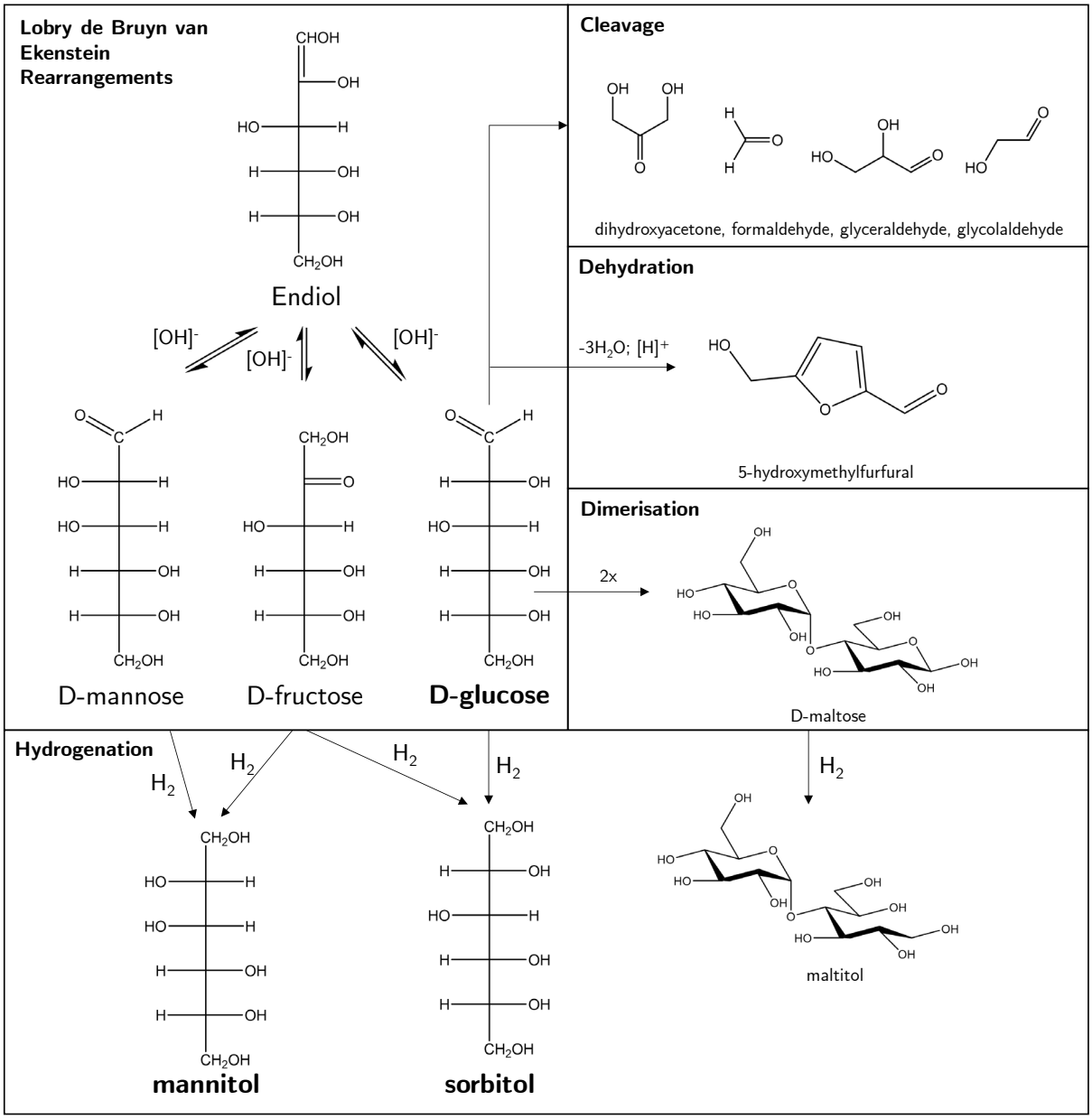

Figure 2-6: Illustrated schematic of the primary products of glucose's hydrogenation/hydrogenolysis. Adapted from Kusserow et al.[26]

2.3: Catalyst Synthesis by Solvothermal Methods

The synthesis of heterogeneous supported metal catalysts takes place by a variety of established techniques, with some more commonly used techniques playing a central role in many catalytic research and development investigations. The most widely used technique in catalyst research investigations is impregnation, conducted by immersing a support material into a metal precursor solution. Whilst this procedure is simple, low-cost, and highly reproducible, it is a time-consuming and energy intensive process. The synthesis of a typical impregnation catalyst also uses a considerable quantity of solvent, both for the impregnation of the metal precursor itself and for subsequent washing steps. An alternative, low-energy and efficient catalyst synthesis method is increasingly receiving research attention, the solvothermal, or "polyol" method. For a typical synthesis, a solution of a selected metal precursor is mixed with a polyol, which acts as the solvent for the precursor, then at elevated temperatures, as a reducing agent for the deposition of its metal onto the support. A wide range of mono-alcohols and polyols have been used in previous investigations into this method. For the synthesis of supported metal catalysts, ethylene glycol is typically used.[29–34]

As a means of improving the efficiency and speed of polyol catalyst syntheses, microwave heating has been employed by researchers investigating the method. Highly cited work by Liu *et al.* published in 2004 detailed a facile microwave-assisted polyol method of synthesising Pt/C catalysts, where a Pt precursor ($H_2PtCl_6{\cdot}xH_2O$) was added to 25 mL of ethylene glycol and Vulcan XC72 carbon, then heated with a conventional household microwave oven. Once the components were mixed, the synthesis took just 50 seconds.[35] The resulting catalyst was then characterised by several methods including TEM, where it was found that the Pt nanoparticles were uniformly dispersed on the carbon support, with an average particle size of 3.8 nm. Okal *et al.* used the method to synthesise Ru/Al_2O_3 catalysts for propane oxidation and found that the Ru particles deposited themselves quickly onto the support. Similarly to Liu *et al.*, the nanoparticles were found to be small and evenly distributed, with an average particle size of 1.6 nm.[36] Other support types have also been found to

work well with this method. Mediavilla *et al.* synthesised a range of Pt/H-ZSM-5 catalysts using a microwave-assisted polyol method and evaluated their activity towards toluene hydrogenation, where they found that the power of the microwave irradiation and the synthesis time had a significant influence on catalytic performance, with longer synthesis times and a higher microwave power producing more active catalysts.[37] The correlations that are seen between synthesis parameters and the catalyst's performance were also observed in our research, the results of which are outlined as part of the fourth chapter of this study. Howe *et al.* synthesised a range of Ru/TiO_2 catalysts for levulinic acid hydrogenation. The effect of varying the ruthenium precursor type, and the preparation time and temperature were investigated. It was also found in this instance that the Ru particles were small and evenly distributed onto the catalyst support, with an average Ru particle size of between 2.35-2.55 nm. When $RuCl_3$ was used as the precursor, the catalysts prepared at the lowest chosen temperature (150 °C) and at the shortest time (5 minutes) were found to be the most active for the hydrogenation reaction.[38] These findings highlight the energy efficiency and green credentials of the synthesis method.

2.4: Levulinic Acid Hydrogenation

In a typical cellulose hydrolysis process, many hydrolysates are formed because of the onward acid-catalysed dehydration reaction of glucose, as shown in Figure 2-7. One of these products is levulinic acid, which is derived from the acid-catalysed ring-opening of 5-HMF.

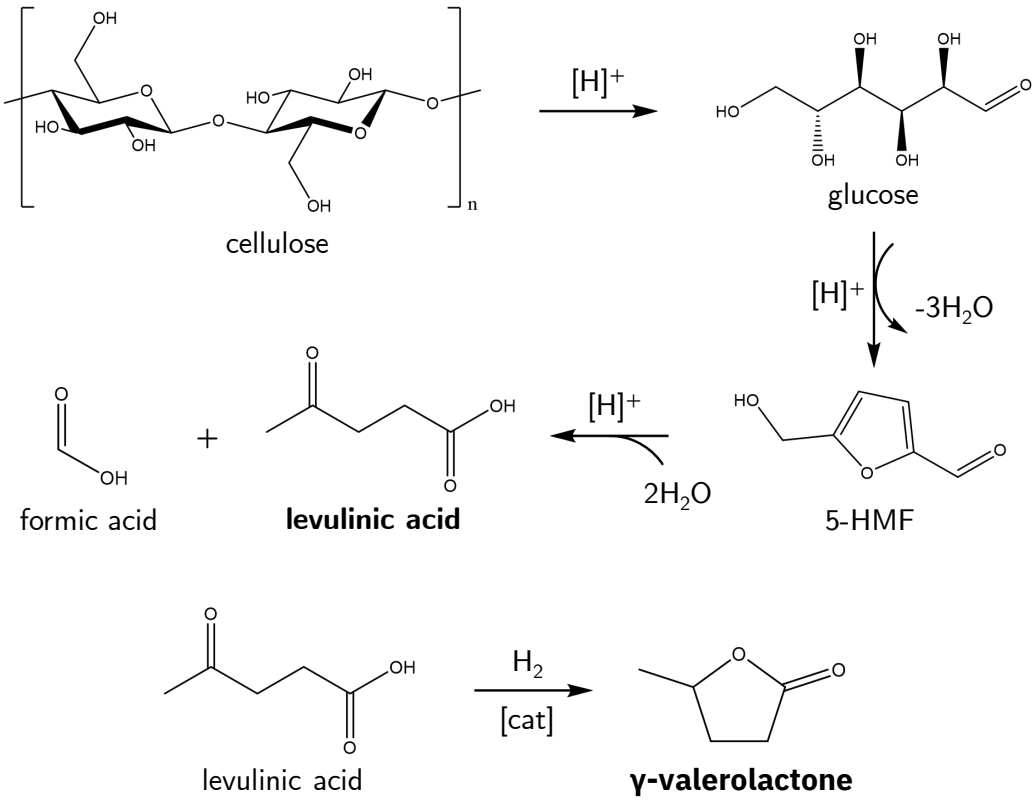

Figure 2-7: The reaction pathway for producing γ-valerolactone from cellulose.

As Figure 2-7 illustrates, one of the products that can be obtained from levulinic acid is one of its hydrogenates, γ-valerolactone (GVL). GVL has received increasing attention for its highly desirable properties as a safe and easy to transport solvent and fuel additive, its benefit in the latter case being comparable to that of ethanol.[39] Levulinic acid hydrogenation is readily performed over a range of supported metal catalysts, however, those based on ruthenium have been reported to be the most active and selective. Luo *et al.* synthesised a range of TiO_2-supported Pd, AuPd, Ru, and RuPd catalysts. Both the AuPd and RuPd catalysts were active for the hydrogenation reaction, however, the monometallic ruthenium catalysts were superior, with their most active producing 51.7 mol_{GVL} g_{metal} h, compared with 1.97 mol_{GVL} g_{metal} h that was achieved by their AuPd catalyst.[40] Li *et al.* found that the choice of catalyst support had a large effect on their 5 wt.% Ru catalysts. Their activated-carbon supported ruthenium catalyst achieved a GVL yield of <90% after 60 minutes of reaction, whereas their γ-Al_2O_3 supported Ru catalyst only achieved a ≈ 40% yield at the same reaction time. They also tested a range of solvents for the reaction, including water, methanol,

ethanol, and hexane and it was concluded that water is the ideal solvent as it minimised the formation of side products,[41] although Jiang *et al.*'s hydrogenations using a mixed metal oxide-supported nickel catalyst, conducted in dioxane, were highly active and selective towards GVL, achieving a near-perfect yield and selectivity (<99%) with their $Ni/MgAlO_{2.5}$ catalyst.[42]

2.5: The Direct Synthesis of Hydrogen Peroxide

Hydrogen peroxide (H_2O_2) is a highly versatile oxidising agent that has many uses in the manufacturing, textiles, and chemical synthesis sectors, amongst others. Over 2.2 million metric tons of H_2O_2 are produced annually for the variety of markets where it is required.[43] The industrial-scale synthesis of hydrogen peroxide is conducted by the anthraquinone oxidation (AO) process, where a functionalised anthraquinone, typically 2-ethyl anthraquinone, acts as a catalytic carrier of H_2 and O_2 to form hydrogen peroxide. The crude H_2O_2 formed during the process is then refined by distillation.

Despite its scalability and ease of implementation, the anthraquinone oxidation process has substantial drawbacks. It is energy-intensive, relying on a series of purification steps *via* solvent extraction, and the process produces a significant amount of waste, generated from sources such as over-hydrogenated anthraquinone and solvent impurities, which must be continually removed from the process stream.[44] For large-scale chemical syntheses, where the commercial viability of a given process is ever more strongly linked to the minimisation of waste, replacements for the AO process are being sought intensely.

An alternative method of synthesising H_2O_2, for applications where it is generated *in situ* and at more dilute concentrations, is its direct synthesis from gaseous H_2 and O_2 with the use of a suitable catalyst. Research has been intensely focussed on the development of a commercially viable method of creating H_2O_2 in this manner.

Palladium catalysts have been known to be active for the synthesis of hydrogen peroxide since the early 20th century,[45] however they were not investigated extensively due to the limitations of the technology of the time. Advancements in the method of

direct H_2O_2 synthesis since have proven the viability of the reaction in experimental settings, with research interest gaining traction in the early-mid 2000's. Blanco-Brieva *et al.*'s sulphonic acid functionalised resin-supported palladium catalysts achieved a H_2O_2 production rate of >1100 mol_{H2O2} mol_{Pd} h^{-1}.[46] A strong Pd particle size effect is observed, with smaller Pd nanoparticles being more active and selective, as Tian *et al.* reported as part of their investigation into the H_2O_2 synthesis activity of their size-controlled Pd catalysts.[47]

Whilst Pd catalysts are active for the synthesis of H_2O_2, they are more active for its subsequent onward hydrogenation to water. The overall reaction for the direct synthesis of H_2O_2 from its constituent gases appears simple ($H_2 + O_2 \rightarrow H_2O_2$), however this representation of the reaction hides a series of competing reactions that are occurring on the catalyst, as Figure 2-8 illustrates.

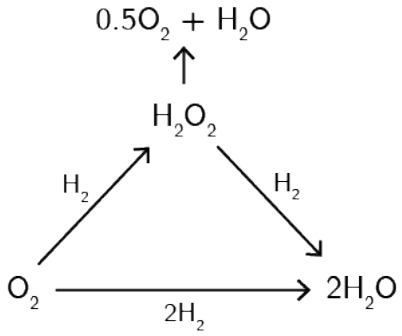

Figure 2-8: The competing reactions that take place over a H_2O_2 synthesis catalyst.

One of the ways that the thermodynamically favourable onwards hydrogenation can be suppressed is to alloy palladium with another metal; most notably, gold. Edwards *et al.* compared the activity and selectivity of monometallic 5 wt.% x/TiO_2 (x = Au, Pd) with 2.5-2.5 wt.% AuPd/TiO_2 catalysts prepared by a modified impregnation method, and found their AuPd catalyst to be over twice as active as its monometallic Pd counterpart.[48] Crucially, its selectivity towards H_2O_2 was 89%, compared to Pd/TiO_2's 40%. The consensus for Au's role in increasing the catalyst's selectivity is that it suppresses the O-O bond scission necessary for the formation of water from H_2O_2.[49]

As well as Au, other, non-precious metals have been investigated for their ability to enhance catalytic activity and selectivity. Crombie *et al.* alloyed palladium with a range of other metals and evaluated their performance as *in-situ* H_2O_2 synthesis and benzyl alcohol oxidation catalysts, and found that there was a modest benefit in doing so, with the benefits being attributed to the increase in the number of smaller Pd sites resulting from its dilution with the secondary metal,[50] with, as previously discussed, smaller Pd sites being more active and selective. Although, it has been reported by Maity *et al.* that the presence of nickel in their NiPd catalysts enhanced their catalytic activity threefold when compared to its monometallic Pd counterpart, indicating that the alloying of Pd with non-noble metals remains a viable route for further investigation.[51]

2.6: References

1 V. Simanzhenkov and R. Idem, *Crude Oil Chemistry*, Taylor & Francis, 1st edn., 2003.

2 E. Lois, E. L. Keating and A. K. Gupta, in *Encyclopedia of Physical Science and Technology*, ed. R. A. Meyers, Academic Press, 3rd edn., 2003, pp. 275–314.

3 R. A. Lee and J.-M. Lavoie, *Anim. Front.*, 2013, **3**, 6–11.

4 S. E. Lebo, J. D. Gargulak and T. J. McNally, in *Kirk-Othmer Encyclopedia of Chemical Technology*, John Wiley & Sons, Inc., Hoboken, NJ, USA, 2001.

5 B. M. Upton and A. M. Kasko, *Chem. Rev.*, 2016, **116**, 2275–2306.

6 A. Webb and D. Coates, *Biofuels and Biodiversity*, Montreal, 2012, vol. 65.

7 J. H. Clark, *J. Chem. Technol. Biotechnol.*, 2007, **82**, 603–609.

8 P. J. Deuss, K. Barta and J. G. de Vries, *Catal. Sci. Technol.*, 2014, **4**, 1174–1196.

9 A. J. Domb, J. Kost and D. Wiseman, *Handbook of Biodegradable Polymers*, CRC Press, 1998.

10 H. Kobayashi and A. Fukuoka, *Green Chem.*, 2013, 15, 1740–1763.

11 F. Parveen and S. Upadhyayula, *Fuel Process. Technol.*, 2017, **162**, 30–36.

12 Y. Liu, L. Chen, T. Wang, X. Zhang, J. Long, Q. Zhang and L. Ma, *RSC Adv.*, 2015, **5**, 11649–11657.

13 P. Lanzafame, D. M. Temi, S. Perathoner, A. N. Spadaro and G. Centi, in *Catalysis Today*, Elsevier, 2012, vol. 179, pp. 178–184.

14 M. Hara, *Energy Environ. Sci.*, 2010, **3**, 601–607.

15 A. Onda, T. Ochi and K. Yanagisawa, *Green Chem.*, 2008, **10**, 1033.

16 X. Wang, X. Wu, K. Guo, J. Ren, Q. Lin, H. Li, X. Wang and S. Liu, *Catal.*

Letters, 2019, **150**, 138-149. DOI:10.1007/s10562-019-02912-6.

17 E. Lam and J. H. T. Luong, *ACS Catal.*, 2014, 4, 3393–3410.

18 X. Fu, J. Dai, X. Guo, J. Tang, L. Zhu and C. Hu, *Green Chem.*, 2017, **19**, 3334–3343.

19 S. J. Dee and A. T. Bell, *ChemSusChem*, 2011, **4**, 1166–1173.

20 Z. Xu, Y. Yang, P. Yan, Z. Xia, X. Liu and Z. C. Zhang, *RSC Adv.*, 2020, **10**, 34732–34737.

21 I. Van Zandvoort, Y. Wang, C. B. Rasrendra, E. R. H. Van Eck, P. C. A. Bruijnincx, H. J. Heeres and B. M. Weckhuysen, *ChemSusChem*, 2013, **6**, 1745–1758.

22 B. Lindman, B. Medronho, L. Alves, C. Costa, H. Edlund and M. Norgren, *Phys. Chem. Chem. Phys.*, 2017, **19**, 23704–23718.

23 H. Kobayashi, Y. Ito, T. Komanoya, Y. Hosaka, P. L. Dhepe, K. Kasai, K. Hara and A. Fukuoka, *Green Chem.*, 2011, **13**, 326–333.

24 Y. Li, Y. Liao, X. Cao, T. Wang, L. Ma, J. Long, Q. Liu and Y. Xua, *Biomass and Bioenergy*, 2015, **74**, 148–161.

25 K. Fabičovicová, O. Malter, M. Lucas and P. Claus, *Green Chem.*, 2014, **16**, 3580–3588.

26 B. Kusserow, S. Schimpf and P. Claus, *Adv. Synth. Catal.*, 2003, **345**, 289–299.

27 A. Shrotri, H. Kobayashi, A. Tanksale, A. Fukuoka and J. Beltramini, *ChemCatChem*, 2014, **6**, 1349–1356.

28 R. Palkovits, K. Tajvidi, J. Procelewska, R. Rinaldi and A. Ruppert, *Green Chem.*, 2010, **12**, 972–97.

29 M. Kang, S. Y. Lee, C. H. Chung, S. M. Cho, G. Y. Han, B. W. Kim and K. J. Yoon, *J. Photochem. Photobiol. A Chem.*, 2001, **144**, 185–191.

30 M. Kang, *J. Mol. Catal. A Chem.*, 2003, **197**, 173–183.

31 W. Chen, J. Zhao, J. Y. Lee and Z. Liu, *Chem. Lett.*, 2004, **33**, 474–475.

32 H. Li, R. Wang, Q. Hong, L. Chen, Z. Zhong, Y. Koltypin, J. Calderon-Moreno and A. Gedanken, *Langmuir*, 2004, **20**, 8352–8356.

33 A. G. R. Howe, P. J. Miedziak, D. J. Morgan, Q. He, P. Strasser and J. K. Edwards, *Faraday Discuss.*, 2018, **208**, 409–425.

34 G. Y. Yu, W. X. Chen, Y. F. Zheng, J. Zhao, X. Li and Z. De Xu, *Mater. Lett.*, 2006, **60**, 2453–2456.

35 Z. Liu, L. M. Gan, L. Hong, W. Chen and J. Y. Lee, *J. Power Sources*, 2005, **139**, 73–78.

36 J. Okal, M. Zawadzki and W. Tylus, *Appl. Catal. B Environ.*, 2011, **101**, 548–559.

37 M. Mediavilla, H. Morales, L. Melo, A. B. Sifontes, A. Albornoz, A. Llanos, D. Moronta, R. Solano and J. L. Brito, *Microporous Mesoporous Mater.*, 2010, **131**, 342–349.

38 A. G. R. Howe, R. Maunder, D. J. Morgan and J. K. Edwards, *Catalysts*, 2019, **9**, 9, 748.

39 I. T. Horváth, H. Mehdi, V. Fábos, L. Boda and L. T. Mika, *Green Chem.*, 2008, **10**, 238–24.

40 W. Luo, M. Sankar, A. M. Beale, Q. He, C. J. Kiely, P. C. A. Bruijnincx and B. M. Weckhuysen, *Nat. Commun.*, 2015, **6**, 1–10.

41 C. Li, X. J. Ni, X. Di and C. H. Liang, *Ranliao Huaxue Xuebao/Journal Fuel Chem. Technol.*, 2018, **46**, 161–170.

42 K. Jiang, D. Sheng, Z. Zhang, J. Fu, Z. Hou and X. Lu, *Catal. Today*, 2016, **274**, 55–59.

43 R. Hage and A. Lienke, *Angew. Chemie*, 2006, **118**, 212–229.

44 J. M. Campos-Martin, G. Blanco-Brieva and J. L. G. Fierro, *Angew. Chemie - Int. Ed.*, 2006, **45**, 6962–6984.

45 United States Patent Office, 1108752, 1914.

46 G. Blanco-Brieva, E. Cano-Serrano, J. M. Campos-Martin and J. L. G. Fierro, *Chem. Commun.*, 2004, **4**, 1184–1185.

47 P. Tian, L. Ouyang, X. Xu, C. Ao, X. Xu, R. Si, X. Shen, M. Lin, J. Xu and Y. F. Han, *J. Catal.*, 2017, **349**, 30–40.

48 J. K. Edwards, B. E. Solsona, P. Landon, A. F. Carley, A. Herzing, C. J. Kiely and G. J. Hutchings, *J. Catal.*, 2005, **236**, 69–79.

49 J. Brehm, R. J. Lewis, D. J. Morgan, T. E. Davies and G. J. Hutchings, *Catal. Letters*, 2021, DOI:10.1007/s10562-021-03632-6.

50 C. M. Crombie, R. J. Lewis, R. L. Taylor, D. J. Morgan, T. E. Davies, A. Folli, D. M. Murphy, J. K. Edwards, J. Qi, H. Jiang, C. J. Kiely, X. Liu, M. S. Skjøth-Rasmussen and G. J. Hutchings, *ACS Catal.*, 2021, **11**, 2701–2714.

51 S. Maity and M. Eswaramoorthy, *J. Mater. Chem. A*, 2016, **4**, 3233–3237.

3: Experimental

3.1: Materials

Commercial Catalysts

Name	*Supplier*
Amberlyst-15 (WET)	Sigma-Aldrich
2.5%:2.5% $AuPd/TiO_2$	Johnson-Matthey

Metal Precursor Solutions

Name	*Concentration*	*Supplier*
$RuCl_3$	10 mg/mL in EG	Sigma Aldrich
$Ru(acac)_3$	10 mg/mL in EG	Sigma Aldrich
$HAuCl_4{\cdot}6H_2O$	5 mg/mL in EG	Sigma Aldrich
$PdCl_2$	2.5 mg/mL in EG	Sigma Aldrich
$Ni(NO_3)_3{\cdot}6H_2O$	5 mg/mL in EG	Sigma Aldrich
$Ag(NO_3)_2$	5 mg/mL in EG	Sigma Aldrich
$H_2PtCl_6{\cdot}6H_2O$	10 mg/mL in H_2O	Sigma Aldrich

EG: ethylene glycol; H_2O: deionised water

Solvents

Name	*Purity*	*Supplier*
Ethylene Glycol	>99%	Acros Organics
Methanol	HPLC Reagent Grade	Sigma Aldrich

Support Materials

Material	*Name/Type*	*Supplier*
Activated Carbon	Vulcan XC72R	Cabot
	Vulcan Black Pearls 2000	Cabot
Titanium Dioxide	P25	Degussa

Other

Name	*Purity*	*Supplier*
Sulphuric Acid	≥95%	Fisher Scientific
Phosphoric Acid	85 wt.%	Acros Organics
Avicel PH-101 Microcrystalline Cellulose		Sigma-Aldrich
Recycled Nappy Fibres		NappiCycle Ltd.
Hydrogen Peroxide	50 wt.% in H_2O	Sigma-Aldrich
Glucose	>99%	Fisher Scientific
Cellobiose	>99%	Sigma-Aldrich
Sorbitol	>99%	Sigma-Aldrich
Levulinic Acid	98%	Alfa Aesar
γ-Valerolactone	98%	Alfa Aesar

3.2: Catalyst Preparation Methods

3.2.1: Microwave-assisted Solvothermal (Polyol) Method

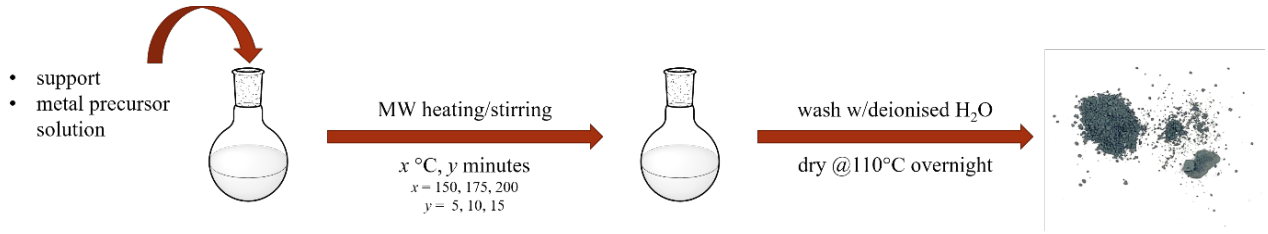

Figure 3-1: A visual schematic of the microwave-assisted solvothermal method of catalyst preparation.

This preparation method was used to synthesise most catalysts for this study. The polyol (in this study, ethylene glycol exclusively) acts as both a solvent for the metal precursor and as a reducing agent for the synthesis of supported metal nanoparticles.

An example catalyst preparation is as follows: for a 1 wt.% Ru/C catalyst, 2 mL of 5 mg/mL $RuCl_3$ is made up to 20 mL with ethylene glycol. This added to a 35 mL glass reactor vessel along with 0.99 g of Vulcan XC72R activated carbon. The vessel is sealed with a Teflon cap then heated with high stirring in a CEM Discover SP microwave reactor for a specified time and at a specified temperature. The resulting catalyst is cooled, washed with deionised water, then dried at 110 °C in a static air oven for 16 hours before use.

3.2.1.1: Catalysts Prepared by the Microwave-assisted Solvothermal (Polyol) Method

#	Supported Metal	Support Material	Metal Precursor	Synthesis Temperature (°C)	Synthesis Time (min)
Activated Carbon-Supported Catalysts					
1	1 wt.% Ru	Vulcan XC72R	$Ru(acac)_3$	150	5
2					10
3					15
4				175	5
5					10
6					15
7				200	5
8					10
9					15
10			$RuCl_3$	150	5
11					10
12					15
13				175	5
14					10
15					15
16				200	5
17					10
18					15
19		Vulcan Black Pearls	$Ru(acac)_3$	150	5
20					10
21					15
22				175	5
23					10
24					15
25				200	5
26					10
27					15
28			$RuCl_3$	150	5
29					10
30					15
31				175	5
32					10
33					15
34				200	5
35					10
36					15

Titanium Dioxide-Supported Catalysts					
37	1 wt.% Ru	Degussa P25 TiO_2	$Ru(acac)_3$	150	5
38					10
39					15
40				175	5
41					10
42					15
43				200	5
44					10
45					15
46			$RuCl_3$	150	5
47					10
48					15
49				175	5
50					10
51					15
52				200	5
53					10
54					15
55	1 wt.% Au		$HAuCl_4$	150	10
56	1 wt.% Pd		$PdCl_2$		
57	1 wt.% Ni		$Ni(NO_3)_3$		
58	1 wt.% AuPd (1:1)		$HAuCl_4 + PdCl_2$		
59	1 wt.% AuPd (1:2)				
60	1 wt.% AuPd (2:1)				
61	1 wt.% NiPd (1:1)		$Ni(NO_3)_3 + PdCl_2$		
62	1 wt.% NiPd (1:2)				
63	1 wt.% NiPd (2:1)				

Table 3-1: A list of all catalysts prepared by the microwave-assisted polyol method.

3.2.2: Wet-Impregnation

Wet impregnation is a ubiquitous catalyst preparation technique as it is simple to perform, reproducible, and produces minimal waste.[1] It was primarily used in this study to compare the activity of catalysts prepared by the microwave-assisted solvothermal preparation method. An example of a synthesis performed using this method is as follows: for a 1 wt.% Pt/TiO_2 catalyst, 10 mL of a H_2PtCl_6 solution ([Pt] = 1 mg/mL) is added to 50 mL of deionised water in a beaker at 60 °C with 0.99 g of P25 titanium dioxide (TiO_2). The mixture is heated at 95 °C in an oil bath until it reaches a paste-like consistency. The mixture is then filtered, washed with deionised water, and dried in a static-air oven at 110 °C overnight (16 hours). A reduction step is then performed in a tube furnace. The catalyst is heated to 400 °C at 10 °C min^{-1} for 4 hours in 5% H_2/Ar.

3.2.2.1: Catalysts Prepared by Wet Impregnation

#	Supported Metal	Support Material	Metal Precursor	Reduction Temperature (°C)	Reduction Time (min)
1	1 wt.% Ru	Vulcan XC72R	$Ru(acac)_3$	400	4
2			$RuCl_3$		
3		Vulcan Black Pearls	$Ru(acac)_3$		
4			$RuCl_3$		

Table 3-2: A list of all catalysts prepared by the wet impregnation method.

3.3: Material Pre-treatment Methods

3.3.1: Ball-Milling

The principle behind the use of ball-milling as a pre-treatment method is that the mechanical action of the milling reduces the abundance of crystalline regions within cellulose's structure, making its glycosidic bonds more susceptible to chemical attack.

The parameters for ball-milling were adapted from previous work by Onda *et al.* and Yang *et al.*[2,3] Figure 3-2 visually illustrates the milling process. The pre-treatment consisted of milling each sample for 2, 12, 24 or 48 hours. To reduce the amount of heat generated during the milling process, ten-minute cycles of milling and rest were used. This is especially important when milling the RNF due to the presence of

materials that become melted at relatively low temperatures, for example, polyethylene begins to melt at approximately 130°C,[4] minimising phase transitions such as this to occur within the milling chamber may avoid altering the sample's physical properties in an uncontrolled fashion.

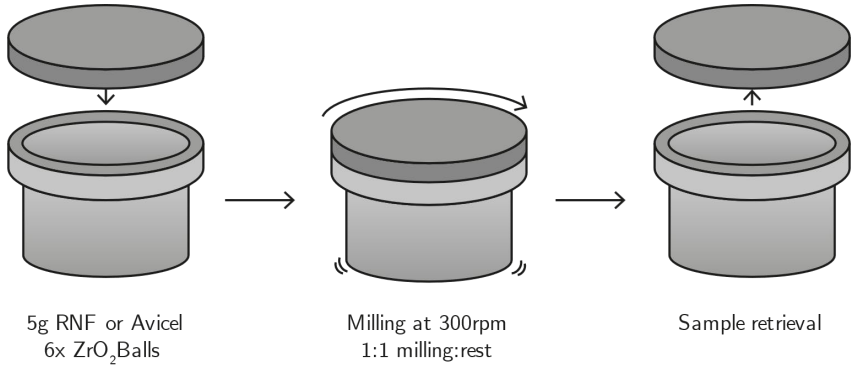

Figure 3-2: Visual schematic of the ball-milling process.

Ball-milling was performed using a Retsch PM-100 planetary ball mill. 5-gram portions, sufficient to fill the milling chamber to the recommended level, of either the Avicel PH-101 or the RNF (Recycled Nappy Fibres) were added, along with six zirconia balls. Milling was conducted at 300 rpm for a predetermined time ranging from 2 to 48 hours to investigate the effect of increasing the milling time on each material's hydrolysis performance.

3.3.2: Phosphoric Acid Regeneration

Highly concentrated solutions of phosphoric acid act as a solvent for crystalline cellulose,[5] and upon reducing its concentration, the cellulose precipitates out, often in a different polymorphic structure. Zhang *et al.* found the technique to be beneficial in their work, where the yield of sugars deriving from their H_3PO_4 treated cellulose increased from 20% to 66%.[6] A technique for treating cellulose with a solution of phosphoric acid was adapted from literature and applied to both the RNF and Avicel.[7]

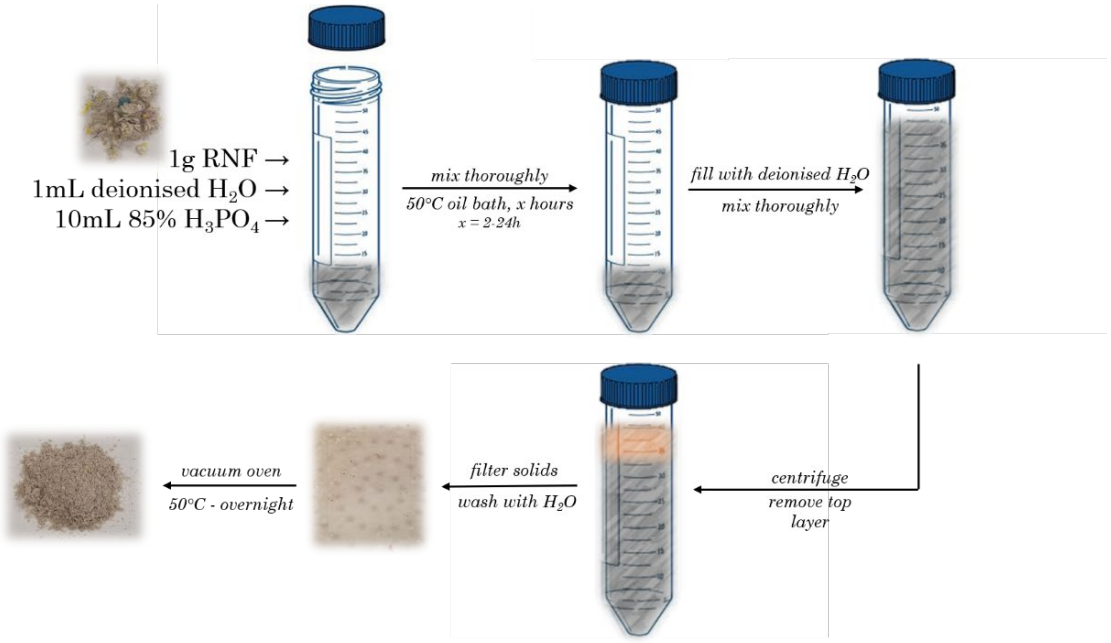

Figure 3-3: Visual schematic of the phosphoric acid regeneration pre-treatment method.

To a centrifuge tube, 1 g of either Avicel cellulose or recycled nappy fibres were added along with 1mL of deionised water. To this, 10 mL of 85 wt.% H_3PO_4 was added slowly with vigorous stirring, to ensure that the acid was fully incorporated into the material/water mixture. The tube was loosely covered then placed into a water bath at 50 °C for a set time, ranging from 2 to 24 hours, to investigate the effect of the duration that the material spent in the acid solution. The tube was then filled to its 50 mL mark with cold deionised water whilst being vigorously shaken, then centrifuged at 4000 rpm for 20 minutes. The solids were filtered, washed with 1 L of deionised water, then dried in a vacuum oven at 50 °C overnight prior to use.

3.4: Catalyst Testing Conditions

3.4.1: Solid Acid Catalyst Hydrolysis

The conditions for both solid and liquid acid hydrolysis reactions were adapted from work by Yang *et al.*[3] Solid-acid hydrolysis reactions were carried out in a Parr stainless-steel high-pressure autoclave, connected to a Parr 4597 reactor controller. To the reactor vessel, 300 mg of either the RNF or Avicel PH-101 were added to 12 mL of deionised water along with 1.2 g of Amberlyst-15, a commercially available solid acid. This was heated and stirred vigorously at 120 °C for 24 hours under autogenous air pressure. The reactor apparatus took 30 minutes to heat up to the desired temperature, after which the reaction was started. The reaction solution was filtered and analysed for hydrolysates using an Agilent 1200 HPLC system fitted with a MetaCarb 67H column.

3.4.2: Liquid Acid Hydrolysis

Due to concerns with reactor corrosion, liquid acid hydrolysis reactions were carried out in a low-pressure glass 'Colaver' brand reactor. To the reactor chamber, 368 µL of concentrated H_2SO_4 was added (to give an approximate parity to the $[H^+]$ of Amberlyst-15) to 12 mL of deionised H_2O, along with 300 mg of either the RNF or Avicel PH-101. This was heated and stirred vigorously at 120 °C in an oil bath for 24 hours under autogenous air pressure. The reaction solution was then filtered and analysed for hydrolysates using an Agilent 1200 HPLC system fitted with a MetaCarb 67H column.

3.4.3: One-Pot Cellulose Hydrogenolysis

The conditions for cellulose hydrogenolysis were adapted from previous research methods.[8,9] Cellulose hydrogenolysis reactions were carried out in a Parr stainless-steel pressure reactor, connected to a Parr 4597 reactor controller, and fitted with a Teflon liner (available volume: 35 mL). To the vessel, 162 mg of Avicel PH-101 or RNF and 50 mg of catalyst was added to 20 mL of deionised water. The reactor was purged three times with the reactant gas (H_2) to remove atmospheric gases, then charged with

1 MPa (10 bar) of H_2. Once the desired temperature of 170 °C was reached, which took 30 minutes, the reaction was started and took place for 24 hours with vigorous stirring. The solids were filtered then the reaction solution analysed using an Agilent 1200 HPLC system fitted with a MetaCarb 67H column.

In the case of cellulose hydrolysis reactions and the one-pot cellulose hydrogenolysis reactions, the yield of glucose was calculated based on the moles of carbon within the input material's cellulose. In the case of the recycled nappy fibres, a correction factor was applied based on the results of thermogravimetric analysis as to the proportion of cellulose within the material.

$$\text{Yield}(\%) = \text{moles of C in detected product} \Big/ \text{moles of C within input material's cellulose}$$

Equation 3-1: Product yield equation from HPLC analysis. In the case of the RNF, a correction factor was applied as the amount of cellulose within the material is 40 wt.%, as determined by thermogravimetric analysis.

3.4.4: Glucose Hydrogenation

Glucose hydrogenation reactions were carried out in a Parr stainless steel autoclave. A typical reaction procedure is as follows: to a Teflon-lined vessel, 162 mg of D-glucose and 50 mg of catalyst was added to 20 mL of deionised water (8.1 g/L glucose solution). The reactor was purged with the reactant gas (H_2) in order to remove atmospheric gases, then charged with 10 bar of H_2. Once the reaction mixture was heated to the desired temperature of 170 °C, which typically took 30 minutes, the reaction was started and took place for 30 minutes with vigorous stirring. The solids were filtered then the reaction solution analysed using an Agilent 1200 HPLC system fitted with a MetaCarb 67H column.

3.4.5: Levulinic Acid Hydrogenation

Levulinic acid hydrogenation reactions were carried out in a Parr stainless steel autoclave connected to a Parr 4597 reactor controller. To a 35 mL Teflon-lined reaction vessel, 25 mg of a 1 wt.% Ru/TiO_2 catalyst was added to 5 wt.% levulinic acid in 10 mL of deionised water. The reactor was purged with the reactant gas (H_2), then charged with 5 bar of H_2. Once the reaction mixture was heated to the desired

temperature of 100 °C, which typically took 15 minutes, the reaction was started and took place for 1 hour with vigorous stirring. The post-reaction solution was then analysed using a Varian GC fitted with a CP-Sil 5CB column. The composition of the reaction solutions was determined by calibration against levulinic acid and γ-Valerolactone standard solutions, in both calibration curves the $r^2 > 0.998$.[10]

3.4.6: Direct Synthesis of Hydrogen Peroxide from Hydrogen and Oxygen

The procedures for H_2O_2 synthesis, hydrogenation, and the measurements of H_2O_2 concentration were applied to this work from previous research within the Cardiff Catalysis Institute.[11] Synthesis reactions were carried out in a Parr stainless steel autoclave connected to a Parr 4597 reactor controller. 2.9 g of deionised water, 5.6 g of methanol and 10 mg of catalyst were added to a 35 mL Teflon-lined vessel. The reactor was purged three times with 5% H_2/CO_2, charged with it to 28.6 bar, then charged with a further 10 bar of 25% O_2/CO_2. The reactions were conducted at room temperature (25 °C) for 30 minutes.

3.4.7: Hydrogen Peroxide Hydrogenation

H_2O_2 hydrogenation reactions were carried out in a Parr stainless steel autoclave connected to a Parr 4597 reactor controller. 0.68 g of 50 wt.% hydrogen peroxide, 2.22 g of deionised water and 5.6 g of methanol was added to a 35mL Teflon-lined vessel, producing a 4 wt.% H_2O_2 solution. 10 mg of catalyst was added before the reactor was purged three times with 5% H_2/CO_2, charged with 5% H_2/CO_2 to 28.6 bar, then charged with a further 10 bar of 25% O_2/CO_2.

3.4.8: Hydrogen Peroxide Concentration Measurements

The concentration of hydrogen peroxide present in each reaction mixture was determined by cerimetry, a method first developed by the Romanian chemist Ion Atanasiu.[12] In this case, hydrogen peroxide reacts with cerium (IV) sulphate, forming cerium (III) sulphate, sulphuric acid, and water (1). A ferroin indicator is added, which changes colour from red to blue when it is reduced by the sulphuric acid generated (2).

(1) $H_2O_2 + 2Ce(SO_4)_2 \rightarrow Ce_2(SO_4)_3 + H_2SO_4 + O_2$

(2) $[Fe(phen)_3]^{2+} + 3H_3O^+ \rightarrow Fe^{2+} + 3phenH^+ + 3H_2O$

A cerium (IV) sulphate stock solution in 0.75 M H_2SO_4 was prepared, with an approximate concentration of 0.0085 M. Anhydrous cerium (IV) sulphate is hygroscopic, therefore the precise concentration of each batch of stock solution was determined by its titration against ammonium iron (II) sulphate hexahydrate.[13]

In a typical titration, 0.5 g of post-reaction solution was acidified with two drops of 2 wt.% H_2SO_4 in a glass vial, followed by the addition of one drop of ferroin indicator solution. The cerium (IV) stock solution was then added until the end point was reached, which was determined by eye and was indicated by a colour change from red to blue. Each titration was repeated three times to ensure accuracy. Due to the burette that was used, the volume of $Ce(SO_4)_2$ that was used was accurate to ± 0.1 cm^3.

Due to the high concentration of hydrogen peroxide used in hydrogenation experiments, a smaller amount of reaction mixture was added to each vial when compared to synthesis reaction solution analyses (≈ 30 mg) to reduce the amount of cerium (IV) sulphate solution required. The concentration of hydrogen peroxide was

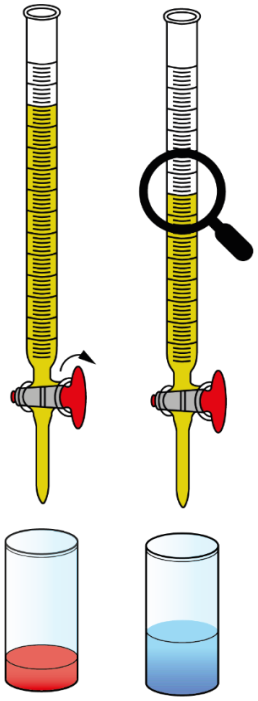

Figure 3-4: Visual representation of the cerium sulphate titration method for hydrogen peroxide concentration determination.

determined before and after each reaction, in each case performing three titrations to ensure an accurate result.

The moles of H_2O_2 present in each solution was calculated using equation 3-2.

$$Moles(H_2O_2) = \left(\left(\frac{average\ titre\ (cm^3)}{mass\ of\ reaction\ solution\ (g)}\right) * total\ solvent\ mass\ (g) * concentration\ of\ Ce(IV) solution\ (M)\right)/2000$$

Equation 3-2: The equation to calculate the moles of H_2O_2 present in each post-reaction solution.

The productivity and degradation activity of the catalyst is then calculated using equation 3-3.

$$\left(mol_{H2O2}\ kg_{cat}{}^{-1}\ h^{-1}\right) = \frac{moles(H_2O_2)}{\left(mass\ of\ catalyst\ used\ (g)/1000\right)} \Big/ Reaction\ duration\ (h)$$

Equation 3-3: H_2O_2 productivity/degradation equation.

3.5: Product Quantification

As previously mentioned in section 3.4, post-reaction solutions were analysed for hydrolysates and hydrogenates using an Agilent 1200 HPLC system fitted with a MetaCarb 67H column. Quantification was achieved *via* the instrument's refractive index detector, and calibration curves for a range of reducing sugars were created, based on what is typically expected from such reactions, and what was economically possible to purchase. A complete list of these is shown in Table 3-3, along with their associated retention times.

Compound	Retention Time
Glucose	8.2 min
Levulinic Acid	15.9 min
Lactic Acid	11.5 min
Formic Acid	12.6 min
5-HMF	33.8 min
Cellobiose	6.7 min
Maltose	6.8 min
Mannose	8.7 min
Fructose	8.9 min
Mannitol	9.4 min
Sorbitol	9.8 min

Table 3-3: The reducing sugars that were calibrated for the purpose of this study using HPLC.

3.6: Characterisation Techniques

3.6.1: Thermogravimetric Analysis

Thermogravimetric analysis (TGA) is a technique that measures the mass of a sample as its temperature increases. It is used to characterise various physical and chemical changes within the sample, such as the adsorption and desorption of species, or as in this instance, to measure the temperature at which constituents in a mixed sample degrade.[14] This information is used to identify the constituent parts of the sample, and to determine their relative abundance. The procedure for TGA analysis was as follows: to a pre-weighed crucible, a quantity (approximately 30 mg) of sample was added. The precise weight of the sample was determined by the instrument prior to the analysis. The sample was then heated to complete decomposition at 800 °C at a constant rate (5 °C min^{-1}) under a flow of N_2 whilst its mass was recorded. The temperatures at which the greatest rate of mass loss was occurring were identified by calculating the 1^{st}-order derivative of the mass losses. These were compared to reference samples of pure cellulose and a mixture of the absorbent core of an unused nappy.

3.6.2: X-Ray Diffraction

X-ray diffraction (XRD) is a phenomenon that occurs when crystalline materials interact with X-ray photons. It is used to elucidate information about the molecular structure of a material. Its main applications include the qualitative identification of crystal phases, and quantitative determinations of each phase's relative abundance in a multi-phase material.[15]

Crystal phase identification is achieved by monitoring a beam of monochromatic X-rays as its emission angle relative to the normal of the sample's surface increases. When an X-ray beam strikes an atom, either an inelastic or an elastic scattering process occurs. In a crystal lattice, rays that are elastically scattered from each plane interfere with each other in accordance with Bragg's law (Equation 3-4).

$$2d\ sin\theta = n\lambda$$

Where:

d is the interplanar spacing distance (Å)

ϑ is the angle between the incident beam and the normal of the crystal surface (°)

n is a positive integer

λ is the wavelength of the incident X-Ray beam

Equation 3-4

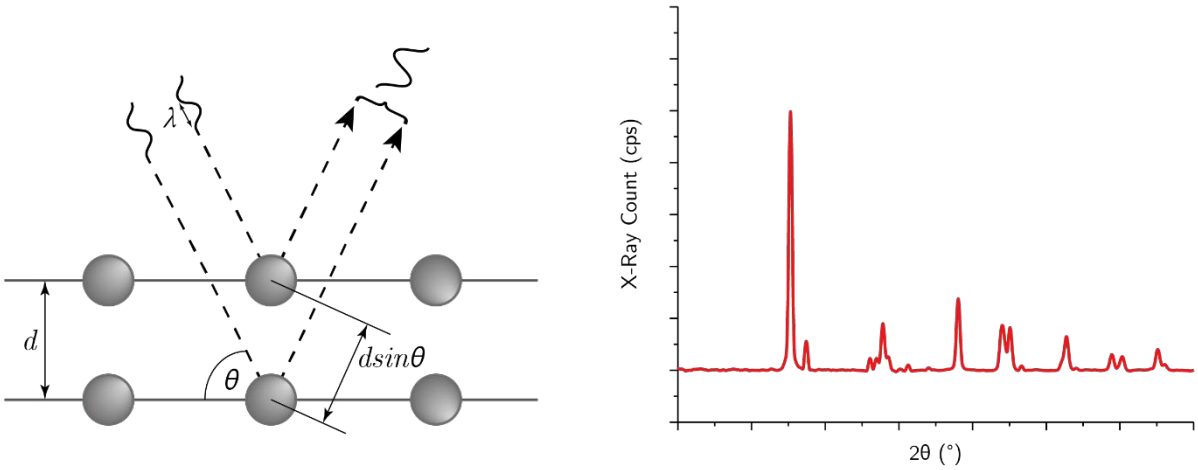

Figure 3-5: An illustration of two parts of a monochromatic X-ray beam colliding with two atoms on adjacent crystal planes. Constructive interference at a given 2Theta angle results in a greater peak intensity in the resulting diffractogram.

Figure 3-5 illustrates an X-ray beam colliding with vertically adjacent crystal planes. The beam that penetrates the first plane travels an extra 2·dsinθ relative to the part of the beam reflected from the surface. When this length is an integer multiple of the wavelength of the incident radiation (λ), constructive interference occurs, and the diffracted beam is amplified by the sum of its constituent beam amplitudes. This is represented as a peak in the resulting diffractogram. Any other length results in the diffracted beams being out of phase, which results in destructive interference of varying amounts.

Identifying a sample from this data is possible due to the reproducibility of the technique. Each material will have its own diffraction pattern that can be compared against a database of known materials.

3.6.3: X-Ray Photoelectron Spectroscopy (XPS)

XPS is a surface-sensitive technique that is used for the analysis of the surface chemistry of a given sample. It can provide information on the oxidation state of elements present in the surface, as well as their relative abundance.[16] The sample to be analysed is irradiated with a beam of single-energy X-rays. The electrons within the sample adsorb this radiation, and are then emitted with a characteristic energy.[17] XPS is used in this study in order to obtain information on the surface composition of each catalyst and the binding energies of the supported metal particles, as well as determining their oxidation states and the extent of their interaction with the support material. XPS data collected for this study was performed by a Thermo Fisher Scientific K-Alpha+ X-ray photoelectron spectrometer fitted with a monochromatic Al Kα X-ray source operating at 72 W.

3.6.4: Microwave-Plasma Atomic Emission Spectroscopy (MP-AES)

When an atom is exposed to enough thermal energy, it emits a characteristic pattern of electromagnetic radiation. This is the fundamental principle of atomic emission spectroscopy. Early examples of atomic emission spectroscopy were reported in the early nineteenth century; work by Henrik Lundegårdh in 1934 is considered to be the basis of modern quantitative analysis using the technique.[18] Thermal excitation can be achieved in many ways. Early techniques used flame excitation; however, this limits the range of elements that can be detected and quantified due to the temperature of the flame. The use of plasma excitation for atomic quantification was first reported in the late 1950s.[19] Its use gives the ability to ionise a greater range of elements, and advancements in equipment technologies allows for the detection of much lower concentrations of a given element within a sample.

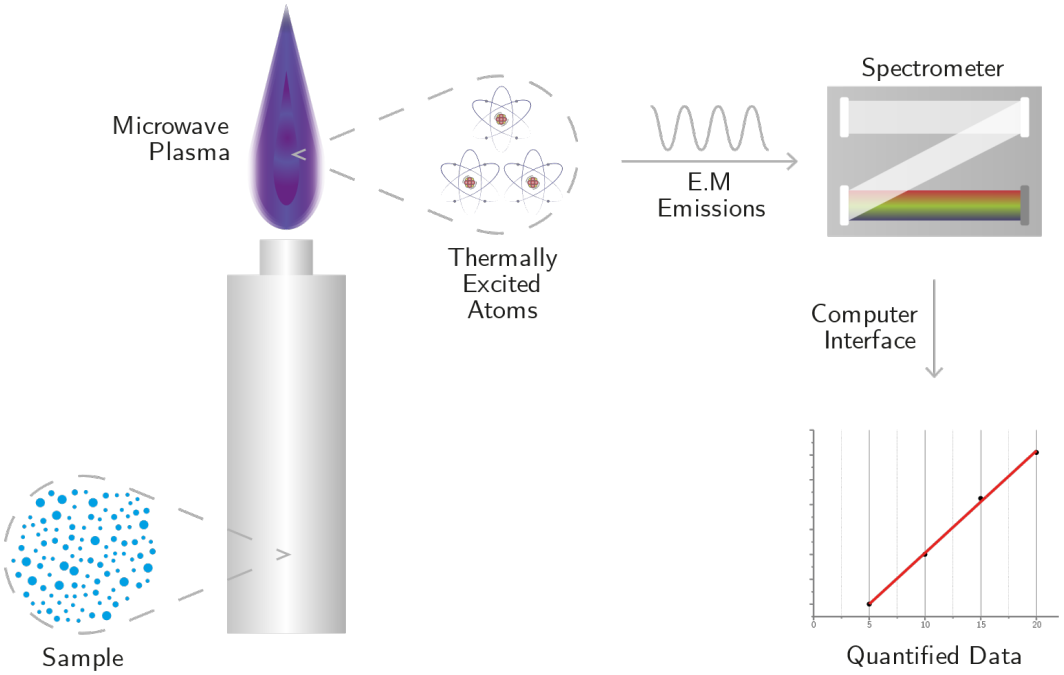

Figure 3-6: Schematic of an MP-AES instrument. Adapted from Agilent's documentation on the instrument.

In this study, MP-AES was used to accurately determine the amount of metal that was deposited on each catalyst, its metal loading. This is typically achieved by dissolving a known amount of each catalyst into a solution of aqua regia, then comparing its metal content to a set of serially diluted reference solutions. The procedure by which this was achieved is as follows:

100 mg of catalyst and 10 mL of aqua regia were added to a glass vial. This mixture was left overnight, then diluted with deionised water to 100 mL in a volumetric flask. A small aliquot of the solution was filtered using a 0.45 µm PTFE syringe filter prior to analysis to ensure that no solids were present. Each sample was analysed three times and at three emission wavelengths appropriate to the metal of interest.

Ruthenium is highly resistant to dissolution in aqua regia,[20] therefore a modified procedure had to be implemented for the analysis of ruthenium-based catalysts. Rather than using the catalyst itself, a comparison was made between the catalyst synthesis solutions before and after the synthesis procedure had taken place. In this case, an absence of ruthenium in the solution correlates to its complete attachment to the support material.

3.6.5: Scanning Electron Microscopy

Scanning electron microscopy (SEM) was used in conjunction with energy dispersive x-ray spectroscopy (EDX) to image and characterise catalysts in Chapter 6. The modern scanning electron microscope is the result of seminal work by several German scientists, most notably Max Knoll and Manfred Von Ardenne, in the 1930s.[21]

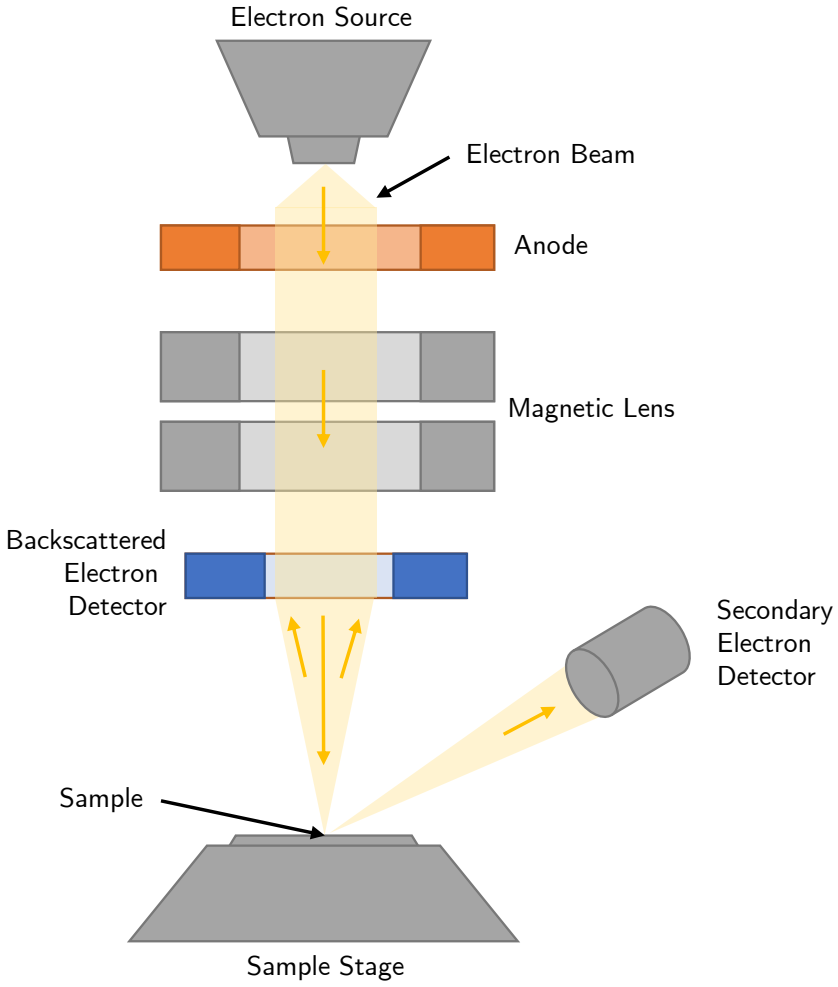

Figure 3-7: Simplified diagram of a typical scanning electron microscope. Based on work by S. Bradbury et al.[22]

An SEM generates images by scanning a sample with a focussed beam of high-energy electrons in a raster pattern.[23] The instrument provides information on the topography and characteristics of the sample's surface, based on the detection of electrons that are scattered by their interaction with the sample's surface.

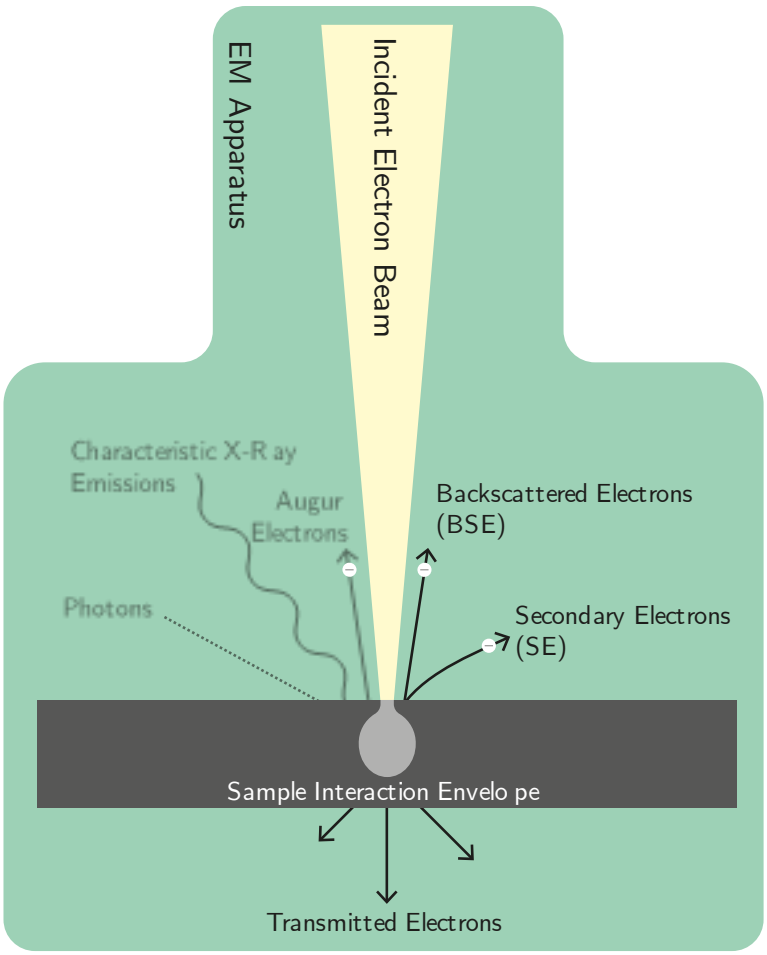

Figure 3-8: The primary emissions that occur because of the scattering of the incident electron beam of a scanning electron microscope.

The detection of inelastically scattered secondary electrons (SE) and backscattered electrons (BSE) are the primary methods of imaging using a scanning electron microscope.[21] Secondary electron imaging has a wide depth-of-field, resulting in an image that appears three-dimensional. The electrons originate from the topmost layers of the sample; the low sample penetration allows for detailed surface images that show topography and surface morphology. Backscattered electrons originate from deeper layers of the sample, BSE emissions have a detected intensity that is proportionally relative to atomic weight. This allows for differences in elemental composition to be viewed, for example, particles of metal deposited onto the support material of a catalyst.

In this study, SEM-EDX was used to obtain information on the surface morphology and particle characteristics of a selected number of catalysts prepared by the

microwave-assisted polyol method. To determine the effect of alloying using the synthesis technique, two monometallic catalysts (1%Au/TiO_2, 1%Pd/TiO_2) and a bimetallic catalyst (1%AuPd(1:1)/TiO_2) were selected. SEM images were captured using a Tescan MAIA3 field emission gun scanning electron microscope (FEG-SEM) fitted with an Oxford Instruments $XMax^N$ 80 energy dispersive X-ray detector (EDX). Images were acquired using both the secondary electron and backscattered electron detector. Samples were dispersed as a finely-ground powder onto 300-mesh copper grids coated with a holey carbon film.

3.6.6: Transmission Electron Microscopy

SEM images are generated by detecting electrons that are scattered by a sample's surface. In contrast, transmission electron microscopy (TEM) is a microscopy technique where images are generated by the detection of electrons as they are transmitted through a thin layer of a sample. This makes it a more suitable technique for obtaining information on a sample's bulk characteristics, such as the arrangement of crystal lattices and particle size distributions.

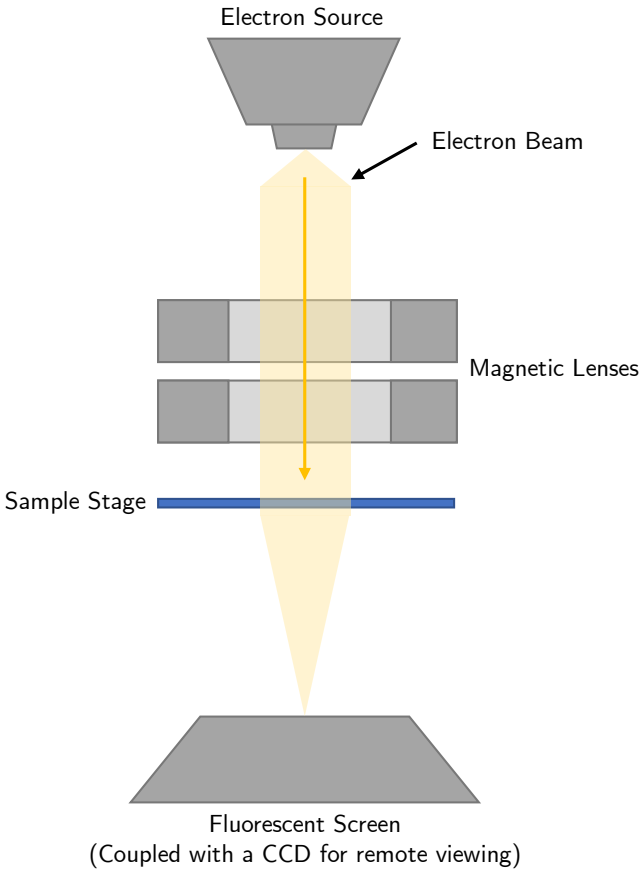

Figure 3-9: Illustrated schematic of a typical transmission electron microscope.

In this study, TEM was used to obtain particle size distribution information on a selected series of Ru/C catalysts that were synthesised by the microwave-assisted polyol method. To investigate the effect that synthesis parameters had on particle size characteristics, three catalysts were chosen from within the same series (1%Ru(Cl)/XC72R 175-x) that were synthesised from the shortest to the longest time. TEM images were captured using a JEOL JEM-2100 instrument operating at 200 kV. Samples were dispersed as a powder onto 300-mesh copper grids coated with holey carbon film.

3.7: References

1 J. R. A. Sietsma, A. Jos van Dillen, P. E. de Jongh and K. P. de Jong, *Application of ordered mesoporous materials as model supports to study catalyst preparation by impregnation and drying*, Elsevier Masson SAS, 2006, vol. 162.

2 A. Onda, T. Ochi and K. Yanagisawa, *Green Chem.*, 2008, **10**, 1033.

3 Q. Yang and X. Pan, *Bioenergy Res.*, 2016, **9**, 578–586.

4 F. C. Stehling and L. Mandelkern, *Macromolecules*, 1970, **3**, 242–252.

5 J. Zhang, J. Zhang, L. Lin, T. Chen, J. Zhang, S. Liu, Z. Li and P. Ouyang, *Molecules*, 2009, **14**, 5027–5041.

6 J. Zhang, B. Zhang, J. Zhang, L. Lin, S. Liu and P. Ouyang, *Biotechnol. Adv.*, 2010, **28**, 613–619.

7 X. Jia, Y. Chen, C. Shi, Y. Ye, P. Wang, X. Zeng and T. Wu, *J. Agric. Food Chem.*, 2013, **61**, 12405–12414.

8 A. Shrotri, H. Kobayashi, A. Tanksale, A. Fukuoka and J. Beltramini, *ChemCatChem*, 2014, **6**, 1349–1356.

9 Z. Li, Y. Liu, C. Liu, S. Wu and W. Wei, *Bioresour. Technol.*, 2019, **274**, 190–197.

10 A. G. R. Howe, R. Maunder, D. J. Morgan and J. K. Edwards, *Catalysts,* 2019, **6**, 713.

11 A. Santos, R. J. Lewis, G. Malta, A. G. R. Howe, D. J. Morgan, E. Hampton, P. Gaskin and G. J. Hutchings, *Ind. Eng. Chem. Res.*, 2019, **58**, 12623–12631.

12 T. Vi, M. Profesor, G. I. Costeanu, P. Universitar, I. A. Atanasiu, C. Toda, S. Ro, M. D. St, C. Societ, C. Orbeci, C. Aplicat, I. Zarafu, C. Na, G. Stanciu, E. Ungureanu and A. Nomares, *Soc. ii Chim. din România*.

13 J. K. Edwards, B. E. Solsona, P. Landon, A. F. Carley, A. Herzing, C. J. Kiely

and G. J. Hutchings, *J. Catal.*, 2005, **236**, 69–79.

14 A. W. Coats and J. P. Redfern, *Analyst*, 1963, **88**, 906–924.

15 S.T.Misture & R.L.Snyder, *Encycl. Mater. Sci. Technol.*

16 R. R. Mather, *Surface modification of textiles by plasma treatments*, Woodhead Publishing Limited, 2009.

17 M. H. Engelhard, T. C. Droubay and Y. Du, *Encycl. Spectrosc. Spectrom.*, 2016, 716–724.

18 M. Ihnat, in *Modern Methods of Food Analysis*, eds. K. K. Stewart and J. R. Whitaker, Springer Netherlands, Dordrecht, 1984, pp. 129–166.

19 K. Ohls and B. Bogdain, *J. Anal. At. Spectrom.*, 2016, **31**, 22–31.

20 A. K. De, *A Textbook Of Inorganic Chemistry*, New Age International (P) Limited, 2007.

21 A. Ul-Hamid, *A Beginners' Guide to Scanning Electron Microscopy*, Springer International Publishing, 2018.

22 S. Bradbury, D. C. Joy and B. J. Ford, Scanning Electron Microscope, https://www.britannica.com/technology/scanning-electron-microscope, (accessed 18 November 2021).

23 H. Schatten, *Scanning Electron Microscopy for the Life Sciences*, Cambridge University Press, Cambridge, UNITED KINGDOM, 2012.

4: Recycled Nappies as a Source of Cellulosic Biomass

4.1: Introduction

Several samples of recycled nappy fibres (RNF) were provided by NappiCycle, in their dried "as- produced" form and in pellets. The initial focus of research was to conduct an in-depth analysis of the material to determine the chemical signature of the RNF. Following identification of the major components of the RNF (likely to be super absorbent polymers and cellulose), the feasibility of using it as an alternative feedstock in upgrading reactions, through its response to a typical cellulose hydrolysis reaction, will be determined.

A detailed investigation into the RNF's physical and chemical properties was the first objective. As its cellulose was the target for conversion into value-added products, a model cellulose, Avicel PH-101, was obtained and subjected to the same procedures as the RNF to provide a comparison and to provide a benchmark in activity to compare the RNF to Avicel. An additional comparison is made between the performance of Amberlyst-15, a commercially available solid acid catalyst used in similar biomass conversion studies,[1–3] and sulphuric acid. In subsequent RNF pre-treatment investigations, Amberlyst-15 is used exclusively.

Cellulose hydrolysis conditions for this chapter of work were adapted from literature by Yang *et al.*[4] In their work, 50 mg of Avicel cellulose was added to 2 mL of water, along with 200 mg of a selected solid acid catalyst. Hydrolysis reactions commenced at 120 °C for a set time, ranging from 12 to 48 hours. Their most active sulfonated polymer catalyst achieved a cellulose conversion of ≈ 50% at the specified reaction conditions after 24 hours. Both Amberlyst-15 and sulphuric acid were used as benchmark catalysts for their study, achieving glucose yields of ≈8% and 14%, respectively. Therefore, these conditions were considered suitable for comparative purposes for this investigation.

4.2: Results and Discussion

4.2.1: Quantitative Composition of the Recycled Nappy Fibres

The RNF were received in two physical forms: as a shredded and dried mixture and as solid cylindrical pellets, as shown in Figure 4-1.

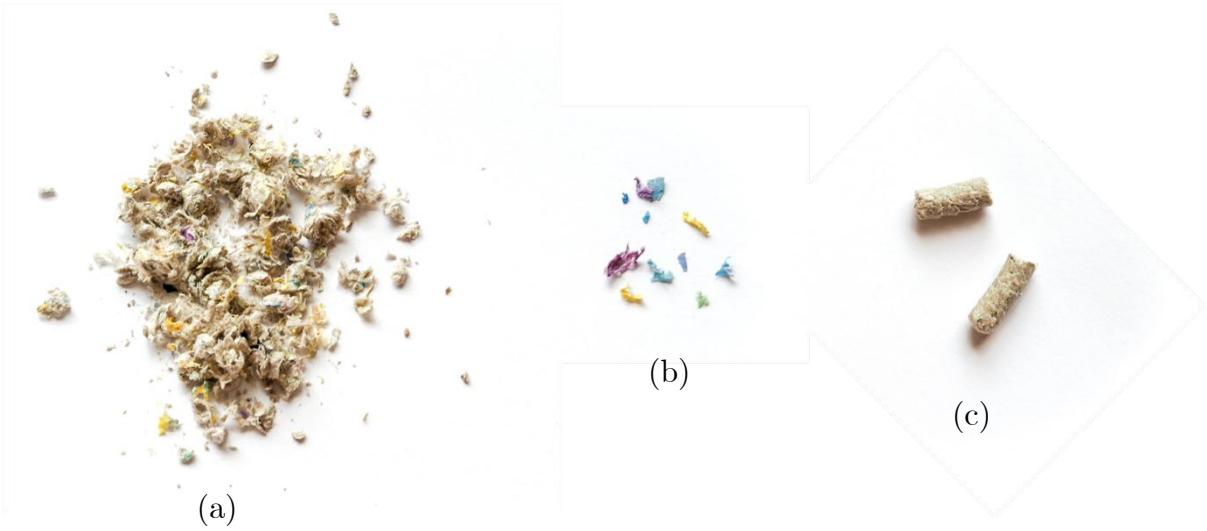

Figure 4-1: The two forms of the material that were received. A shredded and dried form (a) with some coloured plastic films isolated from this shown in (b). A pelletised form of (a) was also received (c).

As discussed in Chapter 2, it was expected that there would be a significant quantity of cellulose present due to its abundance in single use nappies and absorbent hygiene products (AHPs).[5] The presence of plastic films is apparent from visual inspection; some of this was isolated by hand and is seen in Figure 4-1 (b). What was less certain is whether there would be superabsorbent polymers present, as in its deactivated form it may have been able to be washed away in liquid waste streams during the NappiCycle's processing steps.

A measure of the relative abundance of the constituents of the RNF was achieved using thermogravimetric analysis. Samples of both the fibrous and pelletised forms of the material were analysed according to the procedure in Chapter 3, section 4.1. Reference materials were analysed to correlate each mass loss to a specific constituent, based on the temperatures at which the highest rate of mass loss occurs. These mass loss 'events' were identified by calculating the first-order derivative of each mass loss curve, whereby a greater rate of mass loss produces a peak in the derivative curve, with the

midpoint of the peak corresponding to the temperature at which the greatest rate of mass loss is occurring. Figure 4-2 shows TGA curves of both the recycled nappy fibres and its pelletised form at temperatures between room temperature (approximately 30 °C) and 800 °C. For each experiment, approximately 30 mg of material was analysed each time, however mass losses are graphed as a weight percentage of the original mass of each sample, for consistency between each analysis.

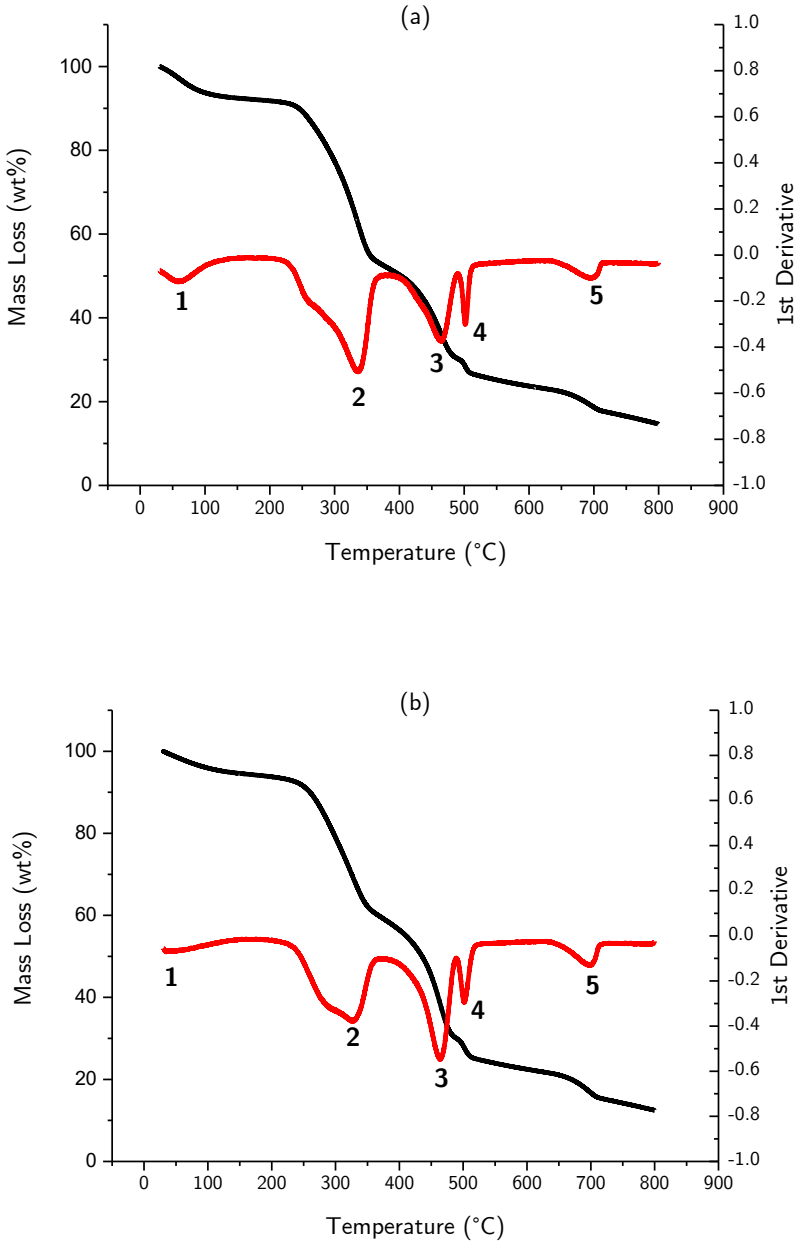

Figure 4-2: TGA curves of the recycled nappy fibres (a) and their pelletised form (b). The black line represents the mass loss as the temperature is increased, expressed as a weight percentage of the sample's mass. The red line represents the peak rate of mass losses by the calculation of the first order derivative of the mass loss curve.

Five distinct mass losses were identified in both samples. These are summarised in Table 4-1.

Recycled Nappy Fibres			**Recycled Nappy Fibres - Pelleted**		
Mass Loss	*Peak Rate of 1st Derivative (°C)*	*Mass Loss (wt.%)*	*Mass Loss*	*Peak Rate of 1st Derivative (°C)*	*Mass Loss (wt.%)*
1	59.5	7.1	1	55.3	5.7
2	335.2	38.8	2	327.4	34.6
3	464.2	22.9	3	464.0	29.7
4	501.8	4.7	4	501.8	5.1
5	694.3	5.1	5	697.4	6.3

Table 4-1: Mass losses identified from samples of recycled nappy fibres and their pelletised form.

Both forms of recycled material have five distinct mass losses at very similar temperatures. This was to be expected, as no additional materials were added or taken away during the production of the pelletised form of the nappy fibres. Each peak mass loss temperature was also the same between the two forms. The first mass loss is attributed to water based on the temperature and the amount of mass lost, which is in keeping with the figure provided by NappiCycle for these materials' moisture content ($<=$ 10%). Mass losses 2 and 3, at $\approx$ 330 °C and $\approx$ 460 °C, represent the two most abundant components of the recycled material at 34-38% and 24-30%. These are cellulose and sodium polyacrylate, respectively. These were differentiated by comparing the peak mass loss temperatures to reference samples of both microcrystalline cellulose and an extract of the absorbent core of an unused nappy, the data from which is shown in Figure 4-3 and Table 4-2.

Previous literature corroborates these findings. Khanylie *et al.*'s investigation into the thermal decomposition of disposable nappies from two popular brands highlighted the presence of two distinct peaks in their TGA data from samples of the core of both nappies, occurring between 350-480 °C. These mass losses were attributed to the decomposition of cellulosic material and superabsorbent polymers, which is in line with the results obtained in this study.[6]

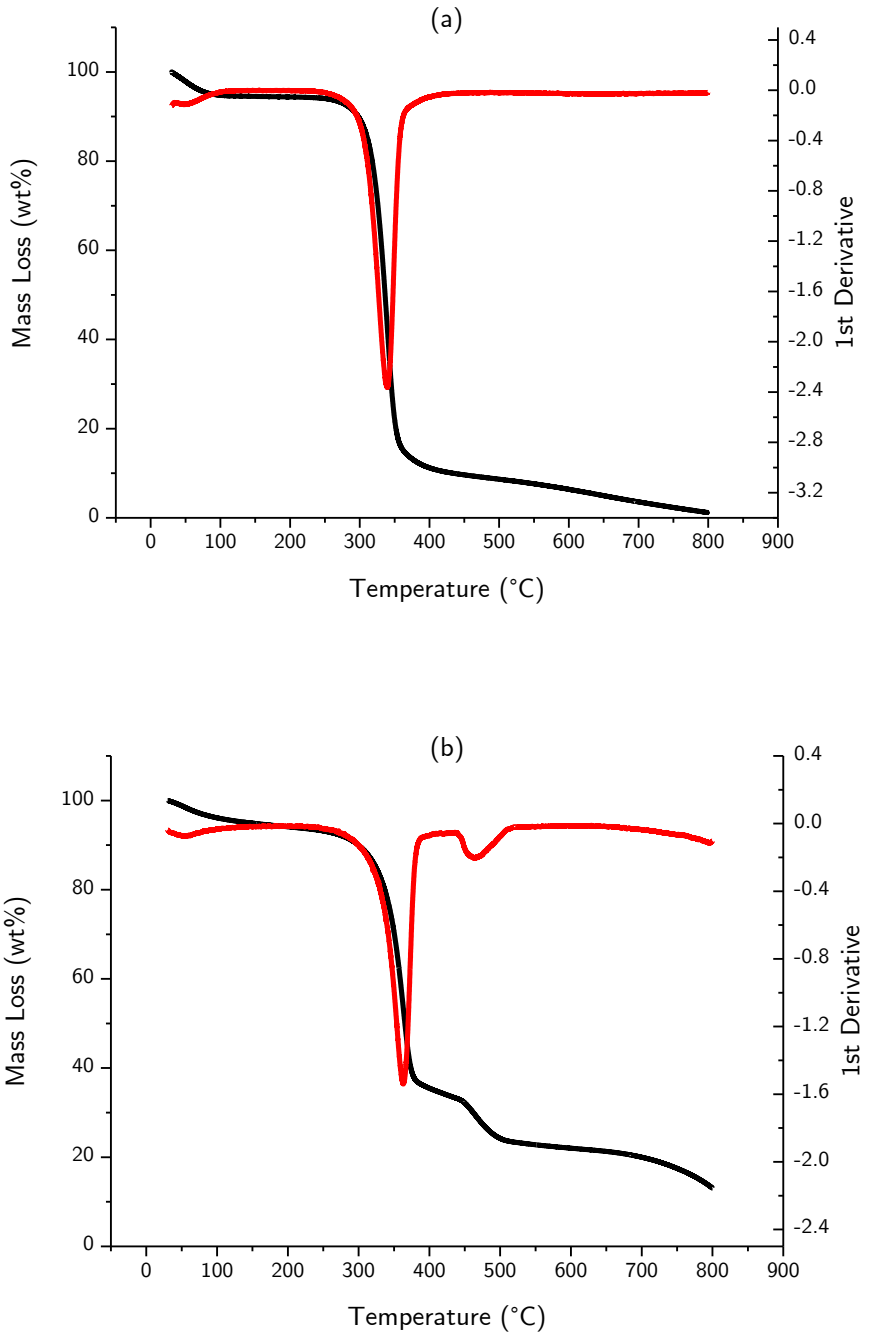

Figure 4-3: TGA curves of pure microcrystalline cellulose (a) and the absorbent core of an unused nappy (b). The data was processed in the same manner as that of the recycled nappy fibre materials, where the black line represents the mass loss as the temperature is increased, expressed as a weight percentage of the sample's mass. The red line represents the 'peak' mass losses, by the calculation of the first order derivative of the mass loss curve.

Microcrystalline Cellulose			Absorbent Core of Unused Nappy		
Mass Loss	*Peak Mass Loss Temperature (°C)*	*Mass Loss (wt.%)*	*Mass Loss*	*Peak Mass Loss Temperature (°C)*	*Mass Loss (wt.%)*
1	339	90.4	1	362.4	64.6
			2	462.3	12.8

Table 4-2: Quantifiable mass losses from TG analysis of pure microcrystalline cellulose and a sample of the absorbent core of an unused nappy. Each TGA run was repeated three times, the average values are presented in this table.

In the RNF samples, cellulose is the most abundant component by weight, representing 39 wt.% of the nappy fibres and 35 wt.% of the pellets. Sodium polyacrylate is the second most abundant component at 23 wt.% in the fibres and 30 wt.% in the pellets.

The presence of such a significant quantity of sodium polyacrylate in the RNF was an unexpected finding. It was initially assumed that a significant amount of it in its deactivated form would be washed away during the recycling process. Methods for re-activating it have been demonstrated in previous literature; the calcium ion bridging that occurs as part of the deactivation process is not permanent,[7] and can be reversed.[8] There have been several proposed uses for non-hygienic superabsorbent polymers, as briefly discussed in Chapter 1, section 1.6. It has been demonstrated to be effective at soil water retention; when mixed with degraded soil it acts as 'artificial humus', controlling the rate of erosion after rainfall.[9] It also may find use in water treatment facilities, and as a chemical modifier for fibre and textile manufacture.[10]

4.2.2: Characterisation of the Materials as Received

Prior to pre-treatment investigations, both the RNF and Avicel PH-101 were tested for their cellulose hydrolysis performance using the conditions described in Chapter 3, sections 3.4.1 and 3.4.2. In short, samples of each were hydrolysed with either a solid acid, Amberlyst-15, or a liquid acid, sulphuric acid at 120 °C for 24 hours. The results of these experiments are shown in Figure 4-4. In addition, both materials were characterised using X-Ray diffraction. This provided the cellulose crystallinity index (CrI%) of each material and a qualitative measure of the polymorphic structures of cellulose present and provides a further means of determining the similarity of the RNF to model cellulose.

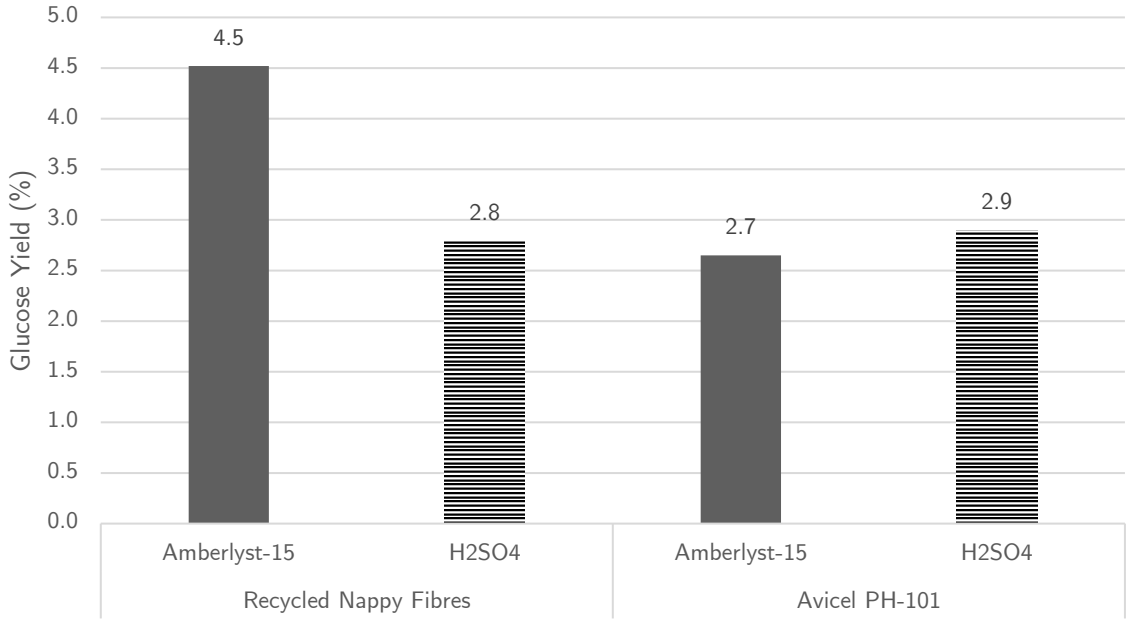

Figure 4-4: Glucose yields obtained from the RNF and Avicel PH-101. Reaction parameters: 300 mg substrate (RNF or Avicel PH-101), 1.2 g Amberlyst-15 (solid acid reactions) or 300 µL H_2SO_4 (liquid acid reactions), 12 mL deionised H_2O, 120 °C, 24 h.

For the hydrolysis reactions, the yield of glucose obtained was low (> 5%) when either the RNF or Avicel were used, and across both the solid acid and liquid acid reactions. The reaction conditions employed were mild when compared to similar cellulose hydrolysis studies, especially temperature. For instance, Onda *et al.* performed solid acid hydrolyses typically at 150 °C and achieved 40.5% yield of glucose using their sulphonic acid-catalysed catalysts. Lanzafame *et al.*'s conversion reactions were performed at 190 °C, and though glucose was produced in a significant quantity, the vast majority of the hydrolysates produced were classed as 'side products', these comprising over 75% of the overall distribution of products when Amberlyst-15 was used.[1] A milder set of reaction conditions (120 °C) were selected in this study primarily in order to minimise the formation of humins within the reactor apparatus.

'Humins' is a term that describes the products of an uncontrolled reaction of cellulose's hydrolysates into a chemically complex, carbonaceous material. It is a dark-coloured solid with an inconsistent chemical structure, as Figure 4-5 illustrates.

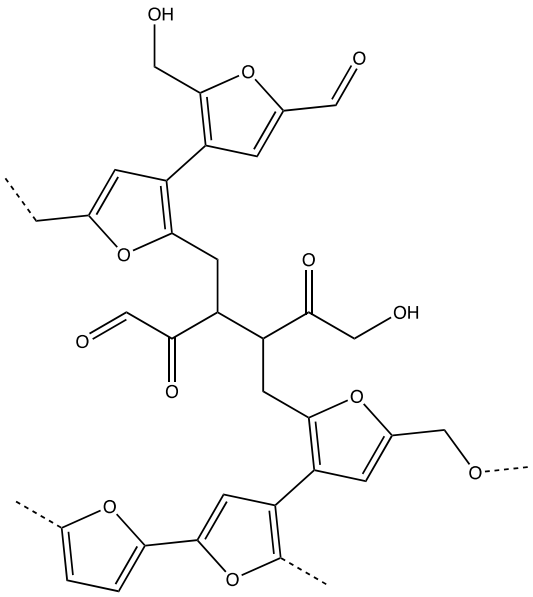

Figure 4-5: A snippet of the proposed structure of humins derived from D-glucose. Based on work by Wang et al.[11]

Due to their inconsistent structures and the high number of functional groups, they are not able to be easily converted into useful compounds, and are therefore considered a waste product.[12] As previously mentioned in Chapter 2, the formation of humins is highly dependent on the reaction temperature that is employed.[12] Their formation during cellulose hydrolysis as a percentage of the overall carbon content increases significantly as temperature is increased.[13,14]

The primary method of characterising the cellulosic materials for this chapter was X-Ray diffraction. For interpretation of the data to be made, the differences between cellulose's polymorphic structures will be explained, and a technique for calculating cellulose's crystallinity index will be introduced and critically discussed. Cellulose has a crystalline structure due to intra- and intermolecular hydrogen bonding between its hydroxyl groups. The arrangement of crystalline cellulose can take on four distinct forms: cellulose I to IV. A simplified schematic of cellulose I and II's structures are shown in Figure 4-6.

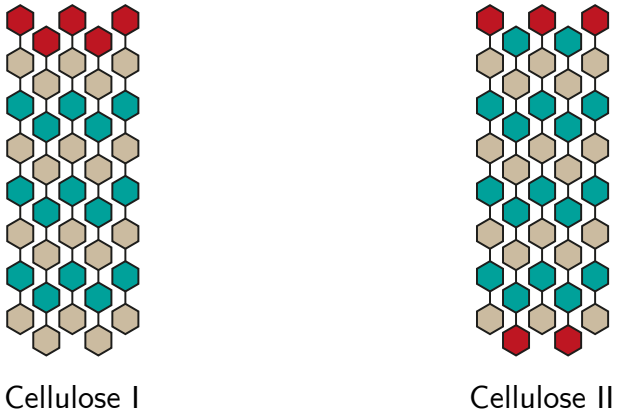

Figure 4-6: A simplified representation of cellulose's two most common polymorphs. The red units indicate the reducing end of each chain. Alternating green and beige colours are used to distinguish between each monomer unit. Adapted from published work by Pérez and Samain.[15]

As Figure 4-6 illustrates, cellulose I is the most common, naturally occurring polymorph. Its chains lie parallel, with the reducing ends orientated in the same direction. In this context, 'reducing ends' refers to the ends of each cellulose fibre that have an unbonded aldehyde group. Cellulose II, also known as regenerated cellulose, is commonly found when cellulose has been subjected to a chemical or physical treatment, such as being dissolved. Its chains lie anti-parallel, with its reducing ends, that is, the terminal anhydro-glucose units that aren't bonded on both ends by a glycosidic bond, lying in opposing directions. The transition of cellulose I to cellulose II is irreversible, indicating that cellulose II is more thermodynamically stable.[16]

In addition to determining the polymorphic structure of the cellulose present in each sample, an estimation of its crystallinity can be achieved using XRD. A highly cited piece of seminal work by Segal *et al.* in 1959 demonstrated that cellulose's crystallinity index can be estimated from its diffraction pattern by Equation 4-1. Cellulose contains both crystalline and amorphous regions. The amount of crystalline material is represented by the height of the greatest diffraction peak (002), and the amount of amorphous material is represented by the height of the minimum intensity between the major peaks. The crystallinity index (CrI%) is the difference between the two intensities, divided by the intensity of the highest peak.[17]

$$CrI\% = {I_{cr}}/{(I_{cr} + I_{am})} * 100$$

Where:

CrI%	is the crystallinity index
I_{cr}	is the peak height of cellulose's (002) diffraction
I_{am}	is the minima of the peaks between cellulose's (101) and (002) diffractions

Equation 4-1: Segal's cellulose crystallinity equation.

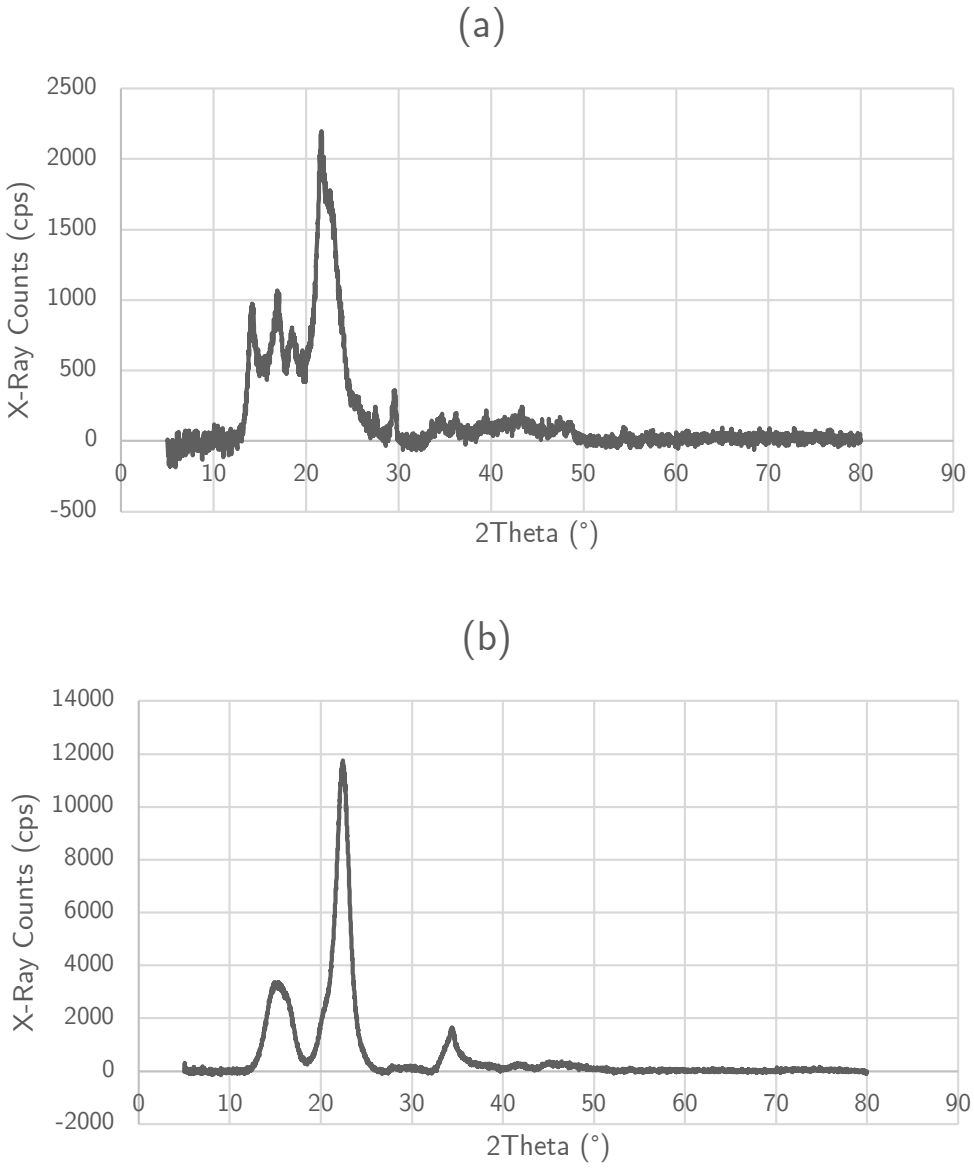

Figure 4-7: XRD Patterns of un-treated RNF (a) and Avicel PH-101 (b). The (002) peak in both instances is located at 2Theta = 22 °.

Recycled Nappy Fibres			Avicel PH-101		
2θ (°)	*Peak Height (cps)*	*Crystal Plane*	*2θ (°)*	*Peak Height (cps)*	*Crystal Plane*
14.2	878	(101)	15.1	3284.9	(101)
16.9	947.8	$(10\bar{1})$	22.5	11498.3	(002)
18.5	802		34.4	1664.5	(040)
21.7	2164.4				
22.6	1680.9	(002)			
29.5	279.2				
34.7	174.9	(040)			

Table 4-3: The identified diffraction peaks from XRD patterns of the un-treated materials.

Both materials' diffraction patterns and the associated peak heights are shown in Figure 4-7 and Table 4-3. Cellulose's crystal phase identification was achieved by referenced literature and through reference libraries.[18]

The diffraction peaks found for Avicel at 2ϑ = 15.1 °, 22.5 °, and 34.4 ° are in line with those of cellulose I, its naturally occurring polymorph. These diffractions were also identified in the sample of RNF. In addition, diffractions at 2ϑ = 16.9 ° and 21.7 ° indicate the presence of cellulose II. The remaining unidentified diffractions are presumed to be due to the presence of other materials within the RNF. Appling Segal *et al.*'s equation to the XRD data results in crystallinity indices of 69% for the RNF and 86% for Avicel PH-101. The RNF's crystallinity index is similar to Trilokesh *et al.*'s calculation of the crystallinity of the cellulose present in their samples of nappy material using Segal's method (65.1%).[19] NappiCycle's recycling process includes several steps (Appendix A, steps 4-7) where the RNF undergoes intensive mechanical forces.[20] These steps may have contributed to the comparably lower initial crystallinity of the RNF's cellulose, as well as the cellulose itself being derived from natural cotton. The CrI% of Avicel as reported in this study is in line with previously published values.[21] Avicel is highly crystalline by design; therefore, its high CrI% is to be expected.

4.2.3: Ball-Milling

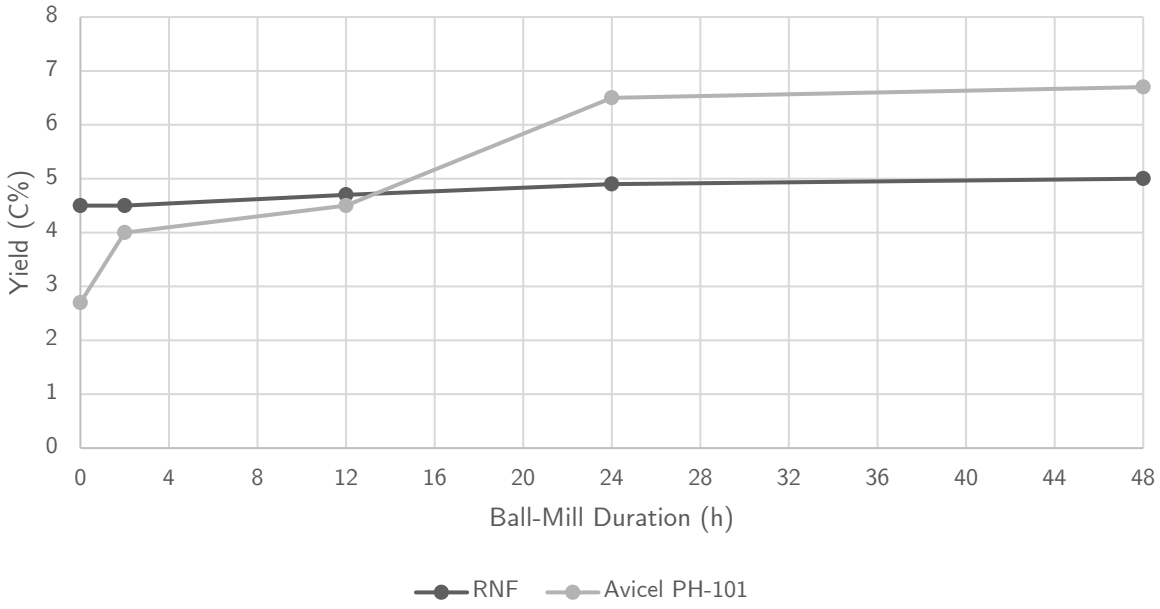

Time (h)	Glucose Yield (C%)	
	RNF	*Avicel PH-101*
0	4.5	2.7
2	4.5	4.0
12	4.7	4.5
24	4.7	6.5
48	5.0	7.0

Figure 4-8: Cellulose hydrolysis data from ball-milled RNF and Avicel PH-101. Reaction parameters: 300 mg substrate (RNF or Avicel PH-101), 1.2 g Amberlyst-15 (solid acid reactions) or 300 µL H_2SO_4 (liquid acid reactions), 12 mL deionised H_2O, 120 °C, 24 h.

Both the RNF and Avicel PH-101 were ball-milled according to the procedure outlined in Chapter 3, section 3.3.1. The purpose of the ball milling experiments was to reduce the abundance of crystalline domains present within the cellulose and increase the yield of hydrolysates obtained from it. This has been observed by Yu *et al.* who showed that ball milling Avicel PH-101 for 7 hours increased the conversion of cellulose to soluble sugars.[22] Briefly, both the RNF and Avicel PH-101 were milled for increasing lengths of time, then used as substrates for cellulose hydrolysis reaction and a comparison was made to untreated "as received" versions. The resulting glucose yields obtained from ball milled RNF and Avicel are shown in Figure 4-8. Selected samples were also analysed for their crystallinity values using XRD.

Ball-milling has a minimal impact upon the yield of glucose obtained with both materials, however the beneficial effect is more pronounced in the case of Avicel, where the yield of glucose increased from 2.7% to 7% after 48 hours of milling time. The beneficial effect became less pronounced after 24 hours of milling. The increase in yield obtained using RNF is minimal, with the yield of glucose obtained from it only increasing from 4.5% to 5% after 48 hours of milling.

X-Ray diffraction was employed to characterise the cellulosic components of both the RNF and Avicel PH-101 post-treatment. Two parameters were investigated: the crystallinity index of the cellulose and the qualitative identification of cellulose's polymorphic structures. The XRD patterns of the RNF and Avicel after 24 hours of ball-milling are shown in Figure 4-9.

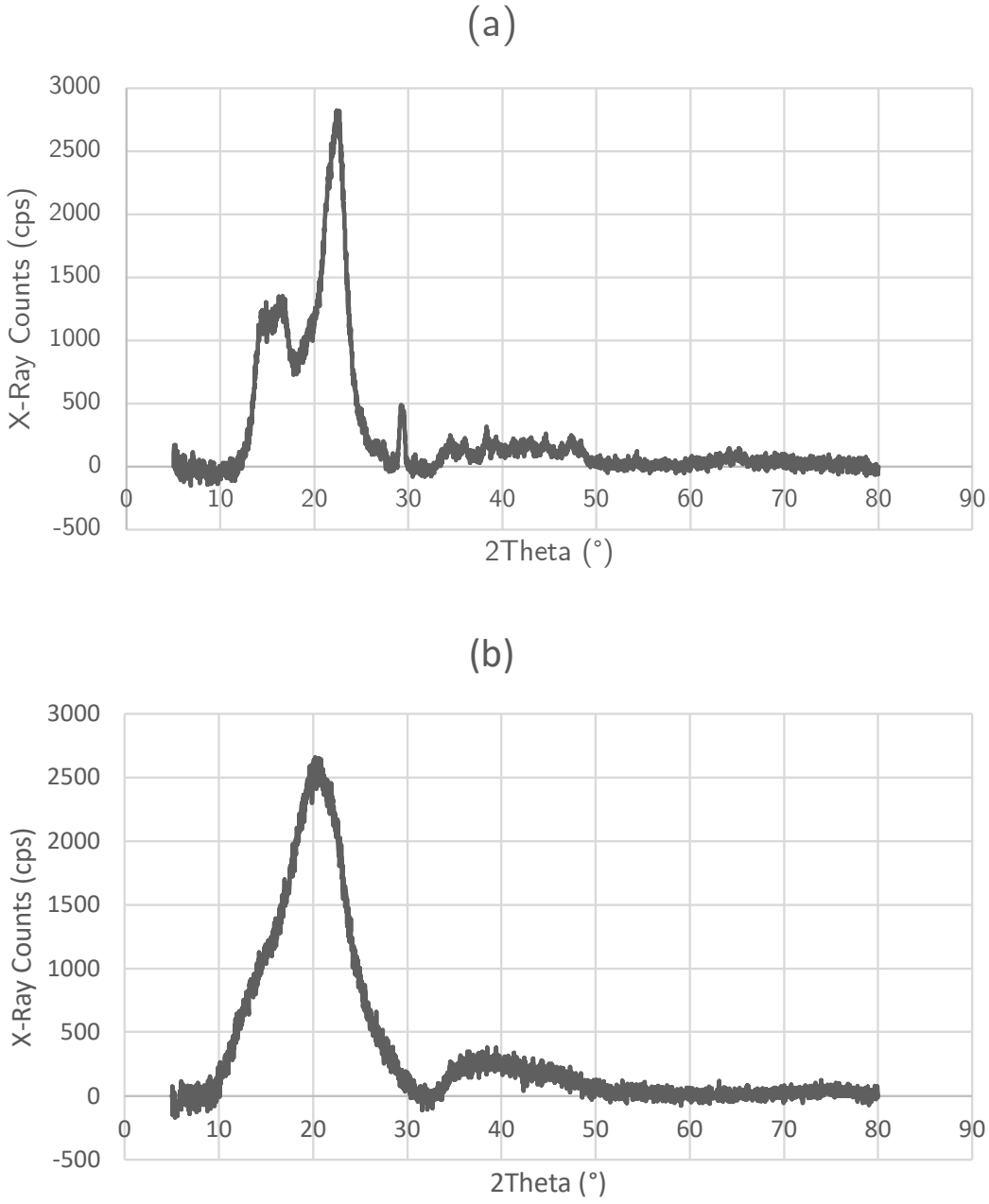

Figure 4-9:XRD Patterns of RNF (a) and Avicel PH-101 (b) after 24 hours of ball-milling.

A reduction in the number of peaks and a general broadening of existing peaks indicates that imperfections in the crystal structure of Avicel cellulose have been introduced.[23] A previous study that investigated the effect of ball-milling cellulose drew the same conclusion, with crystalline peaks decreasing in intensity when the duration of ball-milling is increased.[22] This is correlated with an increased conversion of the cellulose, which is also observed in the findings of this study with Avicel, however as previously mentioned, the hydrolysis performance of the RNF was not affected by this treatment.

Ball-milling results in a significant reduction in the crystallinity of Avicel from 86% to 54% after 24 hours of milling. This reduction correlates to an increased yield of glucose in the associated hydrolysis reaction. In contrast, the RNF's calculated crystallinity remains broadly similar, only decreasing from 69% to 66% after 24 hours of milling. This minimal reduction correlates with the glucose yield obtained from the RNF after ball-milling remaining constant.

4.2.4: Phosphoric Acid Re-generation

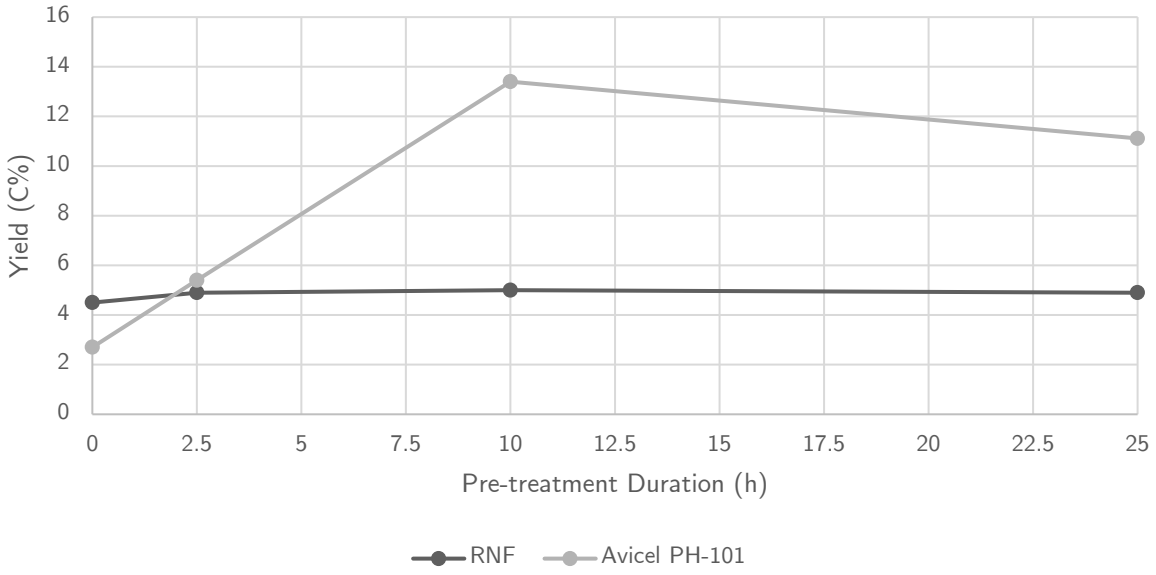

Time (h)	Glucose Yield (C%)	
	RNF	Avicel PH-101
0	4.5	2.7
2.5	4.9	5.4
10	5	14.4
25	4.9	11.1

Figure 4-10: Glucose yields obtained from the RNF and Avicel PH-101 after varying amounts of time in concentrated H3PO4.

The glucose yields obtained from both the RNF and Avicel PH-101 after H_3PO_4 treatments is shown in Figure 4-10. As with ball-milling, the treatment has no noticeable effect upon the RNF's hydrolysis performance. Conversely, as with ball-milling, the treatment improves Avicel's propensity for hydrolysis with treatments up to 10 hours in length. Beyond this time, its hydrolysis performance decreases slightly,

however this cannot be conclusively stated without repeating the experiments to determine the degree of error in the results.

As with ball-milling, X-Ray diffraction was employed to characterise the cellulosic components of both the RNF and Avicel PH-101 post-treatment, as shown in Figure 4-11.

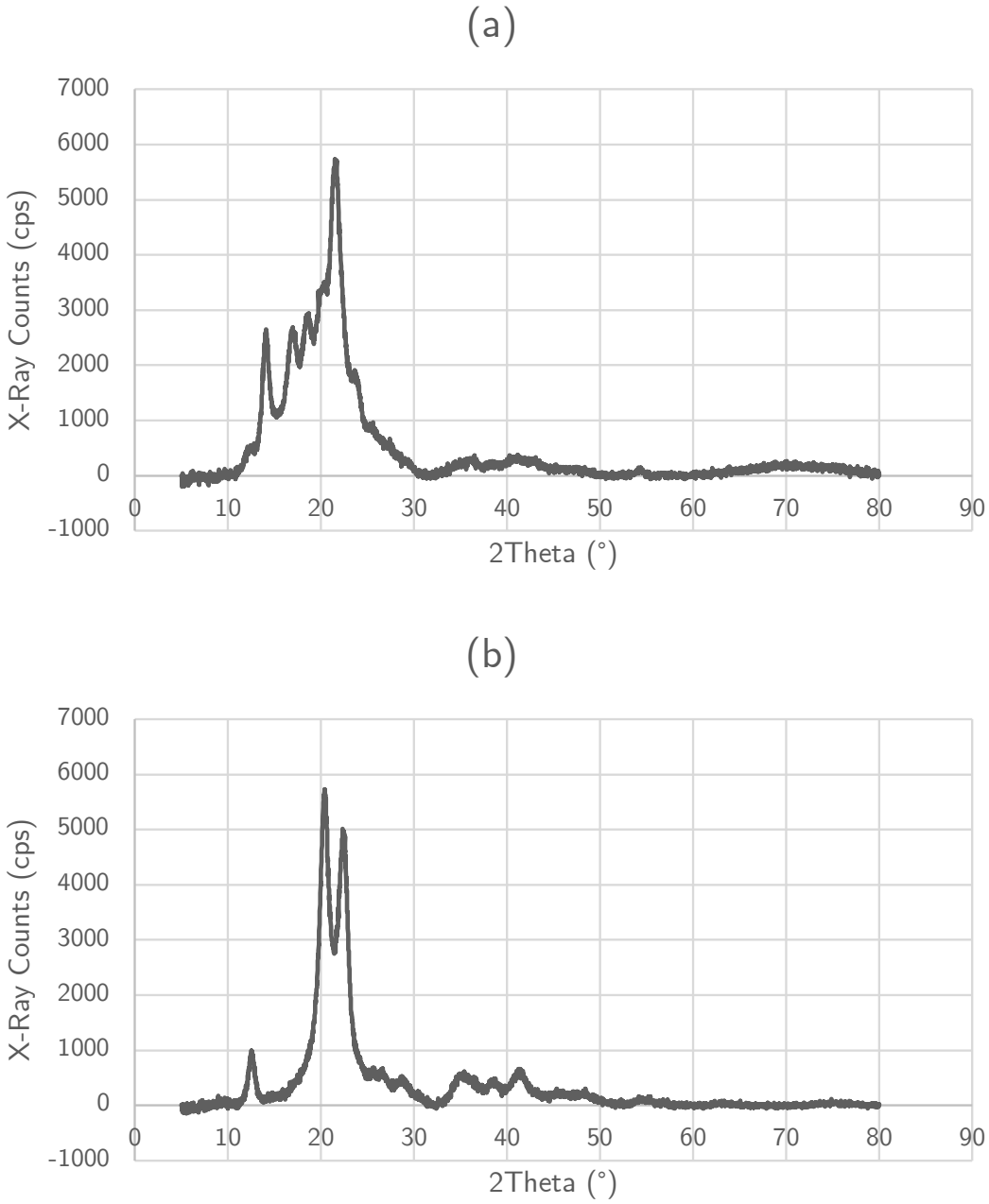

Figure 4-11: XRD Patterns of RNF (a) and Avicel PH-101 (b) after 10 hours of H_3PO_4 treatment.

After the H_3PO_4 treatment, both materials now display evidence of the presence of cellulose II, rather than just the RNF. It can be concluded that the pre-treatment converts some of the Avicel from cellulose I to cellulose II, however the extent of this conversion cannot be determined due to the limitations of Segal's XRD method. As previously mentioned in an earlier section of this chapter, cellulose II is considered to be more thermodynamically stable than cellulose I, however a study on the acidic hydrolysis of cellulose II conducted by Shibazaki *et al.* found that its degree of polymerisation decreased rapidly,[24] a reduction of which correlates to increased hydrolysis activity.[25] Further analysis of the cellulose obtained post-treatment, namely to determine its average degree of polymerisation, would determine the effectiveness of this pre-treatment for both the RNF and Avicel.

A possible explanation for the RNF's resistance to hydrolysis despite the use of these pre-treatments may be the presence of components within the material other than cellulose. It was not deemed necessary to attempt to separate the SAPs or hydrocarbon polymers prior to subsequent cellulose pre-treatment or hydrolysis reactions as they were not expected to interfere in the analysis of hydrolysates. However, this may not be the case. Both polyethylene and polypropylene are highly resistant to degradation in acidic environments; it can be considered a non-interfering component. In the case of the SAPs, research by Singh *et al.* determined that the primary products of sodium polyacrylate's thermal decomposition includes low molecular weight acids and aldehydes.[26] Although these compounds are structurally distinct from glucose, and would not produce any interfering peaks during quantitative analysis by HPLC, it may be the case that a certain portion of the glucose that is produced by the hydrolysis of cellulose reacts further with some of the products of sodium polyacrylate's decomposition. For this to be confirmed, a more comprehensive analysis of the compounds that are present after a hydrolysis reaction with the RNF would need to be carried out. Also, a series of hydrolysis experiments could be carried out where sodium polyacrylate is added to Avicel cellulose to determine if it is indeed their presence that is affecting the yield of glucose.

4.3: Conclusions and Future Works

In this chapter, the data from quantitative characterisation of the recycled nappy fibres using thermogravimetric analysis was presented, which identified the major components and their relative abundance within the material, these being cellulose, sodium polyacrylate and plastic films composed of hydrocarbon polymers. Cellulose was found to be the most abundant component of the RNF by weight, present in a significant quantity within the material at almost 40 wt.%. This draws a parallel with a typical source of lignocellulosic biomass, within which cellulose is usually the most abundant component.[27]

A series of cellulose hydrolysis reactions were carried out to determine the recycled nappy fibre material's potential to be upgraded to value-added products. In addition, two cellulose pre-treatment methods were applied to both the RNF and a reference cellulose, Avicel PH-101, to establish whether they significantly increased the yield of glucose obtained. Here, it was found that despite the significant quantity of cellulose present within the RNF, it was recalcitrant to the hydrolysis reactions, irrespective of whether it was pre-treated or not. It was suspected that this may be due to the other components within the RNF interfering in some manner, with a possible explanation being that the products of the thermal decomposition of RNF's superabsorbent polymers, namely sodium polyacrylate, were reacting with the glucose and producing unknown and unquantified side products. A more in-depth investigation into the compounds that are present in a post-hydrolysis reaction solution where RNF was used may shed some light on whether this is the case.

Both un-treated and treated samples of the RNF and Avicel PH-101 were characterized by X-Ray diffraction to obtain information on their polymorphic structures and crystallinity, as per Segal's method. Whilst this method is widely used, it provides little information on the physical properties of cellulose other than an estimation of the relative abundance of crystalline domains. A value for cellulose's average degree of polymerisation within each sample would be insightful, as it is strongly correlated to its hydrolysis performance. Gel-polymerisation chromatography, as carried out by

Hubbell and Ragauskas on their cellulose samples, is the preferred method,[28] and future work in this area would incorporate this technique for characterising the RNF pre and post treatment.

4.4: References

1 P. Lanzafame, D. M. Temi, S. Perathoner, A. N. Spadaro and G. Centi, in *Catalysis Today*, Elsevier, 2012, vol. 179, pp. 178–184.

2 S. Suganuma, K. Nakajima, M. Kitano, D. Yamaguchi, H. Kato, S. Hayashi and M. Hara, *Solid State Sci.*, 2010, **12**, 1029–1034.

3 G. Gliozzi, A. Innorta, A. Mancini, R. Bortolo, C. Perego, M. Ricci and F. Cavani, *Appl. Catal. B Environ.*, 2014, **145**, 24–33.

4 Q. Yang and X. Pan, *Bioenergy Res.*, 2016, **9**, 578–586.

5 K. Tsigkou, P. Tsafrakidou, D. Zagklis, A. Panagiotouros, D. Sionakidis, D. M. Zontos, C. Zafiri and M. Kornaros, *Renew. Energy*, 2021, **165**, 109–117.

6 A. Khanyile, G. C. Caws, S. L. Nkomo and N. M. Mkhize, *Detritus*, 2020, **9**, 138–149.

7 F. Horkay, P. J. Basser, A.-M. Hecht and E. Geissler, *Spec. Issue Artic. Proc IMechE Part H J Eng. Med.*, 2015, **229**, 895–904.

8 F. Horkay, I. Tasaki and P. J. Basser, *Biomacromolecules*, 2000, **1**, 84–90.

9 A. Hüttermann, L. J. B. Orikiriza and H. Agaba, *Clean - Soil, Air, Water*, 2009, **37**, 517–526.

10 M. J. Zohuriaan-Mehr, H. Omidian, S. Doroudiani and K. Kabiri, *J. Mater. Sci.*, 2010, **45**, 5711–5735.

11 Y. Wang, S. Agarwal, A. Kloekhorst and H. J. Heeres, *ChemSusChem*, , DOI:10.1002/cssc.201600551.

12 I. Van Zandvoort, Y. Wang, C. B. Rasrendra, E. R. H. Van Eck, P. C. A. Bruijnincx, H. J. Heeres and B. M. Weckhuysen, *ChemSusChem*, 2013, **6**, 1745–1758.

13 Z. Xu, Y. Yang, P. Yan, Z. Xia, X. Liu and Z. C. Zhang, *RSC Adv.*, 2020, **10**,

34732–34737.

14 X. Hu, C. Lievens, A. Larcher and C. Z. Li, *Bioresour. Technol.*, 2011, **102**, 10104–10113.

15 S. Pérez and D. Samain, *Structure and Engineering of Celluloses*, 2010, vol. 64.

16 R. C. R. Nunes, *Rubber nanocomposites with nanocellulose*, Elsevier Ltd, 2017.

17 A. D. French and M. Santiago Cintrón, *Cellulose*, 2013, **20**, 583–588.

18 J. Zhang, B. Zhang, J. Zhang, L. Lin, S. Liu and P. Ouyang, *Biotechnol. Adv.*, 2010, **28**, 613–619.

19 C. Trilokesh, P. Bavadharani, M. Mahapriyadarshini, R. Janani and K. B. Uppuluri, *Waste and Biomass Valorization*, 2021, **12**, 4299–4306.

20 C. Trilokesh, P. Bavadharani, M. Mahapriyadarshini, R. Janani and K. B. Uppuluri, *Waste and Biomass Valorization*, 2021, **12**, 4299–4306.

21 T. Komanoya, H. Kobayashi, K. Hara, W. J. Chun and A. Fukuoka, *Appl. Catal. A Gen.*, 2011, **407**, 188–194.

22 Y. Yu and H. Wu, *AIChE J.*, 2011, **57**, 793–800.

23 T. Ungár, *Scr. Mater.*, 2004, **51**, 777–781.

24 H. Shibazaki, S. Kuga, F. Onabe and R. M. Brown, *Polymer (Guildf).*, 1995, **36**, 4971–4976.

25 J. Ni, N. Teng, H. Chen, J. Wang, J. Zhu and H. Na, *Bioresour. Technol.*, 2015, **191**, 229–233.

26 R. K. Singh, D. K. Shrivastava, A. Sarkar and J. P. Chakraborty, *Fuel*, , DOI:10.1016/j.fuel.2020.118115.

27 M. Carrier, A. Loppinet-Serani, D. Denux, J. M. Lasnier, F. Ham-Pichavant, F. Cansell and C. Aymonier, *Biomass and Bioenergy*, 2011, **35**, 298–307.

28 C. A. Hubbell and A. J. Ragauskas, *Bioresour. Technol.*, 2010, **101**, 7410–7415.

5: Ruthenium Catalysts for Biomass Conversion

5.1: Introduction

This chapter investigates the use of supported ruthenium catalysts for the conversion of cellulose to sorbitol directly, and to convert two of the products of its hydrolysis, glucose and levulinic acid, into their hydrogenates, sorbitol and γ-valerolactone, respectively. Figure 5-1 shows the reaction pathway that proceeds to obtain sorbitol from cellulose.

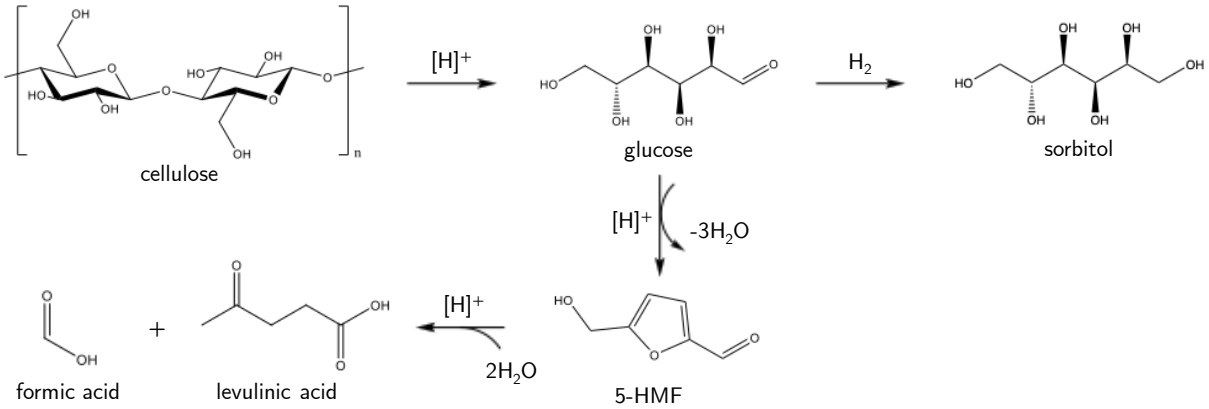

Figure 5-1: A simplified chemical conversion pathway for cellulose, with detail on its hydrogenation into sorbitol from its primary hydrolysate, glucose.

As part of this investigation, the recycled nappy fibres that were characterised as part of Chapter 4 were evaluated to determine their response towards conversion into sorbitol as a real-world cellulose source, with a view to evaluate the plausibility of using the RNF as a "renewable" chemical feedstock. Investigations conducted in Chapter 4 established that the recycled nappy fibres can be used as a feedstock for a typical cellulose hydrolysis process, albeit with unforeseen complications, therefore it was considered pertinent to establish whether they would also be a viable feedstock for a one-pot hydrogenolysis reaction.

A low-energy approach was developed to synthesise the catalysts for this chapter of the study. The microwave-assisted solvothermal method that is used throughout this study for catalyst synthesis has been introduced and discussed in Chapter 2. In short, it is possible to produce a wide variety of heterogeneous supported-metal catalysts in

a one-pot process with the use of polyols, which function as both the solvent for the metal precursor and as a reducing agent for the deposition of their metals at elevated temperatures. There are several polyols that can be used for this purpose. Ethylene glycol is a commonly used polyol for the synthesis of supported metal catalysts in previous literature and is what was selected as the polyol for syntheses in this chapter. Other examples include isopropanol, 1,3-propane diol, 1,5-butane diol and propylene glycol for various solvothermal preparations.[1–6]

After filtration, washing, and drying, the resulting catalyst is ready to use without the need for any additional heat or reducing treatments as it has been reduced *in-situ*, significantly reducing the amount of time and energy taken to produce a catalyst when compared to a more conventional synthesis, such as by an impregnation or sol-gel method.

5.1.1: Cellulose & Glucose to Sorbitol

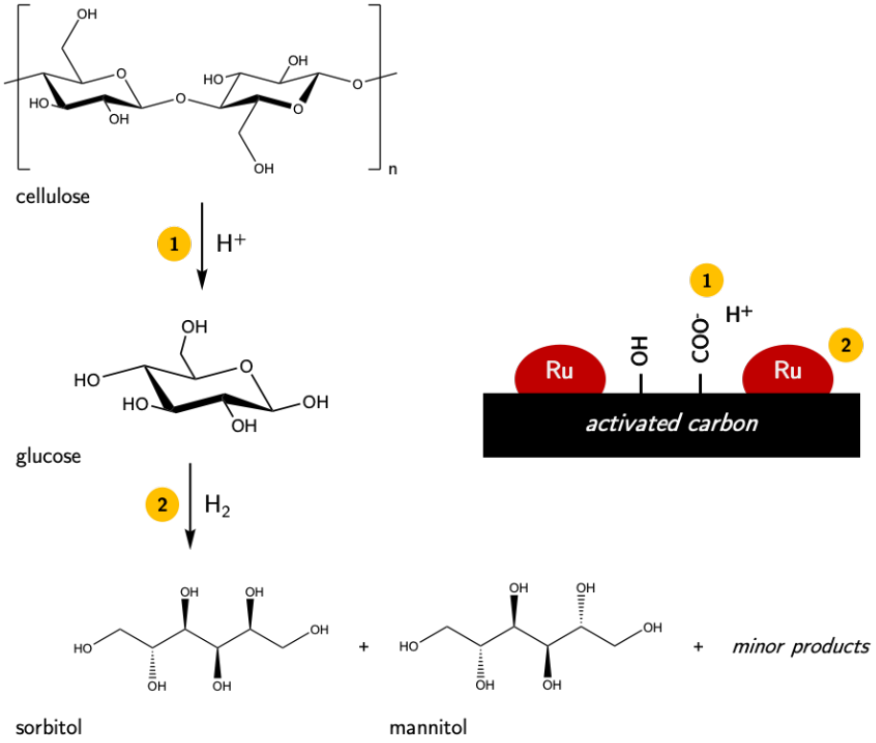

Figure 5-2: A simplified reaction pathway for cellulose hydrogenolysis to sorbitol and other minor products over a typical Ru/C catalyst. Cellulose hydrolysis is a necessary first step prior to the formation of sorbitol, which takes place hydrothermally or via acidic functional groups on the surface of the carbon support (1). Hydrogenation of the reducing sugars then takes place via the ruthenium active site (2).

Sorbitol has been identified as one of the twelve most promising 'building block' chemicals that can be produced in biomass conversion processes.[7] When subjected to elevated temperatures in the presence of an acidic and reducing environment, cellulose undergoes hydrolysis to its monomer, glucose, then hydrogenates to sorbitol at a far greater rate than the initial hydrolysis. This results in a high selectivity to sorbitol and minimises the formation of unwanted side products, namely humins.[8] Activated-carbon supported ruthenium has been shown in previous research to be consistently the most active catalyst type for both the direct conversion of cellulose to sorbitol and the conversion of glucose to sorbitol alone.[8–10] For this reason, synthesis and testing predominantly focused on Ru/C catalysts, however some testing took place with Ru/TiO_2 for comparison. The influence of the carbon support material's surface area on catalytic activity was investigated. Two commercially available activated carbons were chosen as the supports: Vulcan XC72R and Vulcan Black Pearls 2000. These two

activated carbons were chosen as they are both from the same manufacturer, Cabot, and are both placed into the same category of intended use by the manufacturer.[11] The differences between them that were investigated are the surface area and their stated purity; Black Pearls 2000 is designed to have a very high surface area (literature value = 1374 m^2/g)[12]. XC72R's surface area is lower (literature value = 222 m^2/g)[13] and according to the manufacturer also contains lower levels of impurities and contaminants.

The parameters used for catalyst synthesis and testing were drawn and modified from a previous investigation of the polyol method by Howe *et al.*,[14] in which it was shown that the modification of catalyst synthesis parameters, primarily the temperature and duration of the synthesis, the choice of metal precursor, and the choice of polyol solvent, has a significant effect upon their performance and characterizable properties. Aside from initial tests to determine the RNF's viability as a substrate for hydrogenolysis reactions as-received, glucose was used as the substrate for catalyst testing in this section. Due to time constraints, along with the lack of an established experimental procedure in place for measuring the surface acidity of activated carbon, it was decided to focus on obtaining a greater understanding of the Ru/C catalysts as hydrogenation catalysts rather than focussing on their ability to hydrolyse cellulose. There were no attempts to modify the properties of their activated carbon supports in aid of its hydrolysis, such as their acidity or the type of acidic functional groups on their surfaces. The complete list of parameters that were modified are shown in Table 5-1.

Parameter	Range(s)
Precursor Type	- $Ru(acac)_3$ - $RuCl_3$
Support Type	- Vulcan XC72R - Vulcan Black Pearls 2000 - Degussa P25 TiO_2
Synthesis Time	- 5, 10 and 15 minutes
Synthesis Temperature	- 150, 175 and 200°C

Table 5-1: The synthesis parameters for Ru catalysts prepared for cellulose/glucose conversion.

5.1.2: Levulinic Acid to γ-Valerolactone

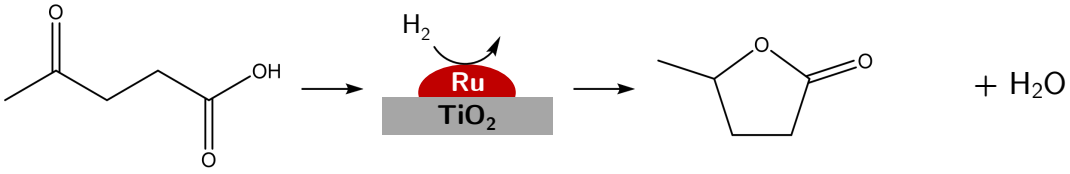

Figure 5-3: Illustrated schematic of levulinic acid hydrogenation over Ru/TiO_2 catalysts.

For a seamless transition to a renewables-based petrochemical industry, where existing infrastructure can be utilised without extensive and costly modifications, the selective conversion of cellulosic biomass to compounds with fewer oxygenated groups is essential.[15] One such compound is levulinic acid (5-oxopentanoic acid). It is used to produce a wide range of valuable chemicals, such as herbicides and acrylate polymers. The product of levulinic acid's hydrogenation, γ-valerolactone (GVL), stands out itself as a useful and versatile compound. If its large-scale production can be feasibly achieved from bio-derived feedstocks, it could find uses as an additive to improve the octane rating of biofuels, as a solvent that is safe easy to transport, and as a platform molecule for the production of a wide range of fine chemicals.[16,17]

The hydrogenation of levulinic acid is readily performed over a range of supported metal catalysts, though ruthenium-based catalysts typically outperform other types in comparative studies.[18] Within the CCI, the Edwards group decided to investigate the performance of a series of Ru/TiO_2 catalysts synthesised by the microwave-assisted

polyol method for the hydrogenation of LA to GVL in a batch reactor process. The list of catalyst synthesis parameters that were modified are shown in Table 5-2:

Parameter	Range(s)
Precursor Type	- $Ru(acac)_3$ - $RuCl_3$
Support Type	- Degussa P25 TiO_2
Synthesis Time	- 5, 10 and 15 minutes
Synthesis Temperature	- 150, 175 and 200°C

Table 5-2: Catalyst synthesis variables and their associated ranges.

5.2: Results and Discussion

5.2.1: Catalyst Testing

5.2.1.1: Cellulose Hydrogenolysis with Ru/C Catalysts

Samples of the RNF and Avicel PH-101 were subjected to the testing procedure outlined in Chapter 3, section 3.4.3. The results of this are shown in Figure 5-4. Briefly, 50 mg of a selected, active, Ru/C catalyst and 162 mg of either Avicel PH-101 cellulose or RNF were added to a Teflon-lined reaction vessel in a stirred autoclave reactor along with 20 mL deionised water. The vessel was sealed, then the reactor charged with 10 bar of H_2. The reaction mixture was heated to 170°C before the reaction commenced for 24 hours. An aliquot of the post-reaction solution was then drawn and analysed using HPLC.

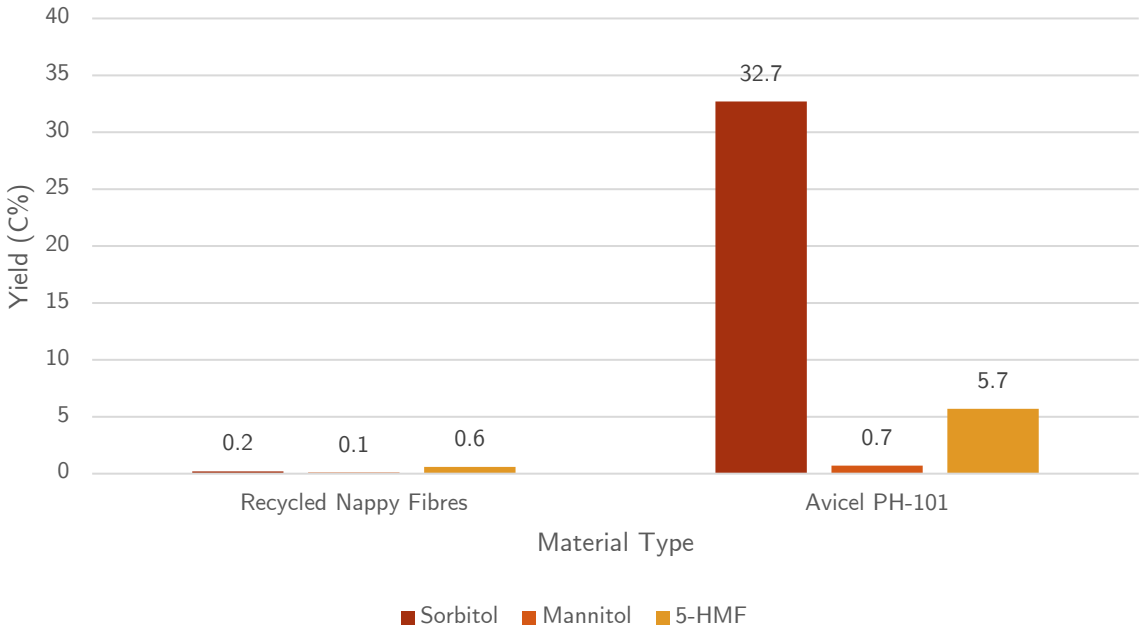

Figure 5-4: Yield of quantifiable products arising from the hydrogenolysis of RNF and Avicel PH-101 using 1%Ru(acac)/XC72R 175-15. Reaction conditions: 50 mg catalyst, 162 mg RNF or Avicel PH-101, 20 mL DI H_2O, 170°C, 10 bar H_2, 24h.

The difference in catalytic activity from both materials is significant. Avicel produced a 32.7% yield of sorbitol after 24 h, however when the RNF was used, only a negligible quantity of it was detected (0.2%). It is also of note that a quantifiable amount of 5-HMF was produced in both instances. When Avicel PH-101 was used as the substrate,

a 5.7% yield of 5-HMF was detected in the reaction mixture. A very low amount was detected in the case of the RNF, at 0.6%. The presence of HMF is an indication that despite the rapid rate of the glucose hydrogenation reaction, a certain degree of acidic dehydration of glucose also takes place, likely due to a combination of the catalyst's acidity, the high reaction temperature and long reaction duration. The presence of HMF in the post-reaction mixture was an expected finding. Kusserow *et al.* list it as one of the major products of a cellulose/glucose hydrogenation process at elevated temperatures.[10]

The cause of the discrepancy in activity between the two materials was investigated. It has been previously reported that the presence of chlorides in a reaction mixture can poison ruthenium catalysts in certain circumstances.[19] NappiCycle disclosed that there was a presence of residual $CaCl_2$ within the nappy fibres as a result of their deactivation process, therefore an investigation was carried out to establish whether this was having a detrimental effect.

A series of reactions were conducted, with glucose as the substrate, where the concentration of calcium chloride within the solution was varied from 0-10 wt.% to investigate the effect of an increased concentration of $CaCl_2$ within the reaction mixture. The results of this are seen in Figure 5-5. Briefly, 50 mg of a selected Ru/C catalyst and 162 mg of D-glucose (8.1 g/L in solution) were added to a Teflon-lined reaction vessel in a stirred autoclave reactor along with 20 mL deionised water. The vessel was sealed, then the reactor was charged with 10 bar of H_2. The reaction mixture was heated to 170°C before the reaction commenced for 0.5 hours. An aliquot of the post-reaction solution was then drawn and analysed using HPLC.

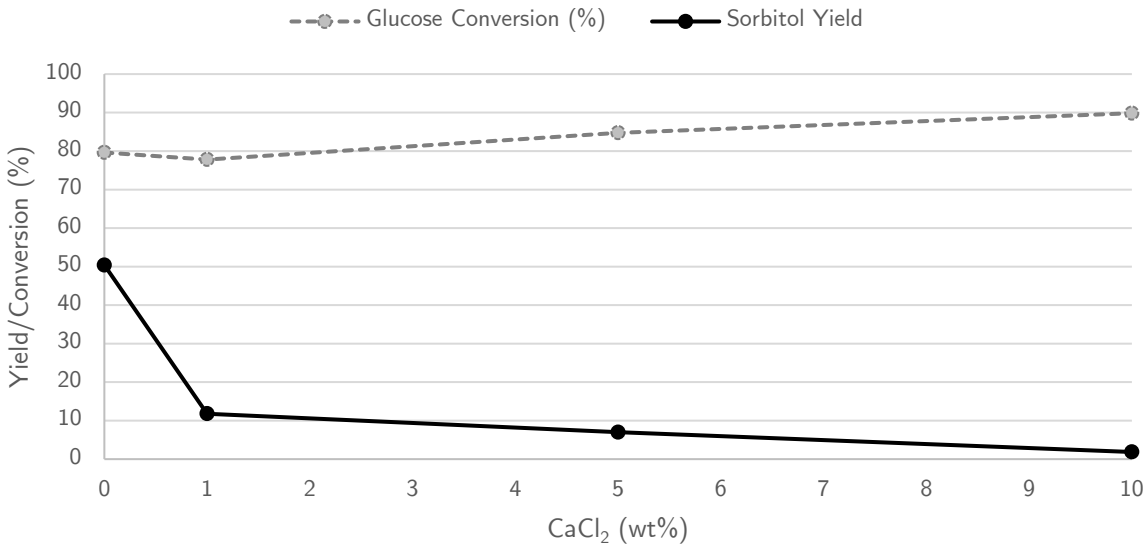

$CaCl_2$ (wt.%)	Glucose Conversion (%)	Sorbitol Yield (%)
0	79.6	50.4
1	77.8	11.8
5	85.8	7.0
10	89.8	1.9

Figure 5-5: The effect of increasing the amount of $CaCl_2$ in a glucose hydrogenation reaction. Reaction conditions: 50 mg catalyst (1%Ru(Cl)/XC72R 150-5), 162 mg D-glucose in 20 mL DI H_2O (8.1 g/L), 170 °C, 10 bar H_2, 0.5h.

The addition of calcium chloride detrimentally affected the activity of catalyst with regards to the yield of sorbitol. The most prominent reduction occurred after the introduction of the lowest concentration of $CaCl_2$, with the yield of sorbitol decreasing from 50.4% to 11.8% with no other changes to the reaction parameters. Sorbitol yield gradually decreased further as the concentration of $CaCl_2$ in the reaction solution was increased. This result indicates that its presence in the nappy fibres is at least partially responsible for the lack of hydrogenation activity observed when using it as the feedstock for the hydrogenolysis reaction in the previous section.

The effect of having chlorides present in solution upon the activity of a catalyst is dependent on the catalyst type and the reaction that is catalysed. For example, it had a promotional effect when added to a Li^+-MgO catalyst in Wang *et al.*'s study on the oxidative dehydrogenation of ethane,[20] however, it is a poison for Ni -based steam

reforming catalysts in Richardson *et al.*'s work.[21] Previous literature that specifically investigates the effect of chlorides upon the performance of supported ruthenium catalysts is predominantly in the context of ammonia synthesis.[22–24] Mieth and Schwarz concluded that the dispersion of ruthenium upon the support's surface is the most significant factor. Catalysts with a high dispersion of ruthenium were poisoned by the presence of chloride, whereas a promotional effect was observed when the dispersion was low.[19] It was noted in this study that the binding of chlorides to ruthenium particles is influenced by the particle's size and the acidity of the support material; in their case, aluminium oxide. Future work in this area should focus on determining if varying the dispersion of ruthenium and the acidity of the carbon support or reaction solution could induce and promote the production of sorbitol from the RNF material in hydrogenolysis reactions without prior treatment to remove residual $CaCl_2$. An analysis of the exact quantity of chloride present in the RNF material itself would also be beneficial to this investigation. A titration method for determining the concentration of chlorides in an aqueous solution was investigated,[25] as well as methods to remove chlorides,[26,27] however due to time constraints, these could not be carried out on the recycled nappy fibres. Future work should also investigate chloride detection and removal methods in more detail.

Despite the drop in sorbitol yield, glucose conversion remained very high as $CaCl_2$ concentration was increased. It was suspected that this was due to the dehydration of cellulose hydrolysates to levulinic acid, formic acid, and 5-HMF, facilitated by the acidic functional groups of the activated carbon support. However, no measurable concentration of these products was observed. One possible explanation considers that there is an absence of oxygen in the reaction environment. When glucose undergoes enzymatic anaerobic digestion it produces gaseous products, namely carbon dioxide, methane and hydrogen, by acidogenesis.[28,29] Future work in this area would therefore focus on the analysis of the reaction gases in order to detect and quantify any gaseous products that may be being produced during these reactions to account for the discrepancy between yield and conversion.

5.2.1.2: Glucose Hydrogenation with Ru/C Catalysts: Time-on-line Study

Ideal reaction parameters to use for glucose hydrogenations was established prior to extensive modifications to catalyst synthesis parameters. To achieve this, a series of 1 wt.% Ru(acac)/XC72R catalysts were synthesised at three temperatures, then each were tested at three reaction times, with all other parameters remaining constant. The results of this investigation are shown in Figure 5-6.

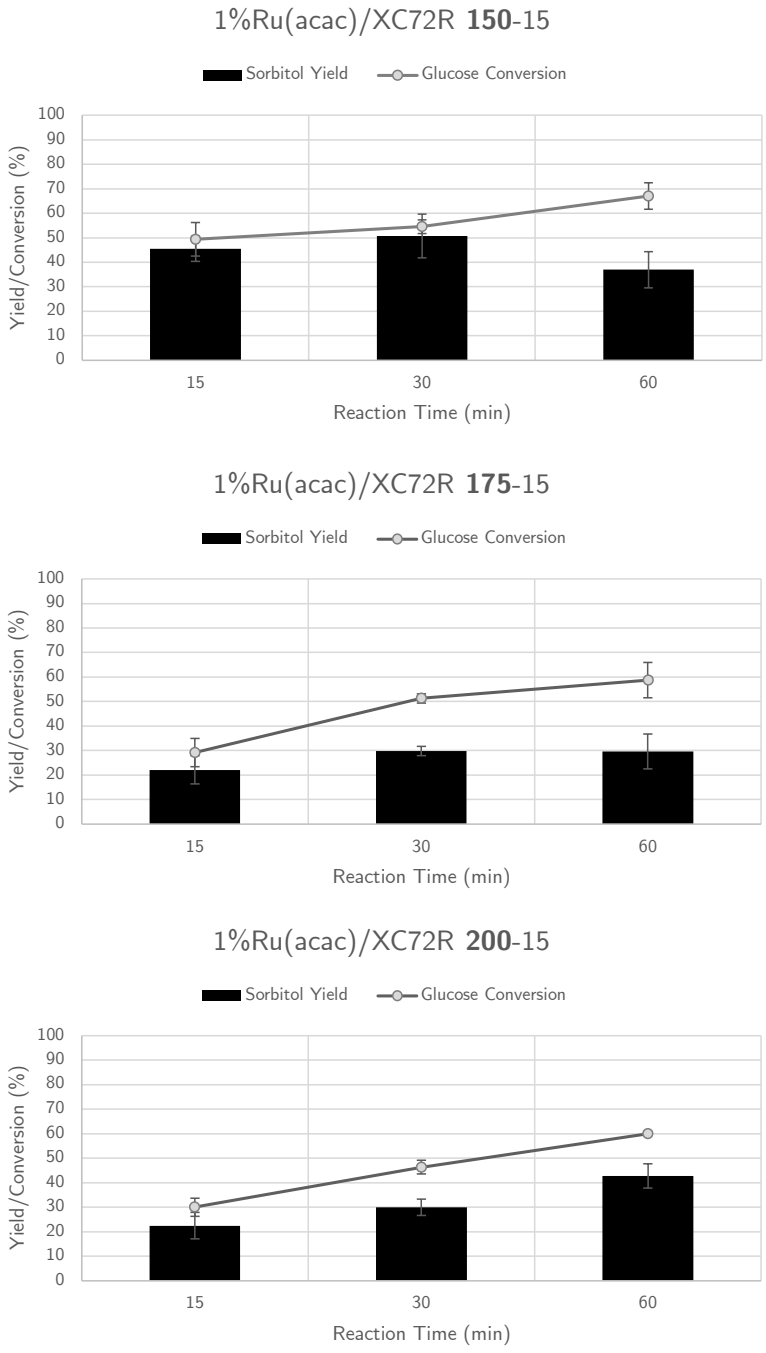

Figure 5-6: Graphis of the yield/conversion data obtained from glucose hydrogenation time-on-line experiments.

Catalyst	Reaction Time (min)	Glucose Conversion (C%)	Sorbitol Yield (C%)
1%Ru(acac)/XC72R 150-15	15	49.4	45.5
	30	55.6	50.7
	60	67.1	37.0
1%Ru(acac)/XC72R 175-15	15	29.2	22.1
	30	51.3	29.8
	60	58.8	29.6
1%Ru(acac)/XC72R 200-15	15	30.0	22.4
	30	46.3	30.0
	60	60.0	42.8

Table 5-2: Tabular data of the yield/conversion data obtained from glucose hydrogenation time-on-line experiments.

The catalyst prepared at the lowest synthesis temperature (150 °C) was the most active overall, with the greatest yield of sorbitol obtained after 30 minutes, at 50.7%. The two other catalysts, prepared at 175 °C and 200 °C had a comparable activity towards the production of sorbitol after 15 and 30 minutes. The 200 °C produced the most sorbitol after 1 hour on average, however due to the amount of experimental error, this cannot be conclusively stated. Significant quantities of sorbitol were produced by many of the catalysts, even at the shortest reaction time of 15 minutes. Glucose conversion correlates well with the yield of sorbitol at the shorter reaction times of 15 and 30 minutes, however the catalysts become less selective as the reaction time is increased to 60 minutes, most evidently in the catalysts prepared at 150 °C and 175 °C. Except for the catalyst prepared at 200 °C, the yield of sorbitol obtained does not increase as the reaction time is increased from 30 minutes to 60 minutes, rather it plateaus, or in the case of the catalyst prepared at 150 °C, decreases. As glucose conversion always increases with an increase in reaction time, this indicates the formation of unquantified side products as the reaction progresses. Kusserow *et al.*'s reaction network for the hydrogenation of glucose, as previously discussed in Chapter 2, contains a variety of other products that can be obtained from the reaction, including various aldehydes and maltitol, the hydrogenated dimer of glucose. Future work in this area would focus on a complete quantification of the products obtained during this reaction.

Based on the data, a 30-minute reaction time was decided upon for future reactions for glucose to sorbitol conversions to provide the most suitable balance between glucose conversion, sorbitol yield and time efficiency.

5.2.1.3: Glucose Hydrogenation with Ru/C Catalysts: Catalyst Synthesis Parameters

After the initial tests for determining the optimal reaction time, the main series of experiments were conducted where a more complete set of catalyst synthesis variables were modified. The results of these are shown in Figure 5-7.

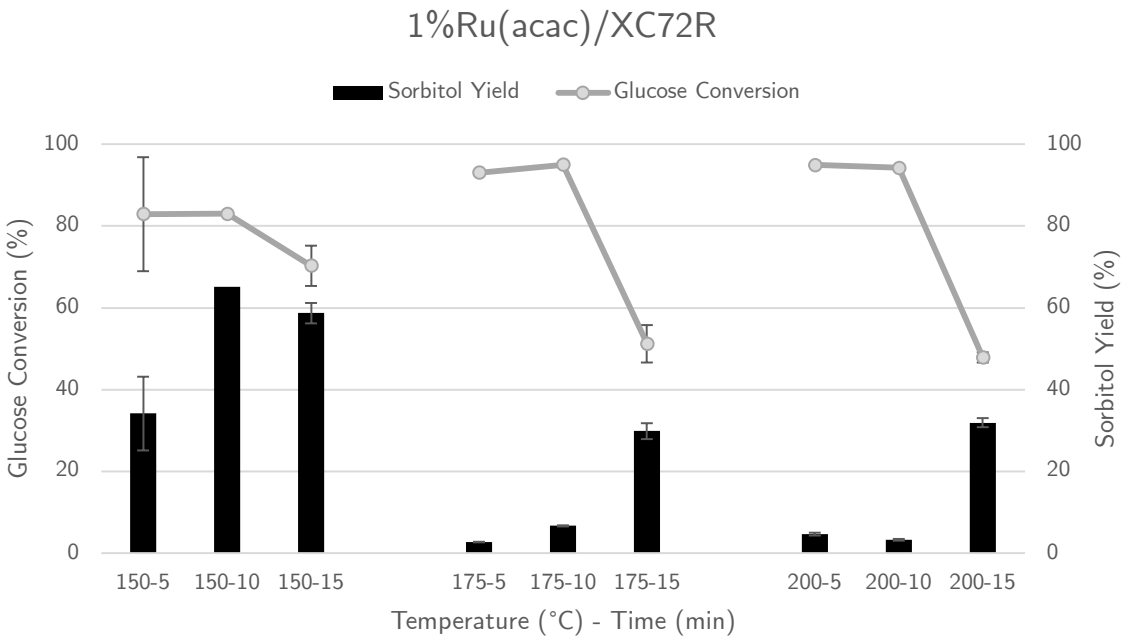
1%Ru(acac)/XC72R
Sorbitol Yield
Glucose Conversion
Glucose Conversion (%)
Sorbitol Yield (%)
0
20
40
60
80
100
150-5
150-10
150-15
175-5
175-10
175-15
200-5
200-10
200-15
Temperature (°C) - Time (min)

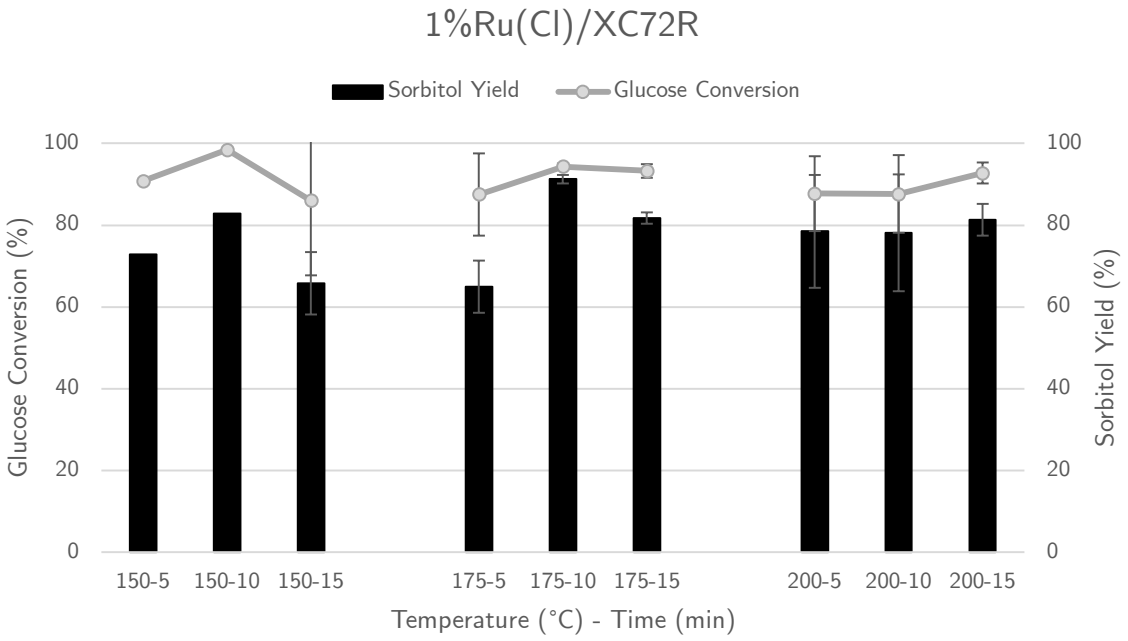
1%Ru(Cl)/XC72R
Sorbitol Yield
Glucose Conversion
Glucose Conversion (%)
Sorbitol Yield (%)
0
20
40
60
80
100
150-5
150-10
150-15
175-5
175-10
175-15
200-5
200-10
200-15
Temperature (°C) - Time (min)

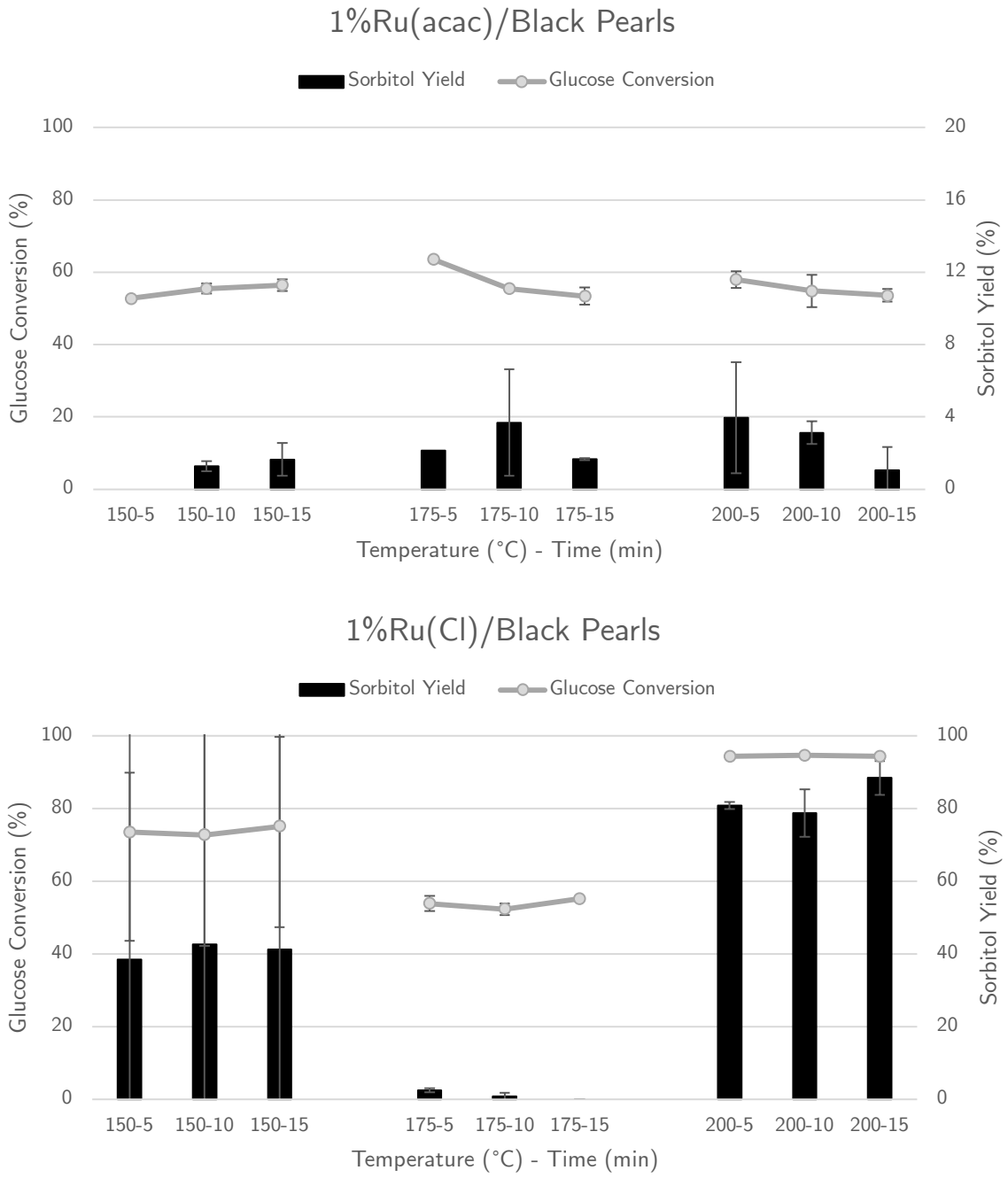

Figure 5-7: Glucose hydrogenation screening data for Ru/C catalysts. Reaction parameters: 50 mg catalyst, 162 mg D-glucose (8.1g/L), 20 mL DI H_2O, 170 ℃, 10 bar H_2, 0.5 h.

1%Ru(acac) /XC72R	Cellulose Conversion (%)	Sorbitol Yield (%)	1%Ru(Cl) /XC72R	Cellulose Conversion (%)	Sorbitol Yield (%)
150-5	82.9	35.1	*150-5*	90.8	72.9
150-10	83.0	65.2	*150-10*	98.4	82.8
150-15	70.3	58.8	*150-15*	86.0	65.8
175-5	93.1	2.8	*175-5*	87.5	65.0
175-10	95.0	6.7	*175-10*	95.4	91.2
175-15	51.3	29.9	*175-15*	93.3	81.8
200-5	95.9	5.7	*200-5*	87.7	78.5
200-10	95.3	3.4	*200-10*	87.6	78.1
200-15	47.9	31.9	*200-15*	92.8	81.3
1%Ru(acac) /BP	**Cellulose Conversion (%)**	**Sorbitol Yield (%)**	**1%Ru(Cl)/ BP**	**Cellulose Conversion (%)**	**Sorbitol Yield (%)**
150-5	52.8	0.0	*150-5*	73.5	38.5
150-10	55.5	1.3	*150-10*	72.7	42.6
150-15	56.4	1.6	*150-15*	75.1	41.3
175-5	63.6	2.1	*175-5*	53.8	2.5
175-10	55.5	3.7	*175-10*	52.3	0.7
175-15	53.4	1.7	*175-15*	55.1	0.0
200-5	58.0	5.0	*200-5*	95.3	80.8
200-10	55.9	3.1	*200-10*	95.5	78.7
200-15	53.6	1.0	*200-15*	95.3	88.4

Table 5-3: Tabular data of the yield/conversion data obtained from glucose hydrogenation screening experiments with Ru/C catalysts.

The catalysts that were prepared with $Ru(acac)_3$ were less active overall when compared with those prepared with $RuCl_3$, with a notable exception being those prepared at the lowest synthesis temperature using XC72R carbon. The XC72-supported catalysts prepared using $RuCl_3$ were the most active set of catalysts. The most active catalyst of the series was 1%Ru(Cl)/XC72R 175-10, achieving a sorbitol yield of 91.2%.

In some experimental runs the degree of error is very large, the notable case being the 1%Ru(Cl)/BP 150-x catalysts. This error could not be reduced, despite efforts to do so. These included re-synthesising the catalysts, thoroughly cleaning the reactor apparatus and ensuring that all apparatus that was used during the synthesis and

testing procedures were free of contaminants. A possible reason was found during XPS analysis of the Ru/C catalysts; a significant presence of sulphur was detected on some samples. This is discussed further in section 5.2.2.3.1.

Correlations can be drawn between the yield/conversion obtained and catalyst synthesis variables when these are isolated, as shown in Figure 5-8.

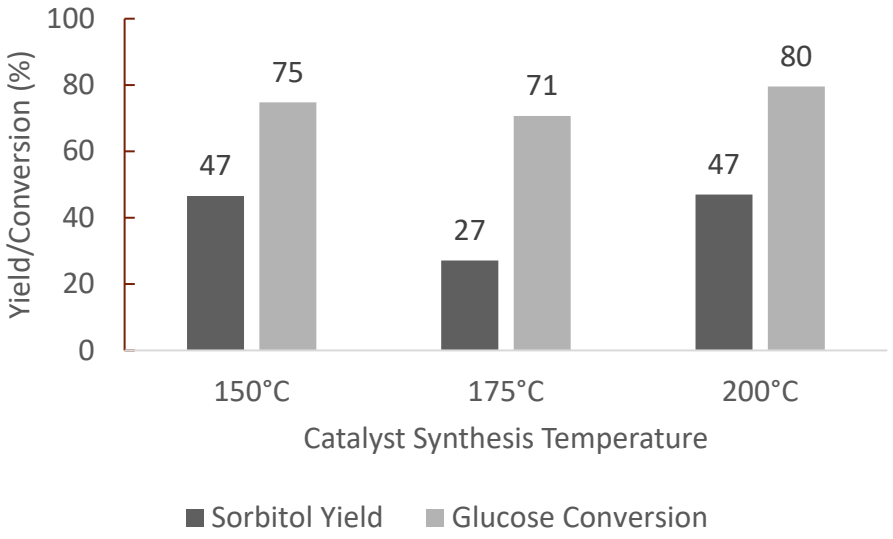

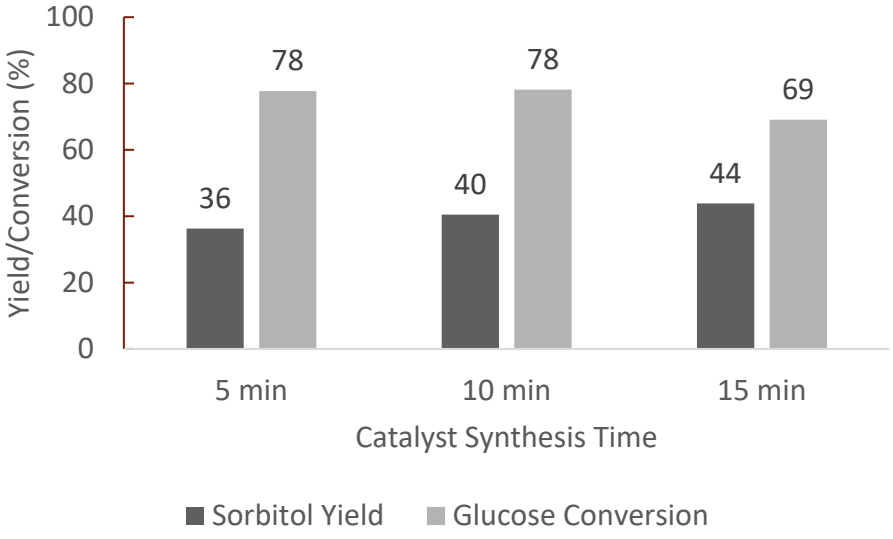

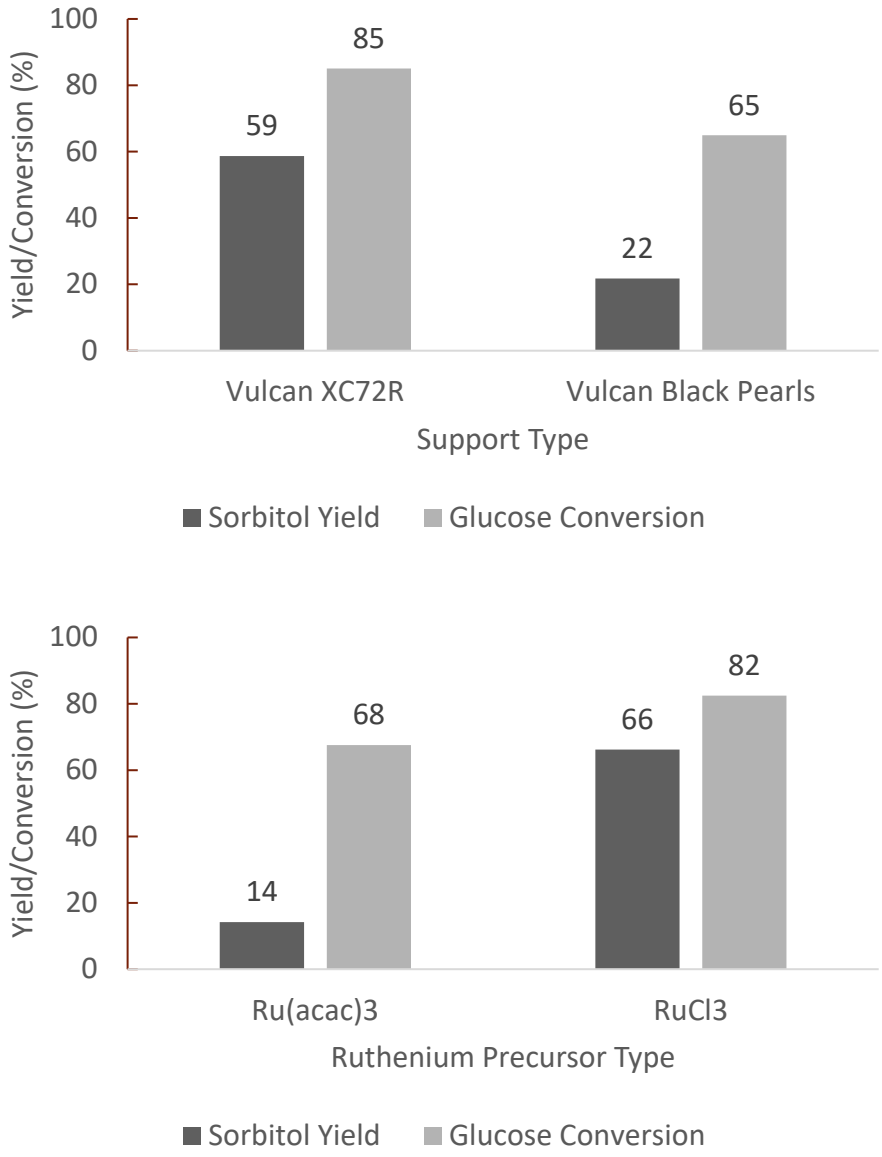

Figure 5-8: Plots of average yield/conversion values from the Ru/C catalysts, isolated by each catalyst synthesis parameter. The averaged value is displayed above each bar, separated by sorbitol yield and glucose conversion.

A longer preparation time has a beneficial effect on the average sorbitol yield. An XC72R-based catalyst is more likely to be the more active type to produce sorbitol than its Black Pearls 2000 equivalent. Catalysts that were synthesised using $RuCl_3$ as the precursor are more consistently active than those synthesised using $Ru(acac)_3$. As observed during the time-on-line experiments, catalysts prepared at the lowest preparation temperature and time are about as active as those prepared at the highest. It has been suggested in previous literature on solvothermally prepared catalysts that shorter synthesis times are beneficial, as it prevents the agglomeration of deposited

nanoparticles.[14] Nanoparticle formation using this catalyst synthesis method occurs rapidly, with Chen *et al.*'s solvothermally prepared Pt/C and Ru/C catalysts taking just 50 seconds to synthesise, as previously mentioned in chapter 2.[3] What appears to influence catalytic activity to a greater extent in this instance is its synthesis time rather than its temperature. An investigation into the effect that catalyst synthesis time has upon nanoparticle formation is presented in a subsequent section of this chapter (5.2.2.4). This may explain the increased activity of catalysts prepared at lower temperatures.

Some of the catalysts that were prepared using $Ru(acac)_3$ were moderately active, with the most active being 1%Ru(acac)/XC72R 150-10, achieving a sorbitol yield of 65.2%, however many of them were inactive, such as 1%Ru/XC72R 175-5, which achieved just 2.8% yield of sorbitol. As was observed during the investigation into the incremental addition of $CaCl_2$ to a glucose hydrogenation catalyst in section 5.2.1.1, the rate of glucose conversion remains high, even when the observed yield of sorbitol is low to none. Again, no additional products could be detected nor quantified in HPLC chromatograms; a more in-depth characterisation of post-reaction solutions and gases would determine the products being generated in this instance.

The average yield/conversion value as synthesis temperature is increased follows a high-low-high pattern as temperature is increased, with catalysts prepared at 200°C having comparable activities in terms of yield and conversion than those prepared at 150°C. A longer preparation time has a beneficial effect on average, however there being such a significant experimental error on some of the catalysts prepared at the longer synthesis times (namely, those in the Black Pearls 2000 series) reduces the validity of this statement.

5.2.1.4: Glucose Hydrogenation: Blank Runs

To determine the extent that the activated carbon alone has on glucose hydrogenation, a series of experiments were carried out with the bare activated carbon supports that

were used to synthesise the Ru/C catalysts. Reactions were carried out in with H_2 and with N_2. The results of these reactions are shown in Table 5-4.

Material	Glucose Conversion (%)	Sorbitol Yield (%)	Fructose Yield (%)	5-HMF Yield (%)
Vulcan XC72R (H_2)	21.3	0.0	3.7	5.6
Vulcan XC72R (N_2)	9.0	0.0	4.6	3.8
Vulcan Black Pearls 2000 (H_2)	20.3	0.0	4.0	0.9
Vulcan Black Pearls 2000 (N_2)	17.5	0.0	3.9	1.6

Table 5-4: Glucose hydrogenation reactions with bare activated carbon support materials. Reaction parameters: 50 mg support material, 162 mg D-glucose (8.1g/L), 20 mL DI H_2O, 170 ℃, 10 bar H_2, 0.5 h.

No sorbitol was produced without the presence of ruthenium, which confirms that ruthenium is the active species for glucose hydrogenation. In this case measurable quantities of fructose and 5-HMF were detected, albeit at low yields. The greatest quantity of fructose was produced by XC72R in the absence of hydrogen, at 4.6%, and the greatest yield of 5-HMF was produced by XC72R in the presence of hydrogen, at 5.6%. A greater rate of fructose and 5-HMF being produced from glucose by the XC72R support material may be due to its surface acidity being greater, as it is bifunctional Lewis/Brönsted acids that catalyse these reactions,[30] however this cannot be conclusively stated without repeating these experiments to determine the degree of error.

5.2.1.5: Activated Carbon as a Dopant

To investigate whether the presence of activated carbon alone can have a promotional effect when other catalyst types are used for glucose hydrogenation, a series of tests were conducted where a Ru/TiO_2 catalyst was doped with the two carbon supports that were used for synthesising Ru/C catalysts in this study. The results of this are shown in Figure 5-9.

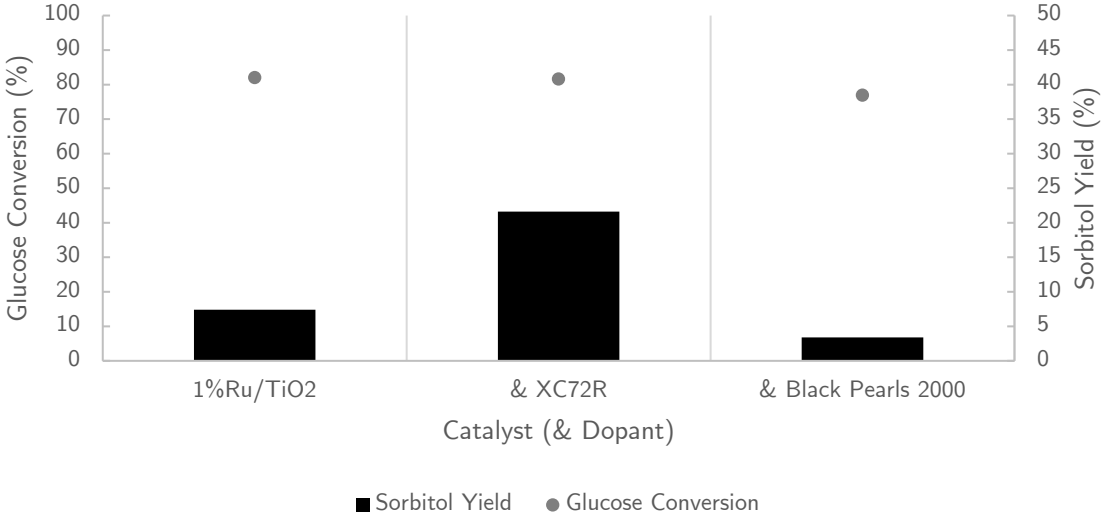

Catalyst (& Dopant)	Glucose Conversion (%)	Sorbitol Yield (%)
1%Ru/TiO_2 175-5	82	7.4
& Vulcan XC72R	81.6	21.6
& Vulcan Black Pearls	76.9	3.4

*Figure 5-**9**: The effect of doping a Ru/TiO_2 catalyst with activated carbon in a glucose hydrogenation reaction. Reaction conditions: 50 mg catalyst (1%Ru/TiO_2 175-5), 50 mg activated carbon, 162 mg D-glucose in 20 mL D.I H_2O (8.1 g/L), 170 ℃, 10 bar H_2, 0.5 h.*

The addition of a small amount of XC72R resulted in a threefold increase in sorbitol yield from the Ru/TiO_2 catalyst. However, adding Black Pearls resulted in a decrease in both yield and conversion. The choice of activated carbon therefore has an important effect as to whether its addition has a promotional effect.

"Activated carbon" encompasses a broad range of carbon-based materials that have a very high surface area due to their highly microporous structure.[31] Many activated carbons are prepared by heat treating carbonaceous materials such as coal or biomass, in the absence of oxygen. Each type will have differing properties due to the differences in the source material used for their production, such as the abundance and types of functional groups on their surfaces. The surface layer of a typical activated carbon contains some combination of oxygenated functional groups. Figure 5-10 illustrates the three most reported, those being carboxyl, hydroxyl, and carbonyl groups, respectively.

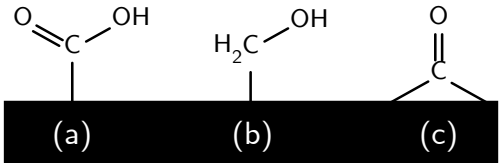

Figure 5-10: The most common surface functional groups of activated carbon: carboxyl (a), hydroxyl (b) and carbonyl (c).

The contribution of activated carbon towards the hydrogenation reaction in this instance is not clear and will require further investigation. However, it is likely that surface acidity plays a large part in the promotional effect observed when Ru/TiO_2 was doped with XC72R. The presence of medium-strength acid groups correlated with increased hydrogenation activity in Venezia *et al.*'s investigation into the effect of support acidity on the hydrogenation of various aromatic compounds over AuPd catalysts, which was attributed to the modification of the active metal's electronic properties by the acid sites.[32] Huang *et al.* also attributed their increased turnover frequencies to active site electronic modification.[33]

5.2.1.6: Ru/TiO_2 Catalysts for Levulinic Acid Hydrogenation

The testing conditions that were employed for the hydrogenation of levulinic acid to γ-valerolactone were milder in comparison to those used for glucose hydrogenation over Ru/C catalysts. Figure 5-11 shows the hydrogenation activity of all Ru/TiO_2 catalysts, plotted by their preparation temperature and time.

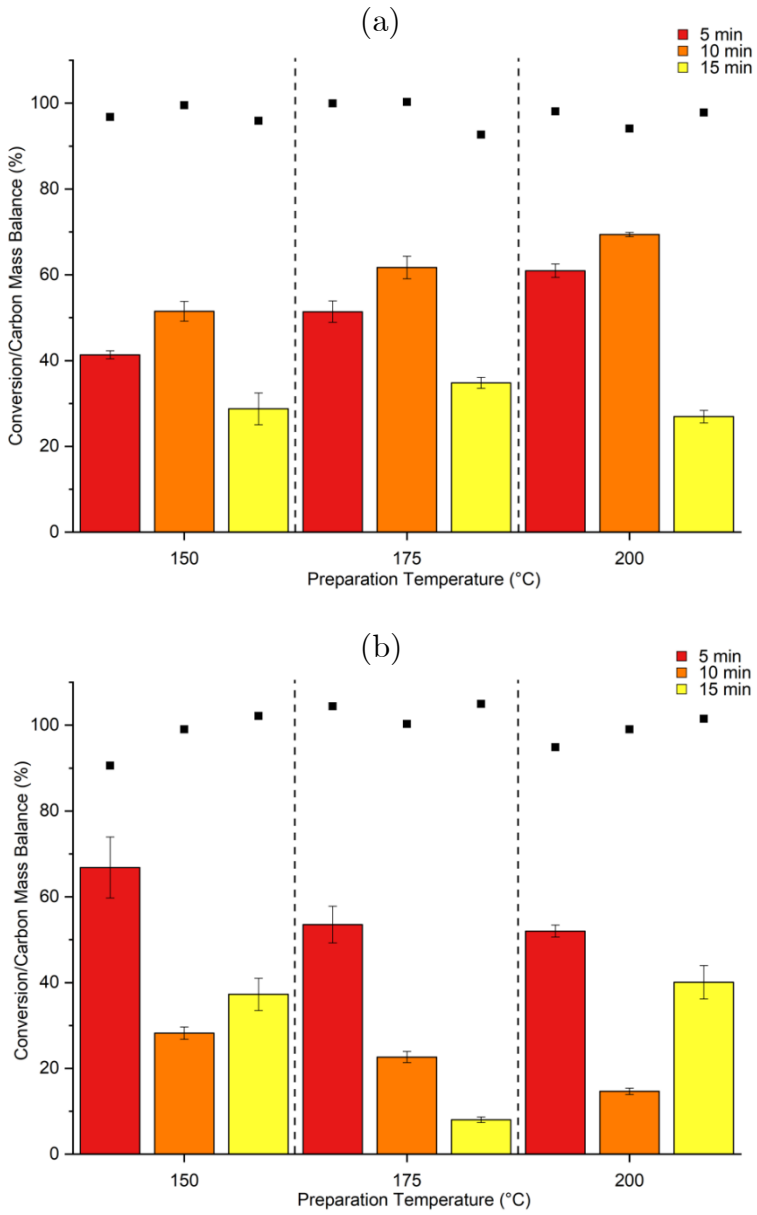

Figure 5-11: The yield of γ-valerolactone/conversion of levulinic acid plotted by each catalyst's preparation temperature. $Ru(acac)_3$-derived catalysts are shown in (a), and $RuCl_3$-derived catalysts in (b). The carbon mass balance values are shown with ■ and are based on the average yield value from each reaction. *Reaction conditions: 25 mg catalyst, 5 wt.% levulinic acid (10 mL), 100°C, 5 bar H_2, 1 h.*

In the case of catalysts prepared using $Ru(acac)_3$, increasing the synthesis temperature generally had a beneficial effect on catalytic conversion, whereas for synthesis time,

the most active catalysts were prepared at 10-minutes across each preparation temperature. The most active catalysts overall being prepared at the highest temperature of 200 °C agrees with the averaged values obtained for the Ru/C catalysts for glucose hydrogenation. In the case of catalysts prepared using $RuCl_3$, the most active catalysts were found to be those made at the shortest synthesis time of 5 minutes. This indicates that this testing regime should be expanded to include catalysts that are synthesised for less time to determine if these would be more active.

5.2.2: Catalyst Characterisation

5.2.2.1: Microwave-Plasma Atomic Emission Spectroscopy

As previously mentioned in chapter 2, section 5.3, ruthenium is insoluble in solutions of aqua regia, therefore the catalysts themselves could not be used as a direct measure of the Ru loading. Rather, each catalyst's post-synthesis solution of ethylene glycol was retained and analysed for its ruthenium content; its absence correlating to complete attachment onto the support material.

5.2.2.1.1: Ru/C catalysts

A complete Table of each catalyst's actual weight loading is shown in appendix B. Generally, the attachment of ruthenium to both activated carbon supports, and using both $Ru(acac)_3$ and $RuCl_3$ precursors, was at or close to the expected value of 1 wt.%. The average discrepancy between the expected and actual weight loadings across all catalysts was 5.4 wt.%, however this figure varied significantly when specific variables were isolated, namely the choice of support material, choice of ruthenium precursor, and the catalyst synthesis time and temperature. Figure 5-12 illustrates the contribution that each variable had upon the deviation between actual and expected values.

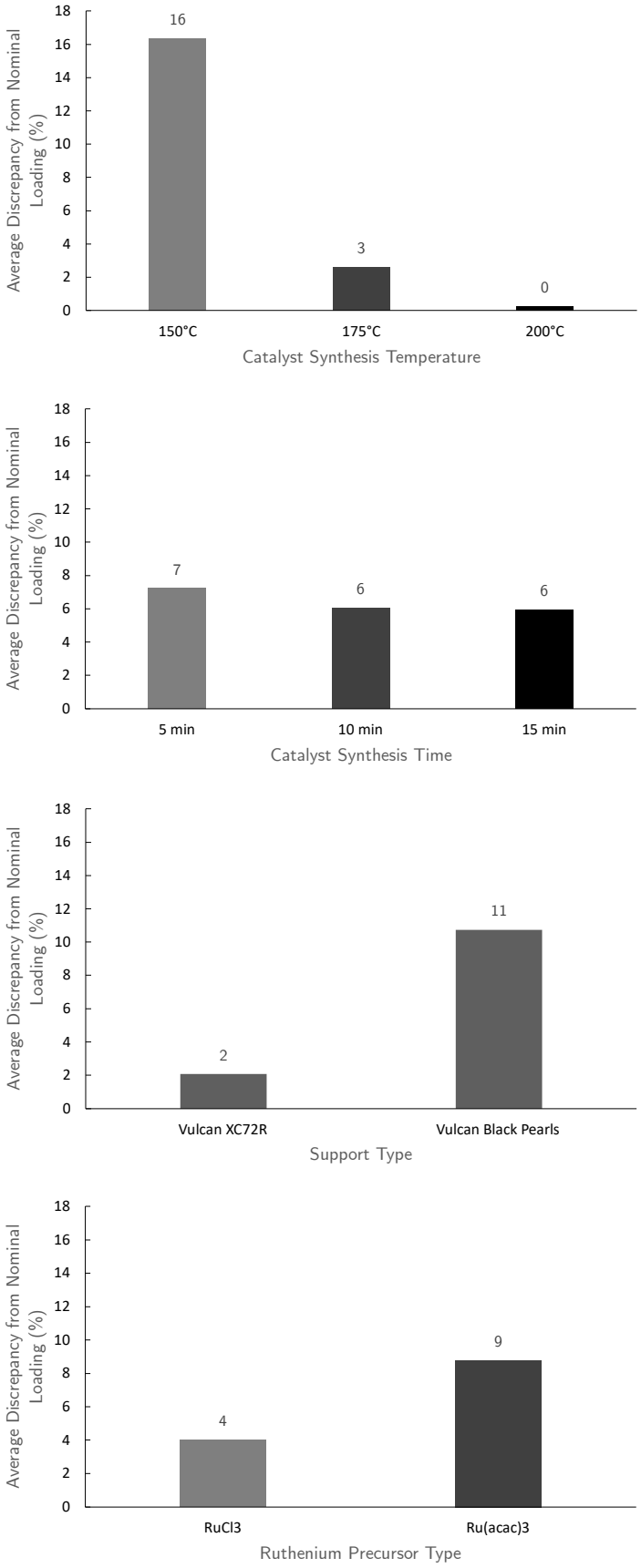

Figure 5-12: The deviation between actual and expected ruthenium loadings for Ru/C catalysts, isolated to take each variable into account.

The carbon support had a large effect, all XC72R-based catalysts having a close agreement between their actual and expected metal loading, however much greater discrepancies were observed with the Black Pearls-based catalysts. Varying the catalyst's synthesis temperature had more of an impact towards the attachment of ruthenium to the catalyst support than varying its synthesis time. The greatest discrepancies were observed in catalysts synthesised at the lowest temperature of 150 °C. The choice of precursor was also a notable factor, with $RuCl_3$-derived catalysts having a lower discrepancy when compared to the average.

When the entire series of Ru/C catalysts' yield/conversion values are considered, the correlation between the discrepancy of each catalyst's metal loading and its yield/conversion value is not particularly strong. Many catalysts whose discrepancies was at or near zero produced relatively low amounts of sorbitol and vice-versa, indicating that variations in metal loading alone cannot account for the general trends that were observed in the catalyst testing data.

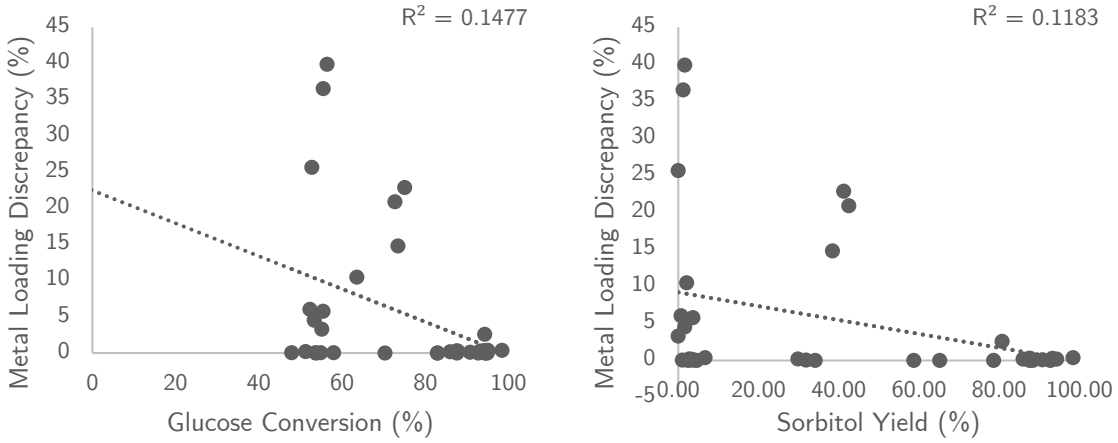

Figure 5-13: A plot of the sorbitol yield obtained from a catalyst against the discrepancy in its metal loading from the expected value.

5.2.2.1.2 – Ru/TiO_2 Catalysts

A selected number of Ru/TiO_2 catalysts, based on the most and least active catalysts synthesised from each ruthenium precursor, were analysed for their metal loading, all of which had close agreement with their expected values, as shown in Table 5-5.

	Expected Ru Loading (wt.%)	Actual Ru Loading (wt.%)
1%Ru(acac)/TiO_2 200-10	1	1.08
1%Ru(acac)/TiO_2 200-15	1	0.97
1%Ru(Cl)/TiO_2 150-5	1	0.96
1%Ru(Cl)/TiO_2 150-10	1	1.02

Table 5-5: The selected number of Ru/TiO_2 catalysts that were analysed for their metal loadings.

5.2.2.2: X-Ray Diffraction

All Ru/C catalysts synthesised by the microwave polyol method were analysed by XRD to establish whether if any differences in crystallographic properties are related to their synthesis parameters or their activities. Figure 5-14 lays out the XRD patterns of all microwave polyol Ru/C catalysts that were tested for their glucose hydrogenation performance, grouped by their carbon support type and precursor type.

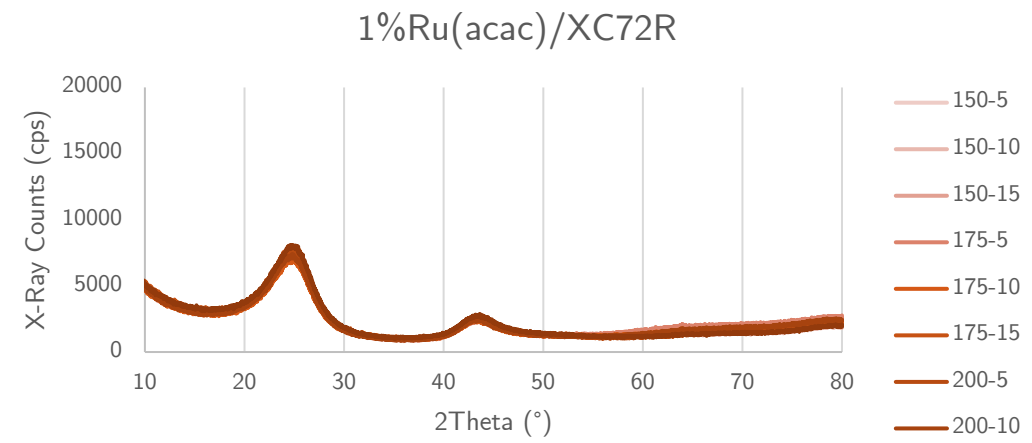
1%Ru(acac)/XC72R
X-Ray Counts (cps)
20000
15000
10000
5000
0
10
20
30
40
50
60
70
80
2Theta (°)
150-5
150-10
150-15
175-5
175-10
175-15
200-5
200-10

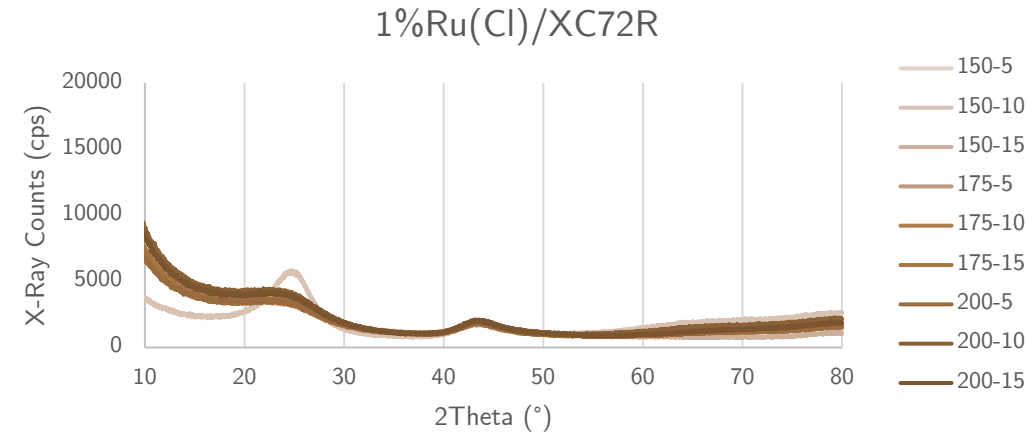
1%Ru(Cl)/XC72R
X-Ray Counts (cps)
20000
15000
10000
5000
0
10
20
30
40
50
60
70
80
2Theta (°)
150-5
150-10
150-15
175-5
175-10
175-15
200-5
200-10
200-15

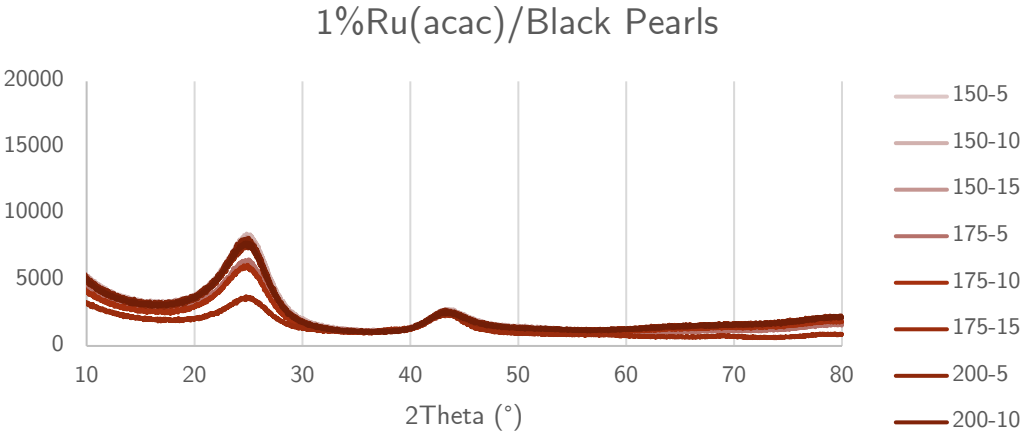
1%Ru(acac)/Black Pearls
20000
15000
10000
5000
0
10
20
30
40
50
60
70
80
2Theta (°)
150-5
150-10
150-15
175-5
175-10
175-15
200-5
200-10

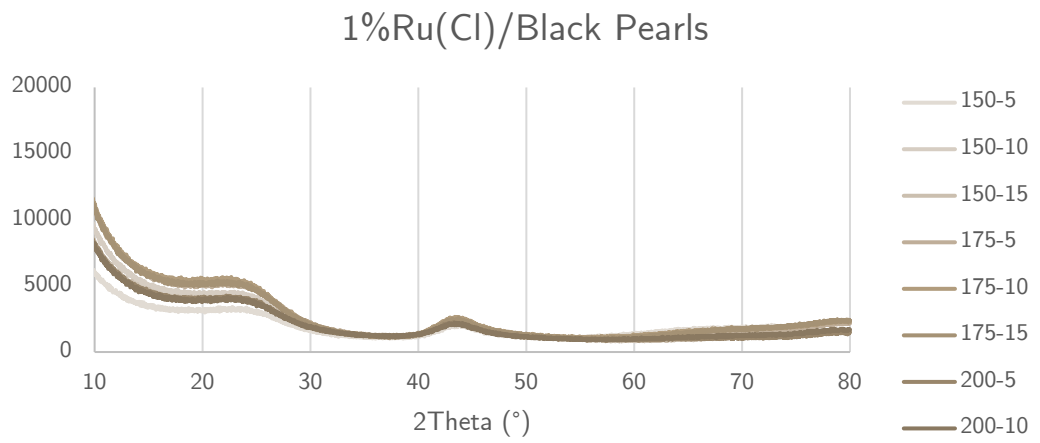

Figure 5-14: XRD patterns of all Ru/C catalysts synthesised by the microwave-assisted polyol method.

The absence of sharp peaks in all instances indicates that the activated-carbon supported catalysts have a predominantly amorphous structure,[34] though in the case of $Ru(acac)_3$ prepared catalysts, sharper peaks at $2\vartheta \approx 24°$ indicates an increased presence of crystalline structures, corresponding to the diffraction of a (002) crystal face.[35] In all instances, there is an absence of peaks that would arise from the diffraction of metallic ruthenium, expected between $2\vartheta \approx 55\text{-}70°$ or that of ruthenium oxide, at $2\vartheta \approx 28\text{-}35°$.[36,37] The absence of these peaks indicates that there are no large ruthenium particles present in a significant quantity; particles that are of a sufficiently small size and present in a sufficiently low quantity will not produce XR diffractions.[38]

5.2.2.3: X-Ray Photoelectron Spectroscopy

A selected number of catalysts were submitted for analysis by X-Ray photoelectron spectroscopy (XPS) to obtain a greater understanding of their surface characteristics; in particular, ruthenium's surface loading, its oxidation state on the surface of the catalyst, and whether these parameters change with changes in catalyst synthesis variables.

5.2.2.3.1: Ru/C Catalysts

Figure 5-15 shows an example of an XPS spectrum of a Ru/C catalyst. There is a significant degree of overlap between C(1s) and Ru($3d_{5/2}$) emissions, which was considered in the peak fitting model.

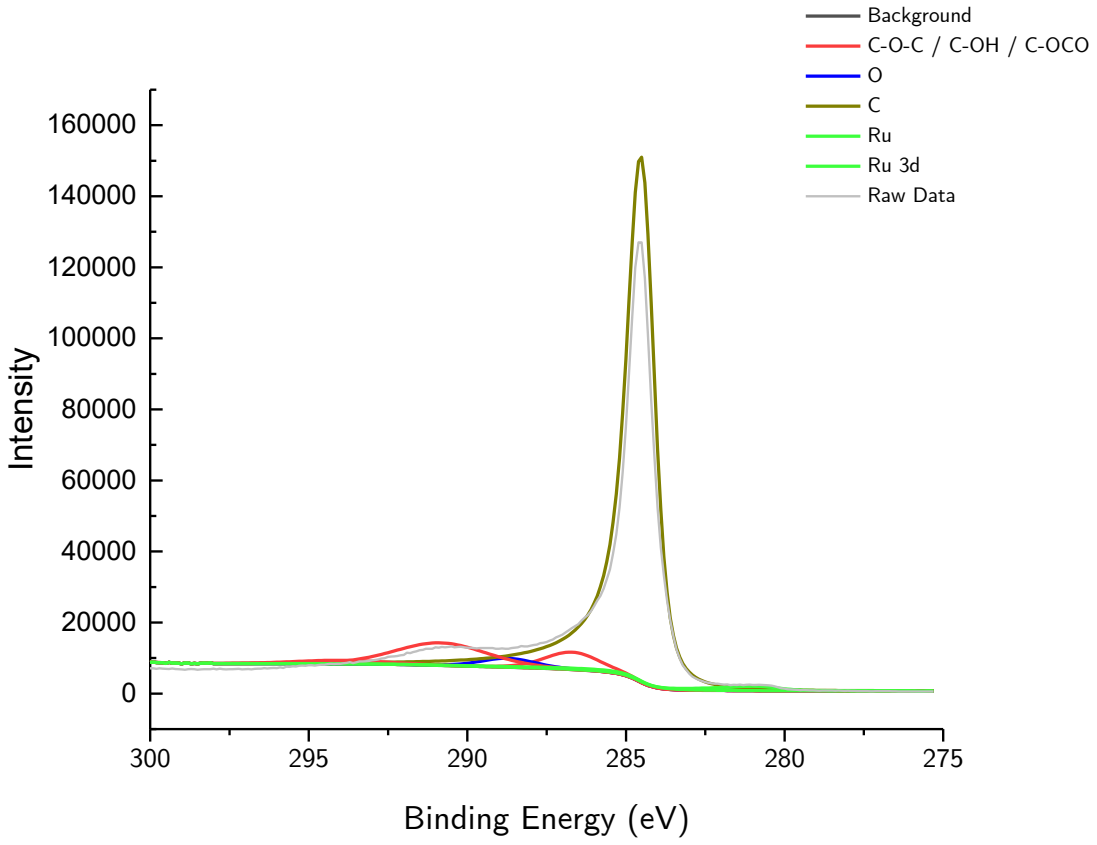

Figure 5-15: Fitted XPS spectrum of 1%Ru(Cl)/XC72R 175-5.

Figure 5-16 shows the Ru($3d_{5/2}$) emissions of the selected series of Ru/C catalysts prepared by the microwave-assisted polyol method.

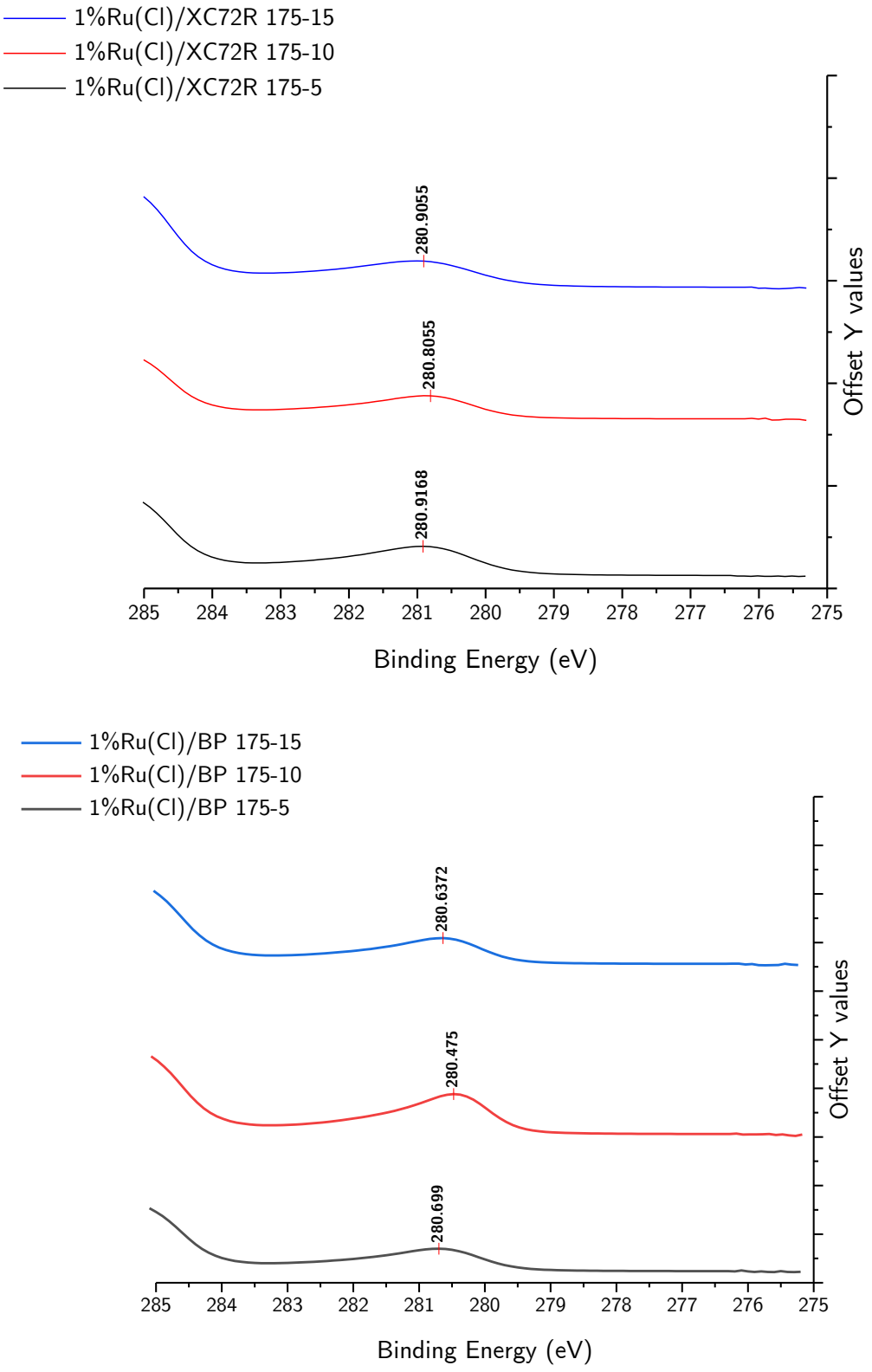

Figure 5-16: The binding energies of Ru(3d) emissions from a selected series of Ru(Cl)/C catalysts.

Catalyst	Element	XPS Surface Concentration (At%)
1%Ru(Cl)/XC72R 175-5	Ru	0.37
	C	77.08
	O	2.29
1%Ru(Cl)/XC72R 175-10	Ru	0.38
	C	77.08
	O	2.13
1%Ru(Cl)/XC72R 175-15	Ru	0.22
	C	81.89
	O	1.35

Table 5-6: XPS elemental surface composition of 1%Ru(Cl)/XC72R 175--x catalysts.

Catalyst	Element	XPS Surface Concentration (At%)
1%Ru(BP)/XC72R 175-5	Ru	0.23
	C	77.85
	O	1.98
1%Ru(BP)/XC72R 175-10	Ru	0.28
	C	82.69
	O	1.34
1%Ru(BP)/XC72R 175-15	Ru	0.17
	C	82.24
	O	1.02

Table 5-7: XPS elemental surface composition of 1%Ru(Cl)/BP 175-x catalysts.

The binding energy of each catalyst's Ru($3d_{5/2}$) emission provides insight into the oxidation state of the ruthenium on the surface of these catalysts. Okal *et al.* state that there is some discrepancy in literature as to the precise binding energies of ruthenium compounds, complicating this analysis. In their investigation into a Ru/Al_2O_3 catalysts prepared by a microwave-assisted polyol method, they reported that ruthenium metal has a binding energy of 279.1 eV, whereas ruthenium oxide (RuO_2) has a binding energy of 279.4 eV.[39] It is of note that they endeavoured to remove as much carbon from the surface of their materials as possible by Ar^+ bombardment to minimise the C(1s) contribution. Mun *et al.* report that this treatment affects the analysis by reducing the surface and broadening the peaks,[40] therefore these binding energies may not be representative of samples that aren't treated in this way. They report Ru($3d_{5/2}$) binding energies of 279.95 eV for un-treated,

metallic ruthenium and 280.77 eV for RuO_2, with higher binding energies at < 281 eV associated with Ru^{3+} and Ru^{4+} as the result of surface defects. This is in agreement with earlier literature, which places metallic ruthenium's $Ru(3d_{5/2})$ emission at ~ 279.9 eV and RuO_2 at ~ 280.7 eV.[41]

The calculated binding energies from the series of Ru/C catalysts that were selected confirm that ruthenium is present predominantly as RuO_2 across each preparation time and carbon support type. This holds true at the highest preparation temperature, as analysis of the series of Ru(Cl)/Black Pearls 200-x catalysts shows. The results of this are shown in Figure 5-17.

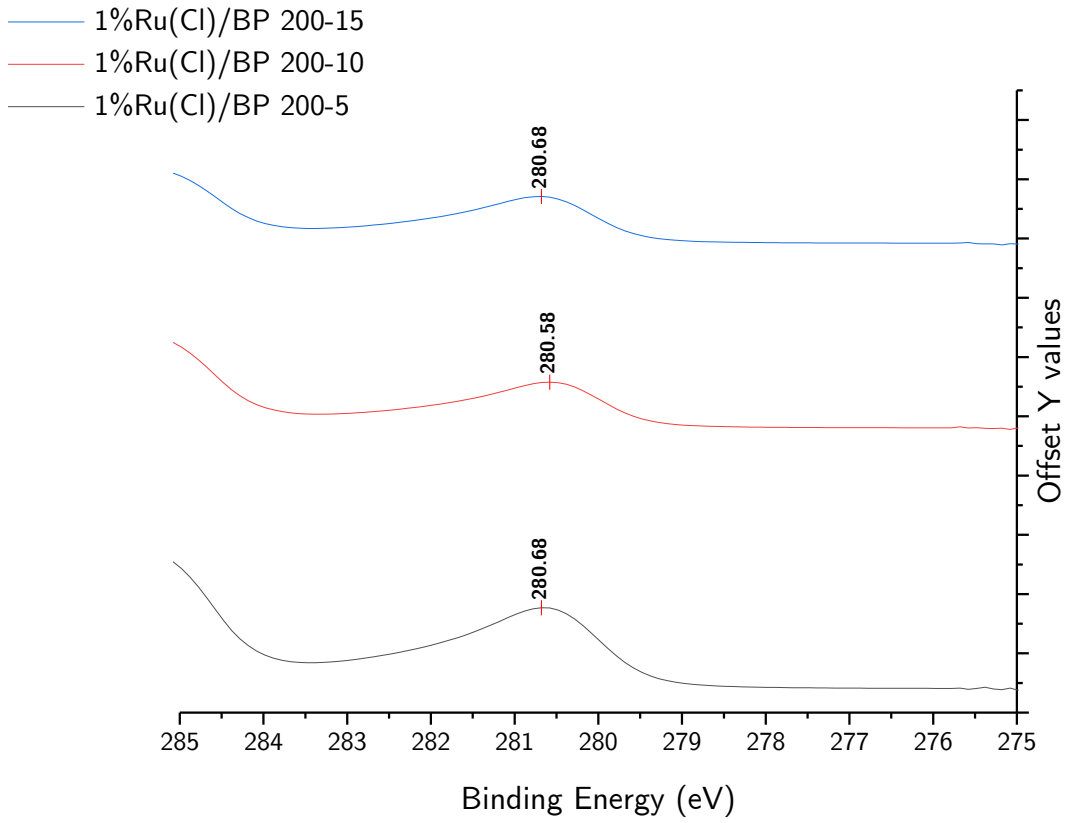

Figure 5-17: The binding energies of Ru(3d) emissions from the series of Ru(Cl)/Black Pearls 200-x catalysts.

Catalyst	Element	XPS Surface Concentration (At%)
1%Ru(Cl)/BP 200-5	Ru	0.40
	C	77.74
	O	2.63
1%Ru(Cl)/BP 200-10	Ru	0.32
	C	78.76
	O	2.29
1%Ru(Cl)/BP 200-15	Ru	0.43
	C	77.98
	O	2.14

Table 5-8: XPS elemental surface composition of 1%Ru(Cl)/BP 200-x catalysts.

To determine if the presence of RuO_2 was a consequence of the polyol preparation method, a series of Ru/C catalysts were prepared using another, more commonly used and well-known preparation method, wet impregnation. In short, 0.99 g of Vulcan XC72R or Vulcan Black Pearls 2000 was added slowly to a heated aqueous solution of either $Ru(acac)_3$ or $RuCl_3$ at the required concentration for a 1 wt.% metal loading. This was then stirred at 95 °C overnight to achieve dryness. The dried catalyst was then reduced in a tube furnace using $5\%H_2/Ar$ at 400 °C for 4 hours, at a heating rate of 10 °C min^{-1}. Each one of the four resulting catalysts were then analysed using XPS in the same manner as those synthesised using the microwave polyol method.

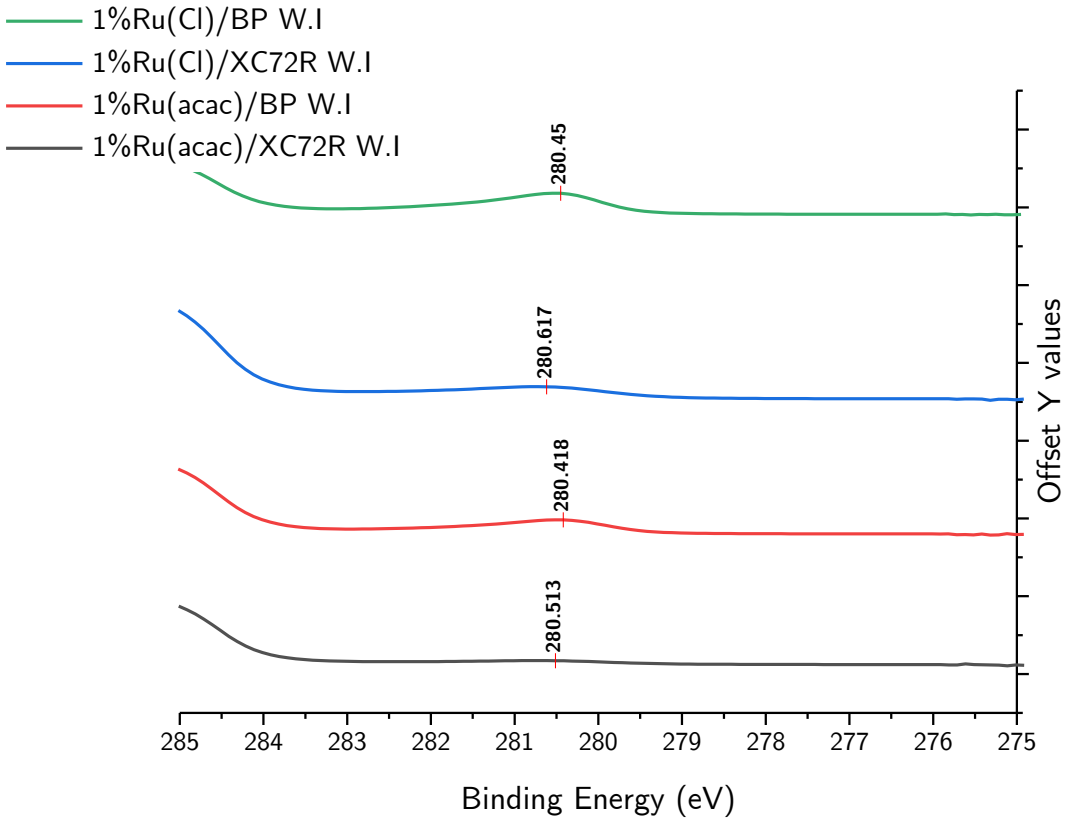

Figure 5-18: The binding energies of Ru(3d) emissions from each Ru/C catalyst synthesised using a wet-impregnation method.

Catalyst	Element	XPS Surface Concentration (At%)
1%Ru(Cl)/BP WI	Ru	0.05
	C	78.82
	O	1.24
1%Ru(Cl)/XC72R WI	Ru	0.10
	C	78.96
	O	1.41
1%Ru(acac)/BP WI	Ru	0.10
	C	83.02
	O	1.08
1%Ru(acac)/XC72R WI	Ru	0.2
	C	83.14
	O	1.05

Table 5-9: XPS elemental surface composition of 1%Ru/C catalysts prepared by wet impregnation, with one catalyst made per carbon support type and ruthenium precursor type.

As was observed with all the catalysts prepared using the microwave polyol method, the binding energies of the Ru(3d) emissions are consistent with the presence of predominantly ruthenium oxide in all instances. It also appears that there is a lower surface concentration of ruthenium present on the surface of these catalysts when

compared with those made by the microwave polyol method. As XPS is a surface sensitive technique, this indicates that a greater amount of ruthenium is present in the bulk of the support.

Thakur *et al.* reported the presence of RuO_2 on their Ru/CNF (carbon nano-fibre) catalysts even after a reduction at 500 °C.[42] It appears that exposing Ru/C catalysts to ambient air oxidises Ru to RuO_2 regardless of any prior reduction of the catalyst, the oxidation occurs between the synthesis of the catalysts and their subsequent analysis by XPS. Jae *et al.* reported that partially oxidised Ru/RuO_2 active sites act as bifunctional hydrogenation/hydrogenolysis catalysts.[43] As RuO_2 is present, hydrogenolysis reactions are likely also taking place, where sorbitol is converted into various polyols including glycerol and propylene glycol.[44] If the presence of these compounds is confirmed in potential future work in this area, this would explain the discrepancy between sorbitol yield and glucose conversion observed during catalyst testing.

During XPS analysis, a significant quantity of sulphur was observed on the surfaces of some of the catalysts, estimated to be at a concentration of ≈ 0.3-0.35 At.%. Sulphur is a common contaminant of activated carbon, and furthermore, its presence has been known to decrease the activity of ruthenium active sites.[45,46] In future work, it would be pertinent to investigate the effect that sulphur contamination has upon catalytic activity for this reaction; its presence in some catalysts may explain the significant variation in yield/conversion values that have no correlation with catalyst synthesis variables. Treatments to remove residual sulphur may prove highly beneficial to catalyst activity and reproducibility when using commercial activated carbons as supports for the synthesis of Ru/C catalysts for this reaction.

5.2.2.3.2: Ru/TiO_2 Catalysts

Two Ru/TiO_2 catalysts in the $Ru(acac)_3$ - derived series (200-10 and 200-15) were selected for XPS analysis to establish whether variations in the oxidation state of ruthenium between them were a contributor to the notable difference in their activity towards levulinic acid hydrogenation. Figure 5-19 shows the fitted spectra of the two catalysts.

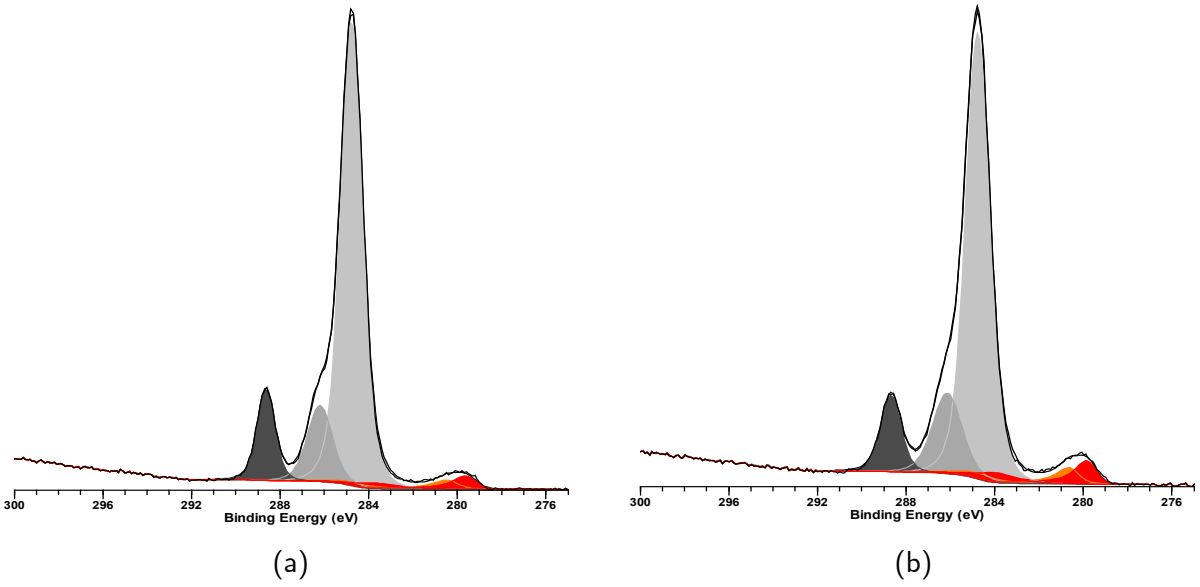

Figure 5-19 Fitted spectra of the Ru(3d)/C(1s) region of Ru(acac)/TiO_2 200-10 (a) and Ru(acac)/TiO_2 200-15 (b) with the contribution of Ru highlighted in red.

The fitted $Ru(3d_{5/2})$ binding energies of Ru(acac) 200-10 were 279.5 eV and 280.4 eV, indicating the presence of metallic Ru and RuO_2, respectively. In both instances, peak fitting of the binding energy of the Ru(3d) emissions suggests that there is a mixture of metallic ruthenium and RuO_2 on the surface of the catalysts. As is the case with the Ru/C catalysts, it is likely that the presence of RuO_2 is a consequence of air oxidation between catalyst preparation and analysis.

5.2.2.4: Transmission Electron Microscopy

A selected series of Ru/C catalysts were imaged using transmission electron microscopy to gather information on their morphology and their particle size distributions in comparison to their synthesis parameters. A representative image of one of the Ru/C catalysts is shown in Figure 5-20, taken at a 150kX zoom level.

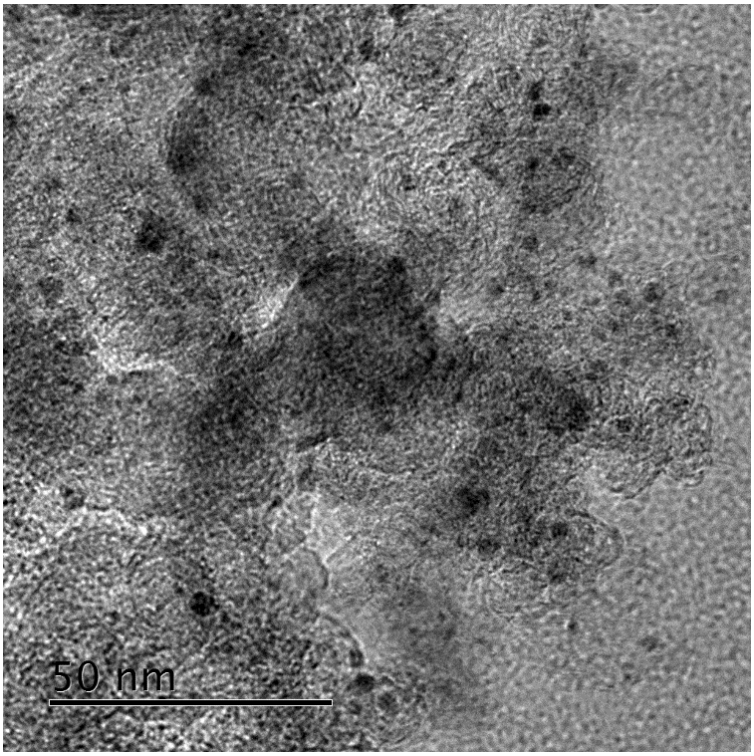

Figure 5-20: TEM image of 1%Ru(Cl)/XC72R 175-5.

All the imaged Ru/C samples displayed small and evenly dispersed nanoparticles, with the average particle size between all samples ranging from 2.8 to 3.8 nm. This makes them slightly larger than Howe *et al.*'s 1 wt.% Ru/TiO_2 catalysts prepared by a similar microwave-assisted polyol method, which had average particle sizes ranging from 2.35-2.55 nm.[14] To investigate the influence of synthesis parameters on particle size distribution, firstly, the series of 1%Ru(Cl)/XC72R 175-x catalysts were imaged, where x denotes the preparation time, which was either 5, 10 or 15 minutes. The result of this analysis is shown in Figure 5-21.

Catalyst	1%Ru(Cl)/XC72R 175-5	1%Ru(Cl)/XC72R 175-10	1%Ru(Cl)/XC72R 175-15
Representative Image (150kX)	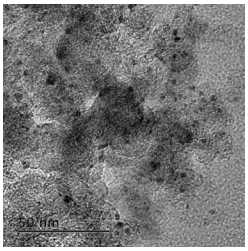	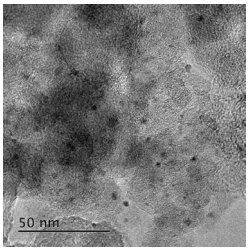	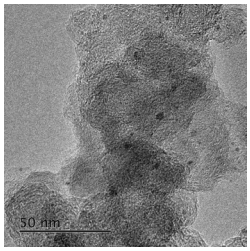
Average Particle Size	3.36	3.78	3.54
Normalised Distribution	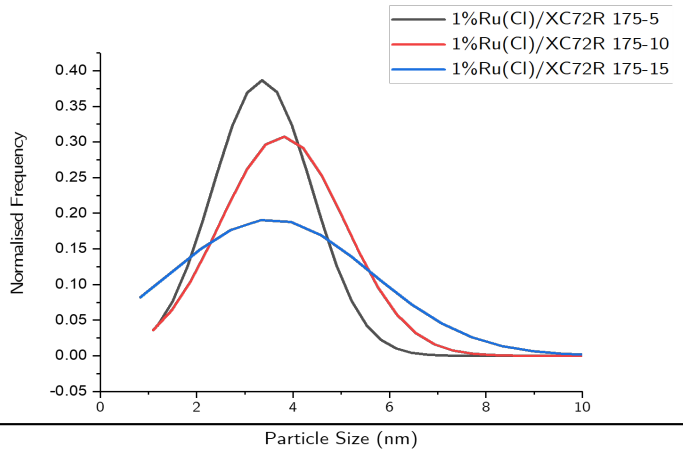		

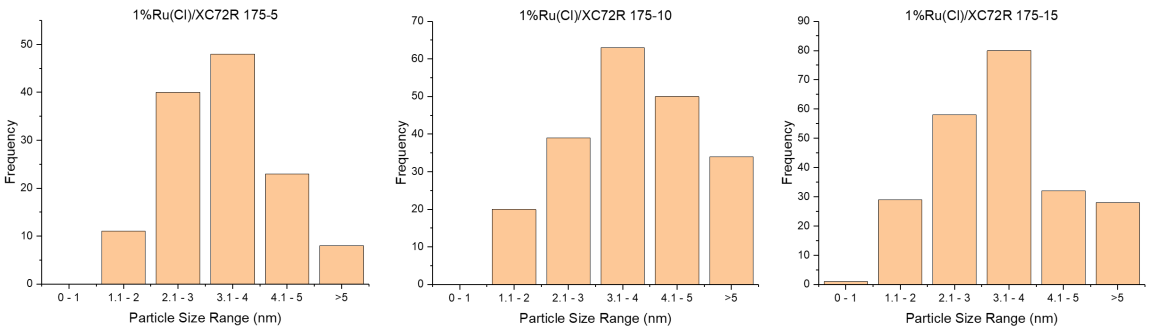

Figure 5-21: Particle Size Distribution Analysis of 1%Ru(Cl)/XC72R 175-x series of catalysts.

The smallest particle size variation was seen in the catalyst synthesised for the shortest amount of time (5 minutes). Whilst the average size of the Ru nanoparticles does not increase appreciably, the range of particle sizes observed broadens as the synthesis time increases. All three of the catalysts imaged by TEM were highly active for glucose hydrogenation, however the catalyst that was synthesised for 10 minutes was the most active of the series. It appears. This corroborates the findings of the catalyst screening investigation in section 5.2.1.3, where it was found that, in general, catalysts prepared at lower synthesis temperatures were more active. It appears that by varying synthesis parameters it is possible to control nanoparticle size distribution using this synthesis method. A glucose hydrogenation study was conducted by Aho *et al.* using Ru/C catalysts; they reported the highest turnover frequency with catalysts whose average particle size was ≈ 3 nm.[47] All three of the imaged catalysts had average particle sizes that were close to this value (3.36 – 3.78 nm), which demonstrates the viability of the microwave polyol method for catalyst design for this reaction. To establish whether average particle size and particle size distribution effects are a major contributor towards the activity of the Ru/C catalysts synthesised during this study, a wider range of catalysts should be sampled in future work, where the particle size distribution and ruthenium dispersion is varied.

Two significant variables were not modified when undertaking the microwave-assisted catalyst syntheses, the polyol solvent that was used and the synthesis solution's pH. In this investigation, ethylene glycol was used exclusively for catalyst synthesis and no modification of solution pH was attempted, however, the modification of both can have a significant effect on particle size. Becker *et al.* achieved significant control over the particle size of ZnO nanocrystals, with particle sizes ranging from 19.8 to 89.6 nm dependent on the solvent type.[48] The average particle size of Pt on Zhao *et al.*'s Pt/C (C = Vulcan XC72) catalysts decreased from 5.5 nm to 2.7 nm as the pH of the synthesis solution was increased from 3.4 to 9.5.[49] In future work, modification of these two parameters is likely to allow for a significant degree of control of Ru particle size in the same manner.

5.3: Conclusions and Future Works

In this chapter, a series of 1 wt.% Ru/C (C = Vulcan XC72R, Vulcan Black Pearls 2000) and 1 wt.% Ru/TiO_2 catalysts, synthesised by a microwave-assisted polyol method, were tested for their activities towards the hydrogenation of cellulose, glucose, and levulinic acid. Firstly, the RNF's response to a one-pot cellulose hydrogenolysis reaction was established and compared with Avicel PH-101, a reference microcrystalline cellulose. It was found that a minimal amount of sorbitol was being produced from the RNF. It was suspected that this was due to the presence of residual $CaCl_2$ from the deactivation of superabsorbent polymers. An incremental amount of $CaCl_2$ was added to the reaction solution of successive glucose hydrogenation reactions, and it was found that the catalyst's activity decreased significantly as the concentration of $CaCl_2$ was increased. It was found in previous research that the poisoning effect of chlorides upon Ru active sites is dependent on their particle size, their dispersion, and the acidity of the support material. Future work in this area should investigate the effect of varying these three parameters upon the activity of Ru/C catalysts for the hydrogenolysis of RNF, as it may not be necessary to remove the residual chlorides from the material if a catalyst can be created that is tailored to the material as-is.

Following this, glucose hydrogenation reactions were carried out as a benchmark for testing 36 Ru/C catalysts, whose catalyst synthesis variables (the ruthenium precursor used, the type of activated carbon support, and the temperature and duration of the microwave synthesis itself) were modified to determine which variables had the most effect on catalyst activity. It was found that the most significant effects were observed when the carbon support type and ruthenium precursor type were modified. XC72R-supported catalysts made with $RuCl_3$ as the Ru precursor were significantly more active on average than catalysts made with Black Pearls 2000 carbon and with $Ru(acac)_3$. On average, benefits to the catalyst's activity were also seen by increasing the catalyst synthesis temperature. The use of the microwave-assisted polyol method had several benefits which have proven useful in the conduction of this study, and that

cannot be overlooked when viewed from an efficiency and green chemistry perspective. When synthesising catalysts for both the glucose hydrogenation reaction using Ru/C catalysts and for the hydrogenation of levulinic acid to γ-valerolactone using Ru/TiO_2 catalysts, the rapidity of the method allowed for many catalysts to be made, tested and characterised, which consequently allowed for the collection of larger datasets than if a more conventional synthesis method was employed. The microwave-assisted polyol method used in this study requires 20mL of solvent for the synthesis, which itself takes place over a timescale of minutes, rather than hours. Future work in this area should involve a wider range of variables for catalyst synthesis, such as the effect of modifying the polyol solvent, increasing, or decreasing the metal loading, and whether alloying ruthenium with a second metal has a beneficial effect. A commonly used second metal that is used to alloy with ruthenium in similar studies is palladium.[18,50]

The isolated averages presented in section 5.2.1.3 provided some insight into the optimum synthesis parameters for future catalyst development in this area. The trends show that a catalyst is likely to be more active if it was synthesised from $RuCl_3$ and XC72R carbon, if its synthesis temperature was higher, and its synthesis time was longer. Many catalysts bucked this trend. Both highly active and inactive catalysts were made at low and high synthesis temperatures, short and long synthesis times, using both carbon support types, and with both types of ruthenium precursor. The reason for the significant variation in catalytic activity towards sorbitol production that was observed when Black Pearls 2000 was used as the carbon support was suggested to be due sulphur contamination, as it was detected on the surface of some of the catalysts submitted to XPS analysis. Therefore, in future work, it would be pertinent to investigate the effect of S contamination on the performance of activated carbon-supported catalysts for cellulose hydrogenolysis/glucose hydrogenation catalysts. Also, it should be determined if the presence of sulphur in XPS analyses was a result of cross-contamination of the samples within the instrument or if the sulphur is indeed present within the catalyst support. This could be achieved by analysing the catalysts with an elemental analysis technique such as ICP-OES.

It is of note that the most active set of catalysts were produced from a chloride-based precursor, when chlorides are a suspected poison for Ru/C catalysts from this reaction, as previously discussed in section 5.1.1. It may be that all residual chloride is successfully removed during the catalyst synthesis steps, however XPS analysis of $RuCl_3$-derived catalysts in future work should be expanded to include chlorine as an analyte to confirm if this is indeed the case.

Future work in this area should also aim to establish the identities of potential side products that are formed during hydrogenation reactions. Figure 5-22 shows a HPLC chromatogram obtained from a typical glucose hydrogenation reaction with Ru/C catalysts from this chapter. Both glucose and its major hydrogenate, sorbitol, were able to be identified and quantified by HPLC, however there were several other peaks whose identity could not be confirmed, despite attempts to do so by spiking reaction solutions with the range of reducing sugars listed in Chapter 3, Table, 3-3.

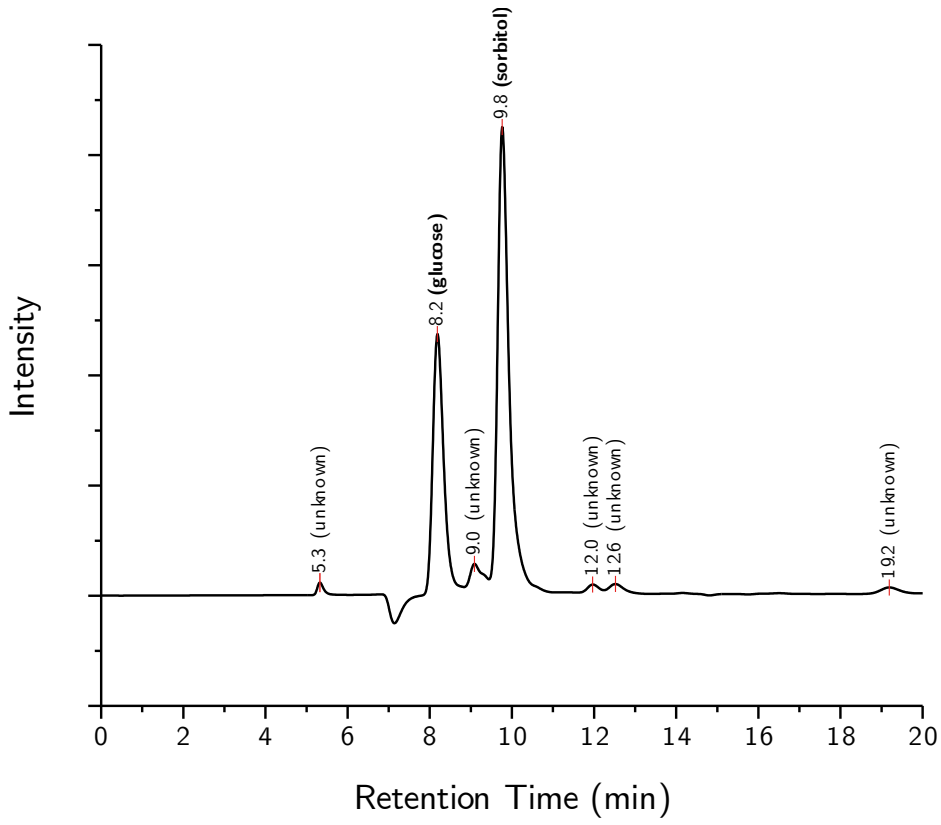

Figure 5-22: HPLC chromatogram of a typical glucose hydrogenation reaction solution using Ru/C catalysts (in this instance, 1%Ru(acac)/XC72R 150-5). Glucose and sorbitol's retention times were 8.2 minutes and 9.8 minutes, respectively.

Considering that the choice of carbon support had such a large effect upon catalyst activity, a wider range of activated carbon support materials should also be investigated, both commercially available and laboratory made. One such route for further research would be the use of mesoporous carbon materials as supports for ruthenium. It has been reported by Kobayashi *et al.* that their Ru/CMK-3 catalysts have a synergistic effect, where the mesoporous carbon facilitates the breakdown of cellulose, then the supported ruthenium further converts the resulting cello-oligomers into glucose and other hydrolysates.[51]

5.4: References

1 M. Kang, S. Y. Lee, C. H. Chung, S. M. Cho, G. Y. Han, B. W. Kim and K. J. Yoon, *J. Photochem. Photobiol. A Chem.*, 2001, **144**, 185–191.

2 M. Kang, *J. Mol. Catal. A Chem.*, 2003, **197**, 173–183.

3 W. Chen, J. Zhao, J. Y. Lee and Z. Liu, *Chem. Lett.*, 2004, **33**, 474–475.

4 H. Li, R. Wang, Q. Hong, L. Chen, Z. Zhong, Y. Koltypin, J. Calderon-Moreno and A. Gedanken, *Langmuir*, 2004, **20**, 8352–8356.

5 A. G. R. Howe, P. J. Miedziak, D. J. Morgan, Q. He, P. Strasser and J. K. Edwards, *Faraday Discuss.*, 2018, **208**, 409–425.

6 G. Y. Yu, W. X. Chen, Y. F. Zheng, J. Zhao, X. Li and Z. De Xu, *Mater. Lett.*, 2006, **60**, 2453–2456.

7 T. Werpy and G. Petersen, *Top Value Added Chemicals from Biomass: Volume I - Results of Screening for Potential Candidates from Sugars and Synthesis Gas*, 2004.

8 R. Palkovits, K. Tajvidi, J. Procelewska, R. Rinaldi and A. Ruppert, *Green Chem.*, 2010, **12**, 972–97.

9 A. Shrotri, H. Kobayashi, A. Tanksale, A. Fukuoka and J. Beltramini, *ChemCatChem*, 2014, **6**, 1349–1356.

10 B. Kusserow, S. Schimpf and P. Claus, *Adv. Synth. Catal.*, 2003, **345**, 289–299.

11 Cabot Corporation, Conductive Carbon Blacks, https://www.cabotcorp.com/solutions/products-plus/carbon-blacks-for-elastomer-reinforcement/conductive, (accessed 26 October 2021).

12 A. P. D'Silva, *Carbon N. Y.*, 1998, **36**, 1317–1325.

13 P. Ferreira-Aparicio, M. A. Folgado and L. Daza, *J. Power Sources*, 2009, **192**, 57–62.

14 A. G. R. Howe, R. Maunder, D. J. Morgan and J. K. Edwards, *Catalysts,* 2019, **9**, 9, 748.

15 S. Van De Vyver, J. Thomas, J. Geboers, S. Keyzer, M. Smet, W. Dehaen, P. A. Jacobs and B. F. Sels, *Energy Environ. Sci.*, 2011, **4**, 3601–3610.

16 I. T. Horváth, H. Mehdi, V. Fábos, L. Boda and L. T. Mika, *Green Chem.*, 2008, **10**, 238–24.

17 H. C. Genuino, H. H. Van De Bovenkamp, E. Wilbers, J. G. M. Winkelman, A. Goryachev, J. P. Hofmann, E. J. M. Hensen, B. M. Weckhuysen, P. C. A. Bruijnincx and H. J. Heeres, *ACS Sustain. Chem. Eng.*, 2020, **8**, 5903–5919.

18 W. Luo, M. Sankar, A. M. Beale, Q. He, C. J. Kiely, P. C. A. Bruijnincx and B. M. Weckhuysen, *Nat. Commun.*, 2015, **6**, 1–10.

19 J. Mieth and J. A. Schwarz, *J. Catal.*, 1989, **118**, 218–226.

20 D. Wang, M. P. Rosynek and J. H. Lunsford, *J. Catal.*, 1995, **151**, 155–167.

21 J. T. Richardson, J. D. Ortego, N. Coute and M. V Twigg, *Catal. Letters*, 1996, **41**, 17–20.

22 K. ichi Aika, T. Takano and S. Murata, *J. Catal.*, 1992, **136**, 126–140.

23 Z. H. Zhong and K. I. Aika, *Inorganica Chim. Acta*, 1998, **280**, 183–188.

24 Y. Li, C. Pan, W. Han, H. Chai and H. Liu, *Catal. Today*, 2011, **174**, 97–105.

25 J. Xu, Y. Song, Q. Tan and L. Jiang, *J. Mater. Sci.*, 2017, **52**, 5908–5916.

26 L. M. G. A. Ferreira, L. Amaral and L. Machado, *Ind. Eng. Chem. Res.*, 2004, **43**, 7121–7128.

27 R. Honkanen and J. Kaila, in *International Chemical Recovery Conference*, 2010, vol. 2, pp. 259–267.

28 C. Y. Lin and R. C. Chang, *J. Chem. Technol. Biotechnol.*, 1999, **74**, 498–500.

29 R. J. Zoetemeyer, J. C. van den Heuvel and A. Cohen, *Water Res.*, 1982, **16**, 303–311.

30 P. Lanzafame, D. M. Temi, S. Perathoner, A. N. Spadaro and G. Centi, in *Catalysis Today*, Elsevier, 2012, vol. 179, pp. 178–184.

31 H. Marsh and F. R. Reinoso, *Activated Carbon*, Elsevier Science, 2006.

32 A. M. Venezia, V. La Parola, B. Pawelec and J. L. G. Fierro, *Appl. Catal. A Gen.*, 2004, **264**, 43–51.

33 J. Huang, Y. Jiang, N. Van Vegten, M. Hunger and A. Baiker, *J. Catal.*, 2011, **281**, 352–360.

34 S. Wang and G. Q. Lu, *Ind. Eng. Chem. Res.*, 1997, **36**, 5103–5109.

35 A. Omri and M. Benzina, *J. la Société Chim. Tunisie*, 2012, **14**, 175–183.

36 M. C. S. Sierra, J. G. Ruiz, M. G. Proietti and J. Blasco, *J. Mol. Catal. A. Chem.*, 1995, **96**, 65–75.

37 T. P. Gujar, W. Y. Kim, I. Puspitasari, K. D. Jung and O. S. Joo, *Int. J. Electrochem. Sci.*, 2007, **2**, 666–673.

38 S. Johnson, Advantages & Disadvantages of XRD and XRF, https://sciencing.com/advantages-disadvantages-xrd-xrf-6054766.html, (accessed 14 January 2022).

39 J. Okal, M. Zawadzki and W. Tylus, *Appl. Catal. B Environ.*, 2011, **101**, 548–559.

40 C. Mun, J. J. Ehrhardt, J. Lambert and C. Madic, *Appl. Surf. Sci.*, 2007, **253**, 7613–7621.

41 H. Y. H. Chan, C. G. Takoudis and M. J. Weaver, *J. Catal.*, 1997, **172**, 336–345.

42 D. B. Thakur, R. M. Tiggelaar, T. M. C. Hoang, J. G. E. Gardeniers, L.

Lefferts and K. Seshan, *Appl. Catal. B Environ.*, 2011, **102**, 232–242.

43 J. Jae, W. Zheng, A. M. Karim, W. Guo, R. F. Lobo and D. G. Vlachos, *ChemCatChem*, 2014, **6**, 848–856.

44 P. A. Lazaridis, S. Karakoulia, A. Delimitis, S. M. Coman, V. I. Parvulescu and K. S. Triantafyllidis, *Catal. Today*, 2015, **257**, 281–290.

45 M. Masuda, T. Tabata, O. Okada, B. J. Wood, G. T. Tong and J. G. Mccarty, *Stud. Surf. Sci. Catal.*, 1991, **68**, 185–193.

46 M. Osada, N. Hiyoshi, O. Sato, K. Arai and M. Shirai, *Energy and Fuels*, 2007, **21**, 1854–1858.

47 A. Aho, S. Roggan, O. A. Simakova, T. Salmi and D. Y. Murzin, *Catal. Today*, 2015, **241**, 195–199.

48 J. Becker, K. R. Raghupathi, J. St. Pierre, D. Zhao and R. T. Koodali, *J. Phys. Chem. C*, 2011, **115**, 13844–13850.

49 J. Zhao, W. Chen, Y. Zheng, X. Li and Z. Xu, *J. Mater. Sci.*, 2006, **41**, 5514–5518.

50 K. Baranowska, J. Okal and W. Tylus, *Appl. Catal. A Gen.*, 2016, **511**, 117–130.

51 H. Kobayashi, T. Komanoya, K. Hara and A. Fukuoka, *ChemSusChem*, 2010, **3**, 440–443.

6: Direct H_2O_2 Synthesis *via* Catalysts Prepared by a Microwave-Assisted Solvothermal Method

6.1: Introduction

Oxidising agents are predominantly used in chemical manufacturing processes in order to synthesise oxygen-functionalised compounds. Whilst molecular O_2 is the prototypical, preferable choice, it is often substituted with a range of compounds, including nitric acid and various halides and perchlorates. These are less hazardous and more practical to use; however, they can yield environmentally damaging by-products.[1] An alternative to these is hydrogen peroxide (H_2O_2). The simplest peroxide, H_2O_2 is a highly reactive compound that is derived from molecular oxygen; it is a potent oxidiser and antiseptic. It is a highly desirable oxidising agent due to the high amount of active oxygen that it contains by weight, and the by-products of its decomposition being the safe and environmentally friendly O_2 and H_2O.

Industrial-scale hydrogen peroxide production takes place using the anthraquinone oxidation (AO) process. The combination of H_2, atmospheric O_2, and an anthraquinone derivative, which acts as a catalytic carrier of the otherwise gaseous reactants, produces crude H_2O_2 which is then purified by solvent extraction and stabilised into various concentrations for subsequent use.

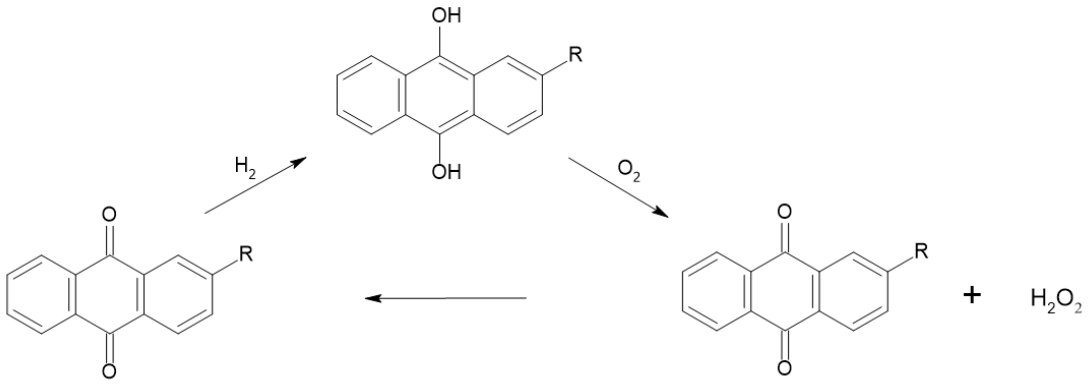

Figure 6-1: A simplified reaction pathway of the anthraquinone oxidation (AO) process for the synthesis of hydrogen peroxide.

The AO process is the source of practically all industrially manufactured hydrogen peroxide. It is well-established and safe, however it is inefficient, mainly due to the need to continuously refine the H_2O_2 that is produced and the need to remove contaminants, including over hydrogenated anthraquinone and solvents.[2] In addition, a centralised production method for producing H_2O_2 results in the need to transport highly concentrated solutions of it to areas where it is required, this being a hazard too great for certain applications.

An alternative to the anthraquinone oxidation process is to directly synthesise H_2O_2 from H_2 and O_2 with the use of a catalyst. In applications where only dilute concentrations of H_2O_2 are required, such as in the decontamination of wastewater,[3] a practical way of performing this is highly sought-after, and as a result, intensive research interest has been devoted to achieving it by several research groups over the previous few decades, with the Hutchings and Edwards groups within the Cardiff Catalysis Institute playing a leading role.[4] Amongst heterogeneous supported-metal catalysts that can produce H_2O_2 directly, those based on Pd, in particular bimetallic AuPd catalysts, are the most active and stable for the reaction.[5,6]

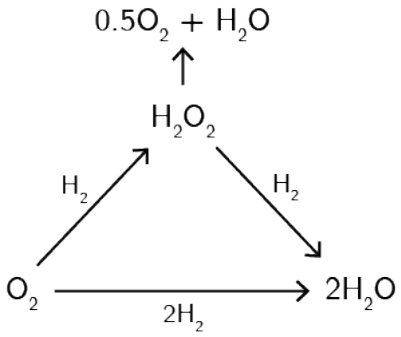

Figure 6-2: The competing reactions that take place over a H_2O_2 synthesis catalyst. This scheme demonstrates that the catalysts are also active for the hydrogenation of the peroxide into H_2O, highlighting one of the key challenges in synthesising H_2O_2 by this method. Adapted from work by Pritchard et al.[7]

Refinements to catalyst synthesis procedures and reaction parameters have resulted in AuPd catalysts with a high activity towards the synthesis of H_2O_2. One of the greatest challenges in their successful implementation, however, is that the same catalysts that are active for H_2O_2 synthesis are also highly active for its onward hydrogenation into water.[7] The greater the extent of this hydrogenation, the lower the selectivity of the

catalyst. As well as developing catalysts to be as active as possible, efforts have been made to inhibit the onward hydrogenation. In this regard, the choice of support material can have a large effect upon the activity of a given AuPd catalyst towards H_2O_2 hydrogenation. Ntainjua *et al.* stated that the isoelectric point of a given support plays a significant role in the extent to which the catalyst decomposes H_2O_2, with more acidic supports having a more selective production of it.[8] Edwards *et al.* reported that an acid pre-treatment of their activated carbon support material caused active site electronic modifications, resulting in a H_2 selectivity of $> 95\%$.[9]

The catalyst synthesis method has been found to influence the activity and selectivity of the resultant catalyst in direct H_2O_2 synthesis reactions. In previous investigations by the Hutchings and Edwards group, it has been found that core-shell structures with a Pd-rich shell are formed in AuPd catalysts when synthesised by impregnation methods, and the formation of these particle types was found to be a factor in the enhancement of catalytic activity for H_2O_2 formation.[10,11] Nanoparticle size and size distribution are also a significant factor in their activity. The use of the sol-immobilisation method for synthesising AuPd catalysts resulted in a higher number of small nanoparticles when compared to impregnation, which resulted in an enhancement in catalytic activity.[7]

In recent studies, it has been established that solvothermal catalyst preparation methods can yield catalysts that have a higher activity for direct H_2O_2 production than catalysts prepared by the aforementioned impregnation and sol-immobilisation methods.[12] Significant differences in the activity of solvothermally prepared catalysts were attributed to the modification of synthesis parameters, including the polyol solvent and the presence of stabilising agents.[13] For example, comparable PdSn catalysts prepared in ethylene glycol versus dimethyl formamide (DMF) resulted in markedly different activities (26 mol_{H2O2} kg_{cat}^{-1} h^{-1} for the PdSn catalyst prepared in DMF and 76 mol_{H2O2} kg_{cat}^{-1} h^{-1} for the catalyst prepared in ethylene glycol.

In previous investigations into solvothermally prepared catalysts for this reaction, AuPd/TiO_2 catalysts have been determined to be the most active compared to its monometallic counterparts, as is true for catalysts prepared by impregnation and sol-immobilisation. There is a desire to substitute both Au and Pd with more abundant and less expensive metals, as doing so would further increase the commercial viability of direct H_2O_2 synthesis catalysts if their efficiency is comparable.

One such metal that is a promising candidate for substituting in part, or replacing AuPd, is nickel. Nickel-based catalysts are widely used for selective hydrogenation processes, such as the conversion of unsaturated alkenes in the petrochemical industry,[14] and NiPd catalysts have already been reported to enhance the activity of Pd when tested for the direct synthesis of H_2O_2.[4] It is a much more abundant metal than Au and Pd, and its cost is a small fraction of that of either. At the time of writing, the trading price of Au and Pd is £42.50 and £46.23 per gram, respectively. Nickel's, conversely, is approximately 1.5p per gram. This study investigates the use of nickel in place of Au at three NiPd molar ratios, and subsequent characterisation will determine if differences in activity can be attributed to each catalyst's properties.

The procedures for the direct synthesis of H_2O_2 and for its degradation will be outlined in brief, as follows. For the direct synthesis reactions, 2.9 g of deionised water and 6.6 g of HPLC-grade methanol were added to a 35 mL Teflon-lined reactor vessel, along with 10 mg of catalyst. The reactor was sealed, then purged three times with 5% H_2/CO_2 in order to remove any atmospheric gases. The reactor was then charged with 28.9 bar of 5% H_2/CO_2, followed by 9.7 bar of 25% O_2/CO_2. The reactions took place at 25°C for 30 minutes before aliquots of the post-reaction solution were analysed for their H_2O_2 concentration by titration with acidified $Ce(SO_4)_4$. For H_2O_2 degradation assessments, 0.68 g of 50 wt.% H_2O_2 in H_2O, 2.22 g of deionised water and 6.6 g of HPLC-grade methanol were added to a 35 mL Teflon-lined reactor vessel, along with 10 mg of catalyst. The reactor was sealed, then purged three times with 5% H_2/CO_2 in order to remove any atmospheric gases. The reactor was then charged with 28.9 bar of 5% H_2/CO_2. The reactions took place at 25°C for 30 minutes before aliquots of the

post-reaction solution were analysed for their H_2O_2 concentration by titration with acidified $Ce(SO_4)_4$.

6.2: Results and Discussion

6.2.1: Catalyst Testing

6.2.1.1: Blank Reactions

To determine the activity of the support material and/or the reaction apparatus blank runs were initially performed with either an equivalent amount (10 mg) of bare P25 TiO_2 or no catalyst at all, added to direct synthesis and degradation reactions. The results of this are shown in Figure 6-3.

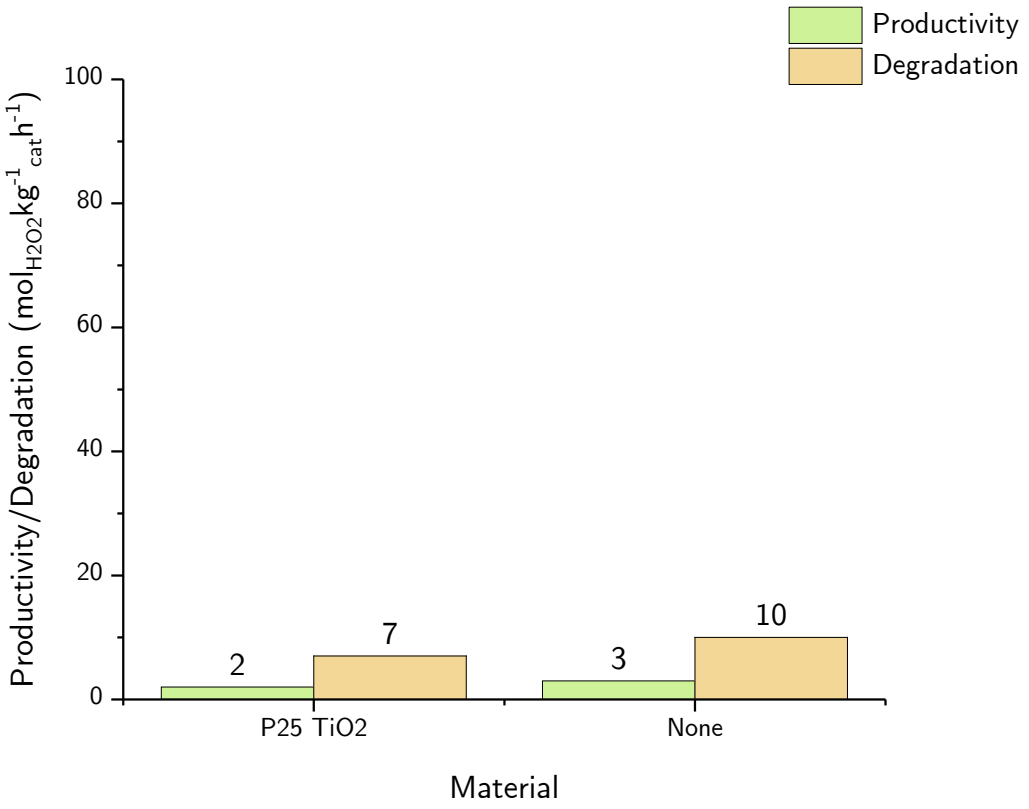

Figure 6-3: H_2O_2 productivity and degradation without the presence of an active catalyst. Reaction parameters: 2.9 g deionised H_2O, 6.6 g MeOH, 28.9 bar 5%H_2/CO_2, 9.7 bar 25% O_2/CO_2, 25°C, 0.5 h.

The synthesis activity of H_2O_2 in the presence of bare TiO_2 was 2 mol_{H2O2} kg_{cat}^{-1} h^{-1}, and in its absence, 3 mol_{H2O2} kg_{cat}^{-1} h^{-1} therefore both tests showed negligible H_2O_2 formation. The same is true for its degradation in the presence and absence of TiO_2, with values of 7 mol_{H2O2} kg_{cat}^{-1} h^{-1} and 10 mol_{H2O2} kg_{cat}^{-1} h^{-1}, respectively. This data shows that undoped P25 TiO_2 is inactive for direct H_2O_2 synthesis under standard conditions and does not contribute towards its degradation under the same conditions.

Therefore, the activity of any catalyst that was tested can be confidently attributed to the presence of the supported metal and the interactions between it and the support. These findings also confirm that the reaction apparatus itself was not playing a part in the reaction, neither was any contaminant present within it, indicating that an adequate level of cleaning and decontamination was being performed.

6.2.1.2: Monometallic x/TiO_2 Catalysts

The activity of monometallic 1 wt.% x/P25 TiO_2 catalysts (x = Au, Pd, Ni) was determined using the method detailed in Chapter 3, section 3.4.6. For all monometallic and bimetallic catalysts synthesised for this study, a 1 wt.% metal loading was chosen, as it was found in a previous investigation by Sankar *et al.* to result in catalysts with similar activities to those synthesised with higher metal loadings, alongside a significant reduction in the amount of metal used.[15] In short, a solution of each metal precursor was prepared in ethylene glycol, such that the concentration of metal in the solution totalled 10 mg in 20 mL of ethylene glycol. To this, 0.99 g of Degussa P25 TiO_2 was added, then the solution was heated and stirred under microwave heating at 150 °C for 10 minutes, then filtered, washed, and finally, dried in an oven at 110 °C overnight (16 hours). Each catalyst was evaluated for its H_2O_2 synthesis and hydrogenation activity using the method specified in Chapter 3, sections 3.4.6 and 3.4.7.

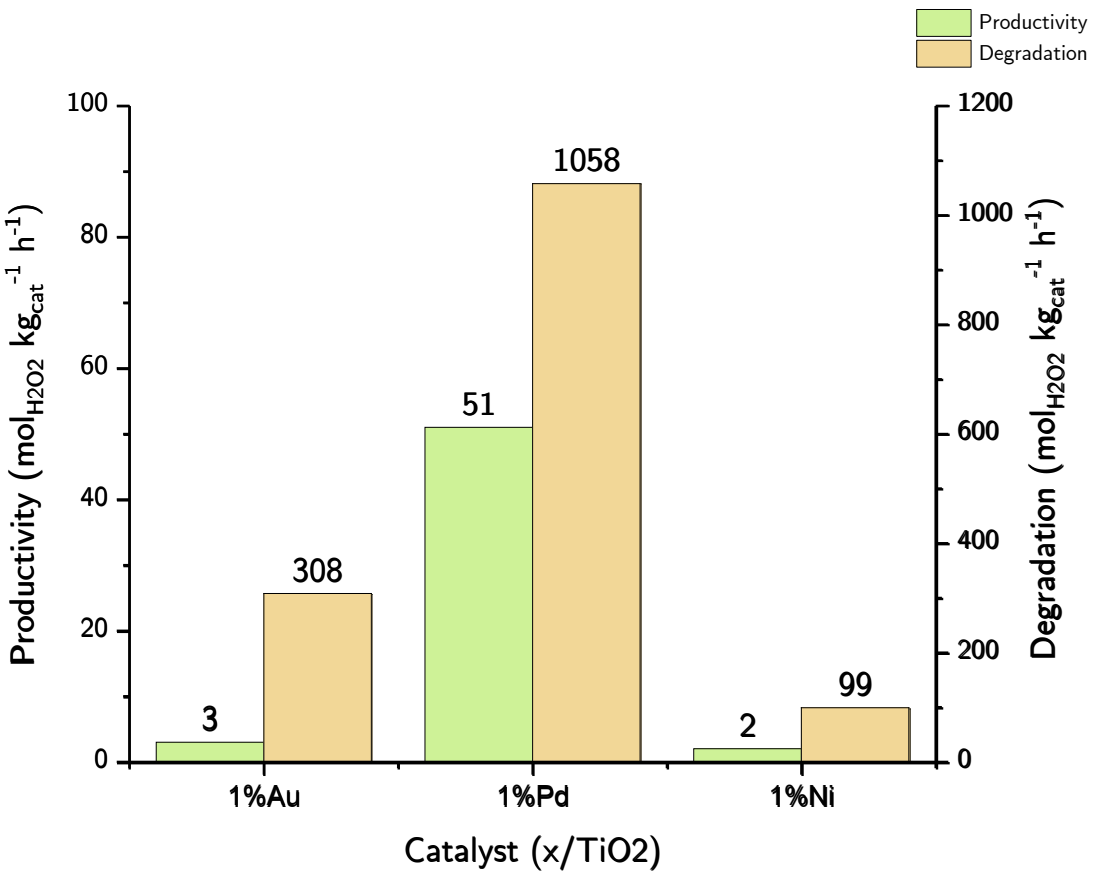

Catalyst	Synthesis Activity (mol$_{H2O2}$ kg$_{cat}^{-1}$ h^{-1})	Degradation Activity (mol$_{H2O2}$ kg$_{cat}^{-1}$ h^{-1})
1%Au/TiO$_2$	3	308
1%Pd/TiO$_2$	51	1058
1%Ni/TiO$_2$	2	99

Figure 6-4: H_2O_2 productivity and degradation over monometallic x/TiO_2 catalysts synthesised by the microwave-assisted polyol method. Catalyst synthesis temperature/time: 150 °C/10 minutes. Reaction parameters: 10 mg catalyst, 2.9 g deionised H_2O, 6.6 g MeOH, 28.9 bar 5%H_2/CO_2, 9.7 bar 25% O_2/CO_2, 25 °C, 0.5 h.

The synthesis activity of 1%Au/TiO_2 was negligible (3 mol$_{H2O2}$ kg$_{cat}^{-1}$ h^{-1}) at the standard conditions. This is in line with previously reported values, Edwards *et al.*'s 5%Au/TiO_2 catalyst prepared by impregnation achieved a H_2O_2 synthesis rate of 7 mol$_{H2O2}$ kg$_{cat}^{-1}$ h^{-1}.[10] Despite its inactivity for synthesis, it was moderately active for its degradation, at 308 mol$_{H2O2}$ kg$_{cat}^{-1}$ h^{-1} . The role of both Au and Pd in the synthesis of H_2O_2 and its further hydrogenation to water has been investigated by Agarwal *et al.* in a DFT study. The initial step in the production of H_2O_2 is energetically feasible to proceed either *via* the hydrogenation of adsorbed O_2 by dissolved H_2, or *via* the

protonation of adsorbed O_2 by solvent water, with the latter being the favoured route based on the available concentration of H_2O in experimental conditions. It was calculated that the oxidation capacity of Pd is far greater than that of Au, the extent of which plays a key role in the formation of H_2O_2, which would explain Au's inactivity when present alone. Rather than directly synthesising H_2O_2 alone, the role of Au in an AuPd system is posed to be, in chief, to limit the oxidation of active sites, thereby limiting the formation of H_2O that is produced by their subsequent re-reduction by H_2,[16] although there are a number of structural and electronic effects that have been attributed to the synergistic effect of the Au/Pd system,[17] which result in AuPd catalysts achieving a greater selectivity towards H_2O_2 than those based on Pd alone.[18]

6.2.1.3: Bimetallic x-y/TiO_2 Catalysts

The preparation of bimetallic x-y/TiO_2 (x = Au, Ni; y = Pd) catalysts was performed using the method detailed in Chapter 3, section 3.2.1. In short, solutions of each metal precursor were prepared in ethylene glycol, such that the total concentration of metal in the solution totalled 10 mg in 20 mL of EG. To this, 0.99g of Degussa P25 TiO_2 was added, then the solution was heated and stirred under microwave heating at 150 °C for 10 minutes, then filtered, washed, and finally, dried in an oven at 110°C overnight (16 hours). Each catalyst was then tested for its H_2O_2 synthesis and hydrogenation activity.

A variety of metal concentrations were investigated to determine the optimum concentrations of metal in the final catalysts for the direct synthesis reaction. As mentioned in the previous section, it has been demonstrated that AuPd/TiO_2 catalysts display a synergistic effect towards H_2O_2 synthesis when compared to their monometallic counterparts. In addition, when a series of AuPd catalysts were prepared using a modified impregnation method and tested at a comparable temperature to that used during this study (20 °C), the synthesis activity of reduced AuPd catalysts increased from 60 to 67 $mol_{H2O2}\ kg_{cat}^{-1}\ h^{-1}$ when the total metal loading was reduced from 5 wt.% to 1 wt.%.[19] Once a total metal loading of 1 wt.% was decided upon, it was then decided to investigate the effect of modifying the ratio of each metal within

its 1wt.% loading. Here, the exact amount of each metal added for the bimetallic catalysts was based on a molar ratio. For example, 1%AuPd(1:1)/TiO_2 signifies that a 1:1 ratio of atoms within an overall metal-support ratio of 1 wt.% was the intended result. 1 wt.% AuPd/TiO_2 and NiPd/TiO_2 catalysts were synthesised using an overall metal-support ratio of 1 wt.%, using three metal-metal ratios (2:1, 1:1, and 1:2) within that quantity. The results of this testing are shown in Figure 6-5.

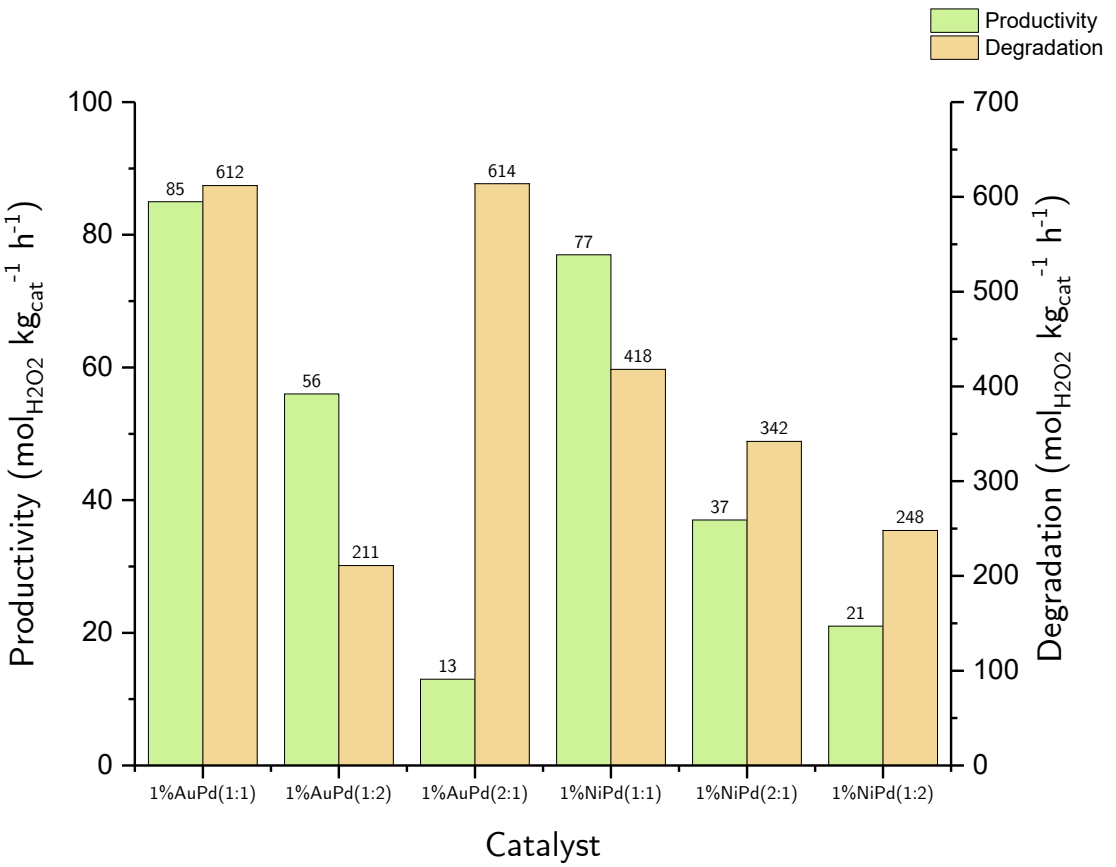

Catalyst	Synthesis Activity (mol$_{H2O2}$ kg$^{-1}_{cat}$ h^{-1})	Degradation Activity (mol$_{H2O2}$ kg$^{-1}_{cat}$ h^{-1})
1%AuPd (1:1)/TiO_2	85	612
1%AuPd (1:2)/TiO_2	56	211
1%AuPd (2:1)/TiO_2	13	614
1%NiPd (1:1)/TiO_2	77	418
1%NiPd (2:1)/TiO_2	37	342
1%NiPd (1:2)/TiO_2	21	248

Figure 6-5: H_2O_2 productivity and degradation over bimetallic x-y/TiO_2 catalysts synthesised by the microwave-assisted polyol method. Catalyst synthesis temperature/time: 150°C/10 minutes. Reaction parameters: 10 mg catalyst, 2.9 g deionised H_2O, 6.6 g MeOH, 28.9 bar 5%H_2/CO_2, 9.7 bar 25% O_2/CO_2, 25°C, 0.5h.

The most active catalyst for both the synthesis and degradation reactions was AuPd(1:1)/TiO_2, with a synthesis activity of 85 mol_{H2O2} kg^{-1}_{cat} h^{-1} and a degradation activity of 612 mol_{H2O2} kg^{-1}_{cat} h^{-1}. The 1:2 Au:Pd catalyst showed a reduction in the synthesis activity (56 mol_{H2O2} kg^{-1}_{cat} h^{-1}) with a much more pronounced reduction in hydrogenation activity of 211 mol_{H2O2} kg^{-1}_{cat} h^{-1} compared to the 1:1 catalyst. The Au

rich 2:1 catalyst showed a much-reduced synthesis activity of 13 mol_{H2O2} kg^{-1}_{cat} h^{-1} but interestingly had a degradation activity similar to the 1:1 catalyst, at 614 mol_{H2O2} kg^{-1}_{cat} h^{-1}. In short, increasing or decreasing the Au:Pd ratio from the optimum 1:1 ratio has a detrimental effect upon H_2O_2 productivity. A significant reduction in degradation activity was observed with a higher Pd to Au ratio, whereas the opposite is true when the amount of Au is greater.

For the NiPd catalysts, a similar trend was observed. The 1:1 molar ratio was also optimal in the case of the NiPd/TiO_2 catalysts. This catalyst performed comparably well against its 1:1 AuPd counterpart, with a synthesis activity of 77 mol_{H2O2} kg^{-1}_{cat} h^{-1} and degradation activity of 418 mol_{H2O2} kg^{-1}_{cat} h^{-1}, respectively. This makes it more active than Huynh *et al.*'s NiPd/C catalyst, which had a H_2O_2 synthesis activity of 43.3 mol_{H2O2} kg^{-1}_{cat} h^{-1}, however when they combined activated carbon with TiO_2, their mixed-support NiPd catalysts had a superior synthesis activity of 83.3 mol_{H2O2} kg^{-1}_{cat} h^{-1}. This indicates that carbon-doping may increase the activity of the NiPd catalysts synthesised for this study. In a similar pattern to the AuPd catalysts, a higher or lower Pd-Ni ratio away from this optimum 1:1 molar ratio resulted in lower H_2O_2 productivities, with the most pronounced reduction occurring for the 1:2 NiPd catalyst.

From this series of tests, it can be concluded that the optimal ratio of metals for each catalyst is a 1:1 molar ratio for catalysts prepared by this synthesis methodology and evaluated for H_2O_2 synthesis. The 1:1 AuPd catalysts are the most active for the H_2O_2 synthesis reaction at 85 mol_{H2O2} kg^{-1}_{cat} h^{-1}, which is higher than values previously reported in the reviewed literature for 1 wt.% AuPd catalysts that were tested for this reaction. The NiPd catalysts show almost the same synthesis activity (77 mol_{H2O2} kg^{-1}_{cat} h^{-1}) with a reduced degradation activity compared to the AuPd catalyst (418 mol_{H2O2} kg^{-1}_{cat} h^{-1} vs 612 mol_{H2O2} kg^{-1}_{cat} h^{-1}) respectively.

6.2.2: Catalyst Characterisation

6.2.2.1: Microwave-Plasma Atomic Emission Spectroscopy

The exact metal loadings of the monometallic 1wt.% x/TiO_2 (x = Au, Pd, Ni) and bimetallic 1 wt.% x-y/TiO_2 (x = Au, Ni; y = Pd) catalysts was determined by MP-AES. Briefly, 100 mg of each catalyst was digested in 10 mL of aqua regia. Once digestion was complete, the solution was made up to 100 mL, filtered, then analysed for its metal content using the MP-AES instrument. This was done in order to determine if there was agreement between the nominal and actual values in terms of the attachment of the metal to the surface of the support. The results for the monometallic catalysts are given in Figure 6-6.

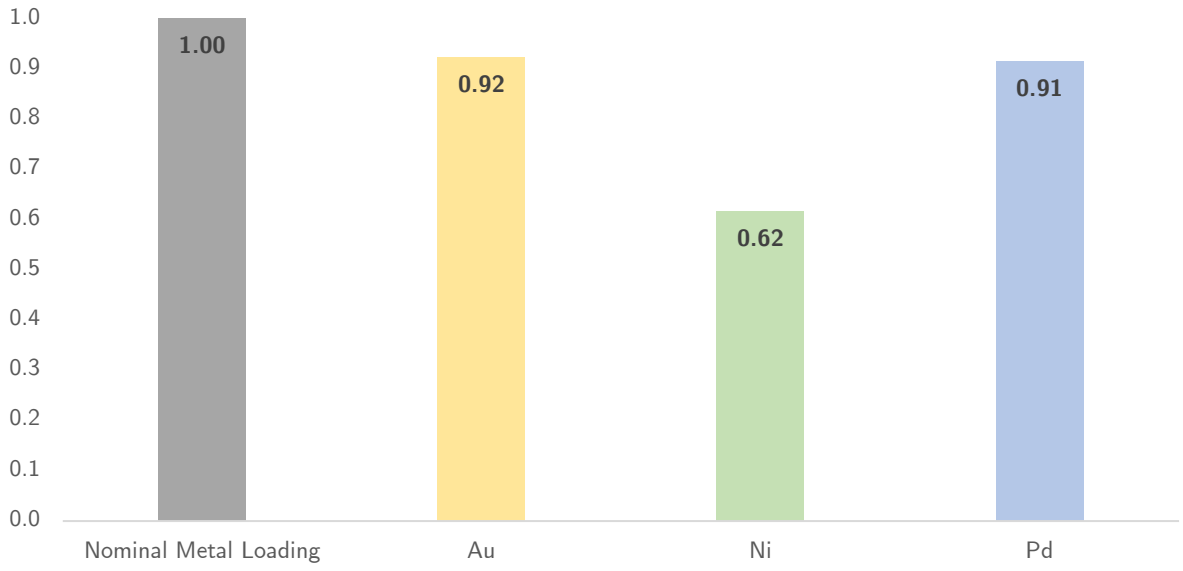

Figure 6-6: Metal loading values of each monometallic catalyst that was tested for their production of H_2O_2.

Both Au/TiO_2 and Pd/TiO_2 had a reasonable agreement with the nominal metal loading of 1 wt.%. Ni/TiO_2 had an incomplete or inadequate Ni attachment to the support, with only 62% of the Ni being deposited. This discrepancy is suspected to be due to the preparation temperature of the catalysts, which was kept constant across the series, at 150 °C. Whilst this data suggests that this temperature is adequate for the attachment of Au and Pd, this may not be the case for Ni. Jaji *et al.*'s solvothermal preparation of Ni nanoparticles takes place at 190°C. Their method for determining the extent of nickel nanoparticle formation from their $NiCl_2$ precursor was by UV/Vis

spectrometry. At 150 °C, nanoparticle formation was determined to be incomplete.[20] In future investigations, the use of a higher temperature for supported Ni catalysts that are prepared by this microwave polyol method may result in a more complete attachment of it to TiO_2.

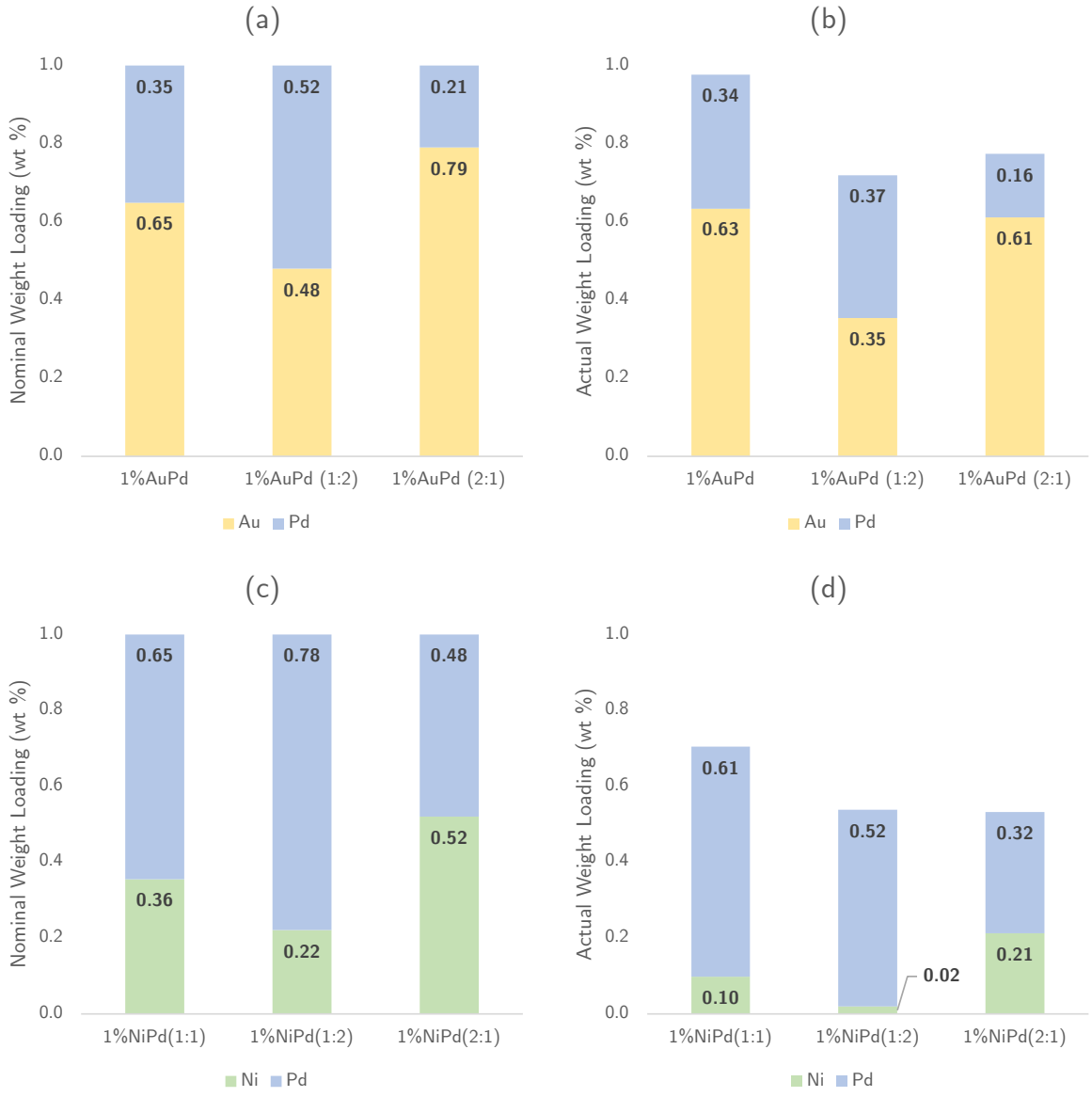

Figure 6-7: Metal loading values of each bimetallic AuPd and NiPd catalyst in the series. Graphs (a) and (c) represent the intended molar ratio of metals, expressed in weight percent, as a comparison to the actual values, shown in graphs (b) and (d).

Figure 6-7 is a visual representation of the expected and actual weight loadings of each bimetallic catalyst that was evaluated for the direct synthesis reaction. Charts (a) and (c) display the expected metal loading of each catalyst, converted to weight percent

from their intended molar ratios. Charts (b) and (d) show the actual values, as calculated from the MP-AES data.

The AuPd catalyst that showed the closest agreement both in terms of its overall metal loading and the ratio between its two metals is AuPd (1:1). The nominal metal loading of Au to Pd in this catalyst was 0.65 wt.% : 0.35 wt.%. The calculated loading was 0.63 wt.% : 0.34 wt.%, therefore it achieved 99% of its expected metal loading. As with AuPd (1:1), the relative composition of Au/Pd in the other two AuPd catalysts showed a good agreement with their expected values; however, less metal overall was deposited on AuPd (1:2) and AuPd (2:1). Palladium-rich AuPd (1:2) showed the greatest discrepancy between its nominal and actual weight loading, with 71% of the intended amount of metal deposited. Gold-rich AuPd (2:1) fared slightly better, with 77% of the intended amount of metal deposited.

Greater deviations are observed in the case of the NiPd catalysts, in line with the results of the monometallic Ni catalyst. As with the monometallic series of catalysts, Ni shows the greatest deviation in its loading, and as a result, the ratio of Ni:Pd within each NiPd catalyst is significantly lower than expected, which supports the statement made in the previous section regarding the catalyst preparation temperature being too low. As with AuPd (1:1), NiPd (1:1) shows the closest agreement with the nominal value, however the deviation itself is much more pronounced, with the catalyst achieving 71% of its overall intended metal loading. Nickel-rich NiPd (2:1) achieved an overall metal loading of 54% of its nominal value, with the greatest contributor to the discrepancy being attributed to Ni, which was deposited at just 6% of the intended amount. Palladium-rich NiPd (1:2) fared slightly better in terms of its Ni deposition, however, contained less metal than its nominal value, with 53% of the metal being deposited overall.

Combining the data for the exact metal loading of each catalyst with the moles of H_2O_2 formed allows for activity to be expressed as a function of the moles of metal present. The results of these calculations are shown in Figures 6-8 and 6-9.

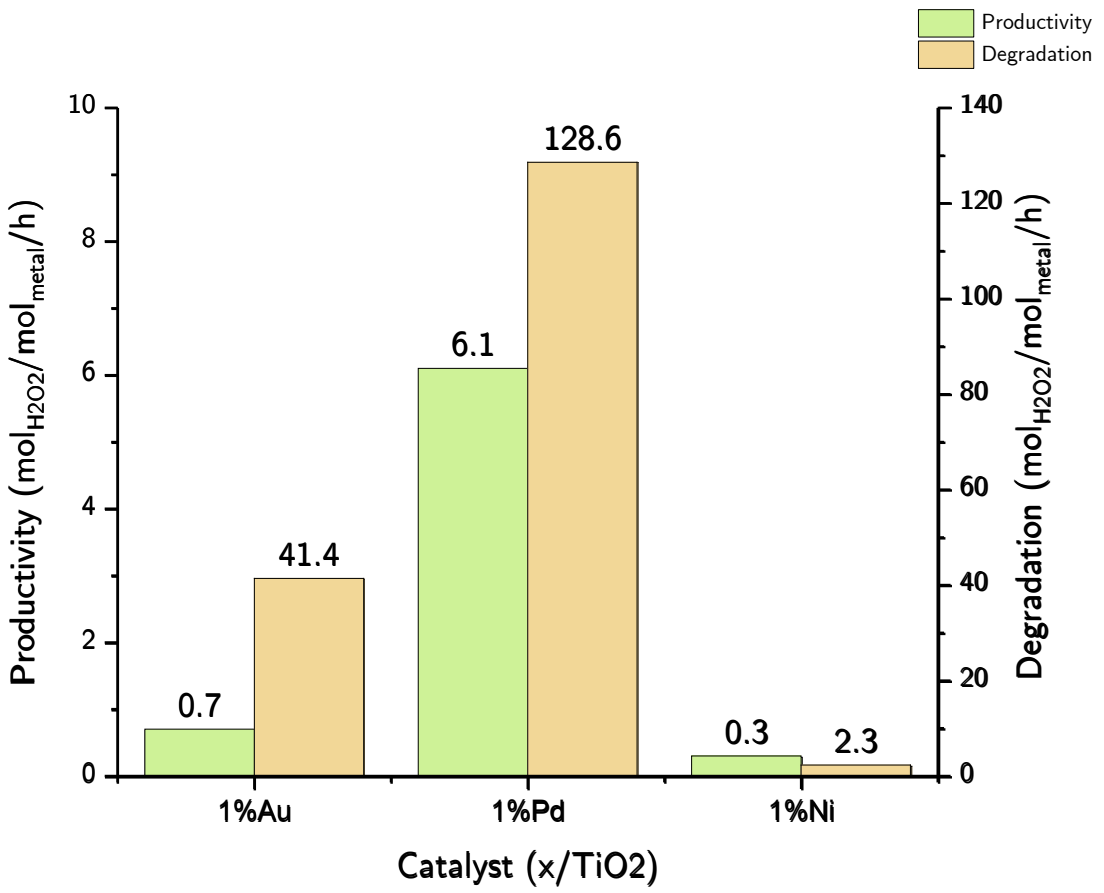

Catalyst	Synthesis Activity (mol_{H2O2} kg^{-1}_{cat} h^{-1})	Degradation Activity (mol_{H2O2} kg^{-1}_{cat} h^{-1})
1%Au/TiO₂	0.7	41.4
1%Pd/TiO₂	6.1	128.6
1%Ni/TiO₂	0.3	2.3

Figure 6-8: H_2O_2 productivity and degradation over monometallic x/TiO_2 catalysts synthesised by the microwave-assisted polyol method, with activity expressed in terms of the moles of H_2O_2 produced per mole of metal per hour. Catalyst synthesis temperature/time: 150°C/10 minutes. Reaction parameters: 10 mg catalyst, 2.9 g deionised H_2O, 6.6 g MeOH, 28.9 bar 5%H_2/CO_2, 9.7 bar 25% O_2/CO_2, 25°C, 0.5h.

In the case of the monometallic catalysts, expressing the activity in terms of the moles of H_2O_2 produced per mole of metal results in comparable trends to those seen when these values are expressed in terms of the moles of catalyst present. 1%Pd/TiO_2 remains the most active catalyst by a significant margin, at 6.1 mol_{H2O2} mol_{metal} h^{-1}, when compared to 1%Au/TiO_2 and 1%Ni/TiO_2, with activities of 0.7 and 0.3 mol_{H2O2} mol_{metal} h^{-1}, respectively. Both Au and Pd had a much closer agreement to their nominal values for weight loading than Ni, and although Ni's metal loading in

1%Ni/TiO_2 was lower than that of Au or Pd, its lack of activity for H_2O_2 synthesis is even more pronounced in this instance.

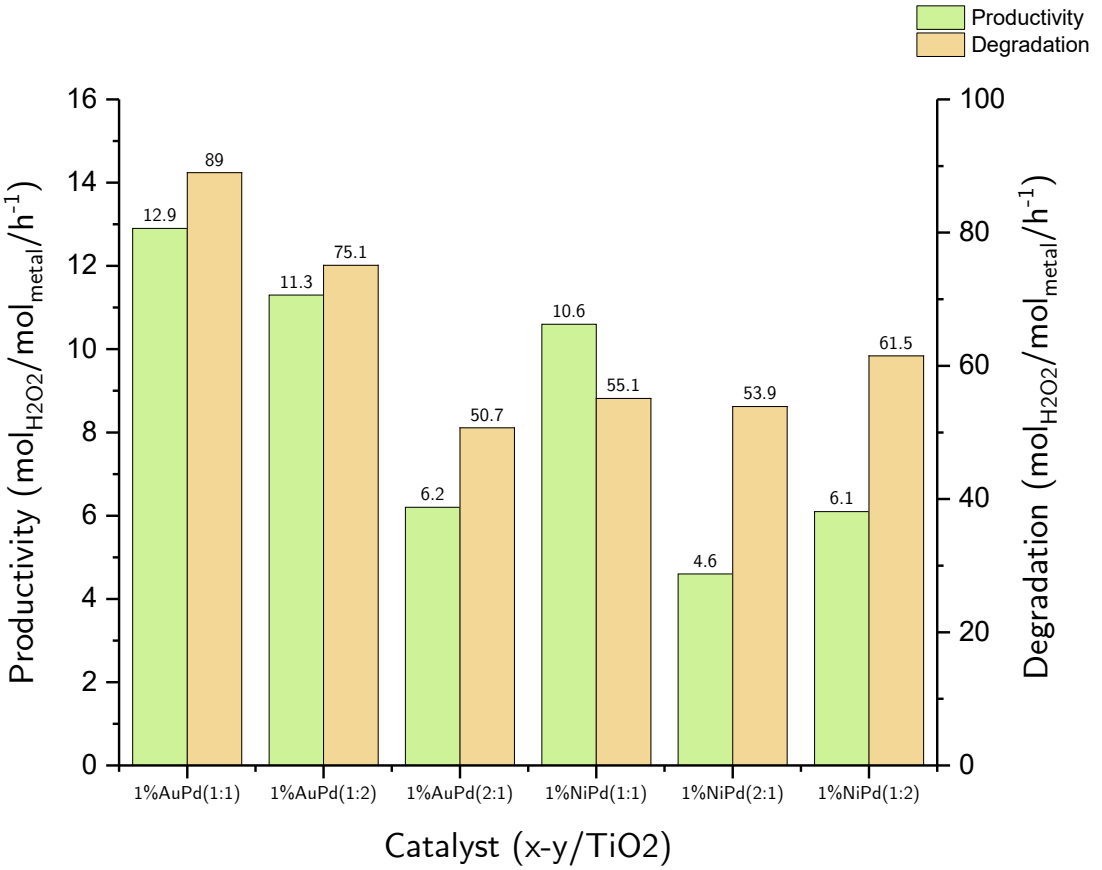

Catalyst	Synthesis Activity (mol_{H2O2} mol_{metal} h^{-1})	Degradation Activity (mol_{H2O2} mol_{metal} h^{-1})
1%AuPd (1:1)/TiO_2	12.9	89
1%AuPd (1:2)/TiO_2	11.3	76.1
1%AuPd (2:1)/TiO_2	6.2	50.7
1%NiPd (1:1)/TiO_2	10.6	56.1
1%NiPd (2:1)/TiO_2	4.6	53.9
1%NiPd (1:2)/TiO_2	6.1	61.5

Figure 6-9: H_2O_2 productivity and degradation over bimetallic x-y/TiO_2 catalysts synthesised by the microwave-assisted polyol method, with activity expressed in terms of the moles of H_2O_2 produced per mole of metal per hour. Catalyst synthesis temperature/time: 150 °C/10 minutes. Reaction parameters: 10 mg catalyst, 2.9 g deionised H_2O, 6.6 g MeOH, 28.9 bar 5%H_2/CO_2, 9.7 bar 25% O_2/CO_2, 25°C, 0.5h.

When the actual metal loadings of each catalyst are taken into account, the H_2O_2 synthesis activity of the AuPd and NiPd catalysts have a greater parity with each

other. AuPd (1:1) remains the most active catalyst, producing 12.9 mol_{H2O2} mol_{metal} h^{-1}. Palladium-rich AuPd (1:2) produced 11.3 mol_{H2O2} mol_{metal} h^{-1}, again placing it in the middle of the range, followed by gold-rich AuPd (2:1), which produced 6.2 mol_{H2O2} mol_{metal} h^{-1}. The NiPd catalysts follow the same pattern of activity as their AuPd analogues, with NiPd (1:1) being the most active catalyst of the series, producing 10.6 mol_{H2O2} mol_{metal} h^{-1}. Palladium-rich NiPd (1:2) produced 6.1 mol_{H2O2} mol_{metal} h^{-1}, whereas nickel-rich NiPd (2:1) produced 4.6 mol_{H2O2} mol_{metal} h^{-1}.

6.2.2.2: Inductively Coupled Plasma Mass Spectrometry (ICP-MS)

An important parameter to consider when investigating the suitability of a catalyst is the amount of metal that is leached from the support material during the catalytic reaction. An excessive rate of leaching can pose significant challenges to the implementation of a catalyst. The loss of valuable platinum group metals to the waste stream is both a financial and environmental concern, and the costs of replacing the catalyst increase significantly along with an increased rate of leaching/deactivation.

The amount of leaching from a selected number of bimetallic catalysts after a H_2O_2 synthesis reaction was determined by ICP-MS, a highly sensitive quantification technique based on atomic emission spectroscopy. The ICP-MS instrument's limit of quantification and detection is of an order of magnitude lower than that of the MP-AES instrument used for the calculation of metal loadings. The lower limit of detection/quantification that is possible using ICP-MS allowed for the direct analysis of post-reaction solutions to take place in order to determine the amount of metals present.

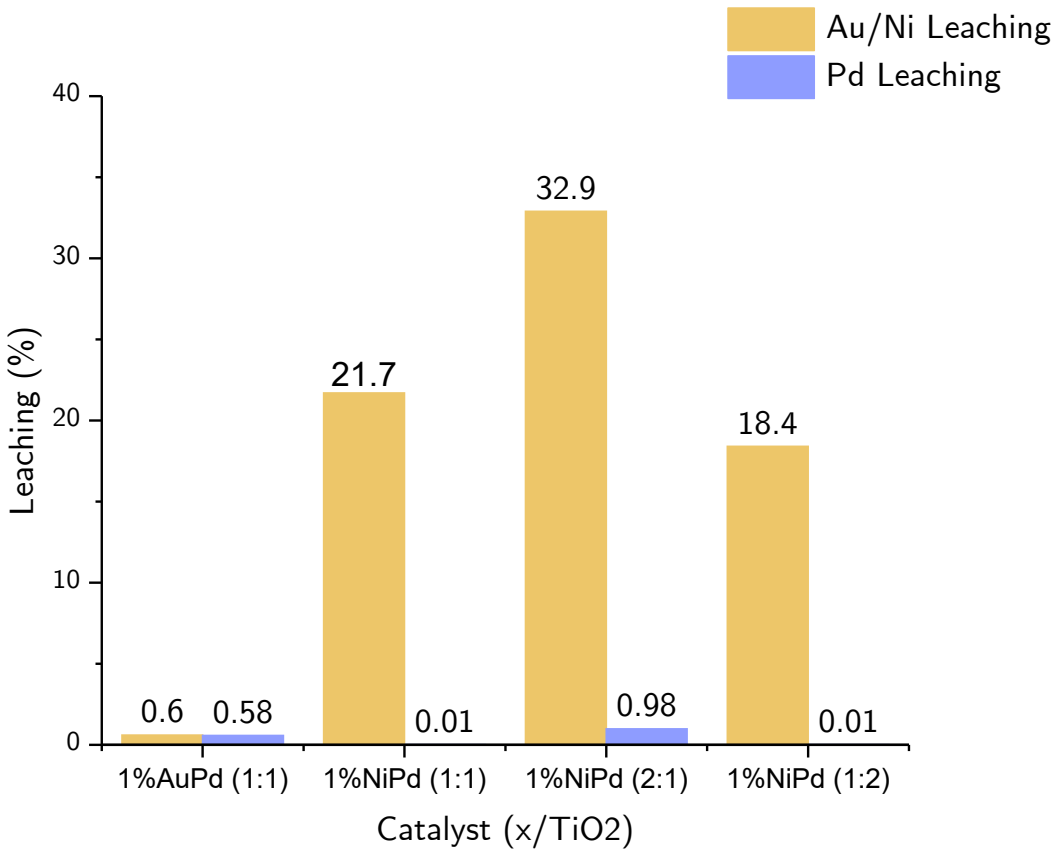

Figure 6-10: The extent of metal leaching from each NiPd/TiO_2 catalyst, along with a comparison with AuPd (1:1)/TiO_2.

To determine the extent of metal leaching, direct synthesis reactions were performed under the standard reaction conditions, the catalyst filtered, and the filtrate retained and submitted for ICP-MS analysis. The results are presented as a percentage of the measured metal loading of the original, untested catalysts, as determined by MP-AES. The results are shown in Figure 6-10.

AuPd (1:1) leached 0.6% of its Au and 0.58% of its Pd after the reaction. Edwards *et al.*'s 2.5%Au:2.5%Pd/TiO_2 catalysts that were prepared by an incipient wetness method did not leach any of its supported metal when calcined at 400 °C in air,[21] which indicates that although the extent of the leaching in the case of AuPd catalysts prepared by the microwave-assisted polyol method is minimal, it is not optimal. All NiPd catalysts leached significant amounts of their Ni after each reaction. The most nickel-rich catalyst, NiPd (2:1), leached the most amount of Ni, at 32.9%. Palladium-

rich NiPd (1:2) leached the least amount of Ni, at 18.4%. NiPd (1:1) leached 21.7% of its Ni, placing it in the middle of the range. From this data, it can be concluded that the more nickel that is present within NiPd catalysts prepared by the microwave-assisted polyol method, the greater the amount of it that is leached as a percentage of its overall content within the catalyst. This reinforces the statement that was made in section 6.2.2.1, where it was concluded that the catalyst synthesis temperature that was selected for this study did not adequately deposit Ni onto the catalyst's surface. Maity *et al.* reported that in their direct H_2O_2 synthesis reactions with NiPd catalysts, nickel was leaching significantly into their reaction solutions, based on ICP-AES analysis of their spent catalysts.[4] Soaking the catalysts for 0.5 hours eliminated this phenomenon, indicating that a pre-treatment of this nature for the NiPd catalysts may resolve the significant amount of leaching observed during this study.

6.2.2.3: X-Ray Photoelectron Spectroscopy

XPS analysis was performed on all monometallic and bimetallic TiO_2 catalysts. This was done in order to obtain information on each catalyst's surface loading, the oxidation state of the supported metals, and whether these parameters varied when the ratio of metals in bimetallic catalysts was varied.

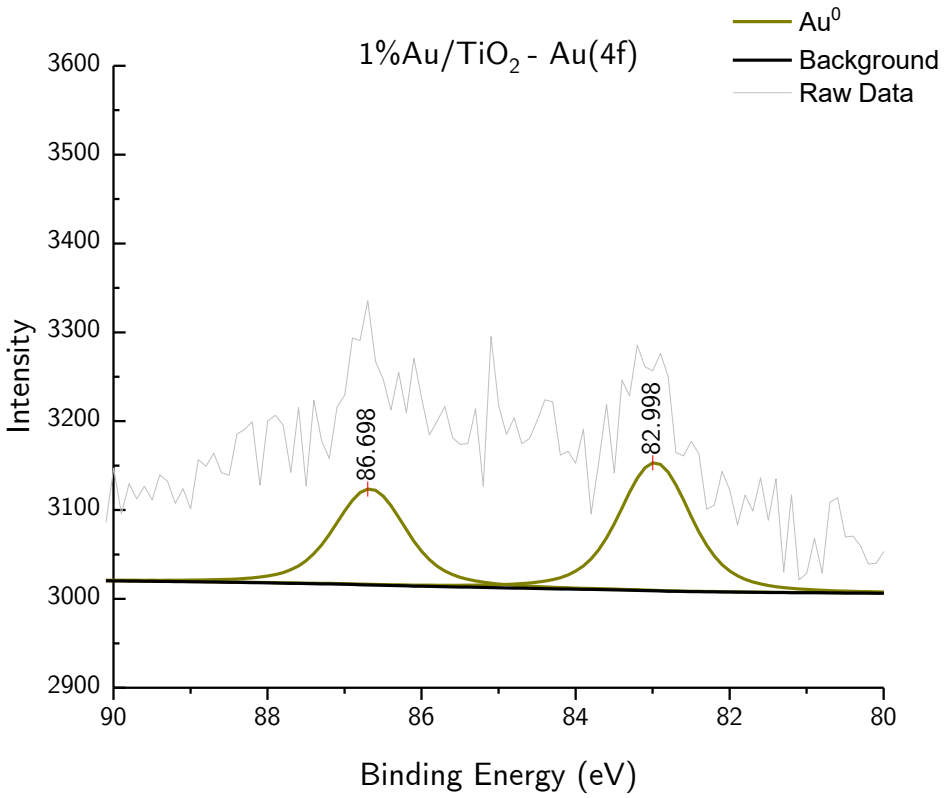

Figure 6-11: XPS narrow scan of the Au(4f) region of 1%Au/TiO_2, showing a spin-orbit component separation of 3.7 eV.

The Au($4f_{7/2}$) binding energy of Au^0 is 84.0 eV, however in 1%Au/TiO_2, this is shifted by ≈ 1 eV. This shift is attributed to the binding of Au to a metal oxide support, which has been reported to shift its binding energy by as much as 1.4 eV depending on the support type. Table 6-1 shows the elemental composition of the surface of the catalyst.

Element	XPS Surface Concentration (At%)
Au^0	0.02
Ti	21.32
O	53.64
C	26.02

Table 6-1: XPS elemental surface composition of 1%Au/TiO_2

The significant quantity of carbon detected on the surface of the catalyst is attributed to the catalyst preparation method. Howe *et al.* noted the deposition of complex carbonaceous species onto the surface of Ru/TiO_2 catalysts prepared by a similar microwave-assisted solvothermal method, attributed to the decomposition of the polyol

at elevated temperatures. Its presence did not appear to detrimentally affect catalytic performance.[22]

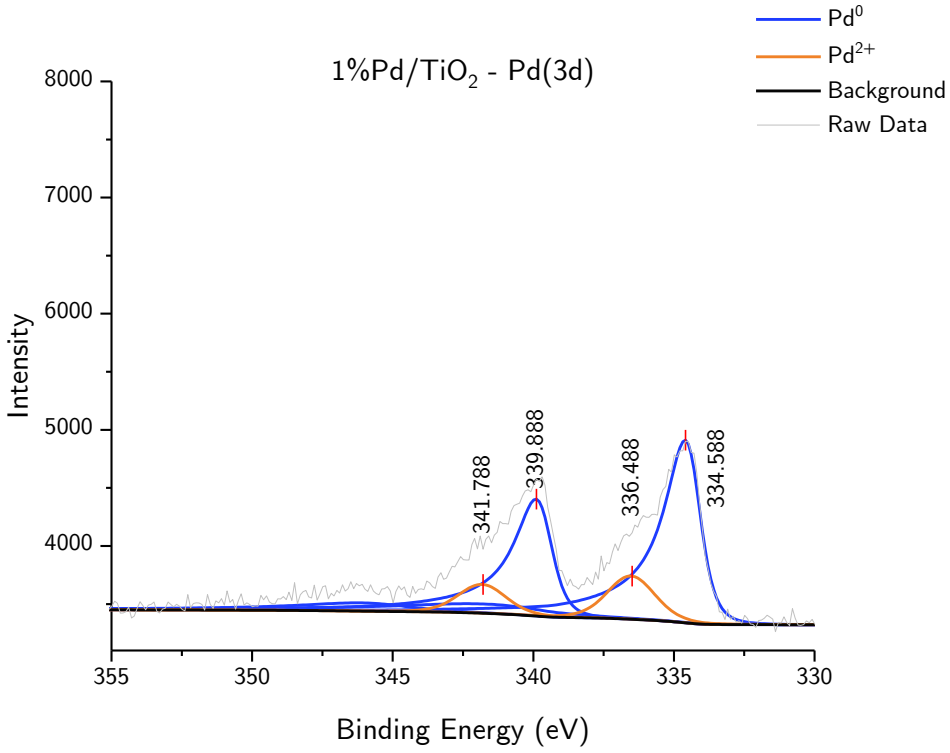

Figure 6-12: XPS narrow scan of the Pd(3d) region of 1%Pd/TiO_2, with its spin-orbit separation of 6.3 eV. Both Pd^0 and Pd^{2+} were observed.

In a similar fashion to 1%Au/TiO_2, the observed binding energy of the Pd($3d_{5/2}$) is 334.588 eV, which is shifted from the binding energy of Pd foil by 0.41 eV, attributed to the binding of Pd to a metal oxide support. The binding energy at 336.488 eV is attributed to Pd^{2+}, present as PdO.

Element	XPS Surface Concentration (At%)	
Pd^0	0.4	**Pd^0/Pd^{2+} Ratio** = 5:1
Pd^{2+}	0.08	
Ti	22.19	
O	47.35	
C	22.37	

Table 6-2: XPS elemental surface composition of 1%Pd/TiO_2

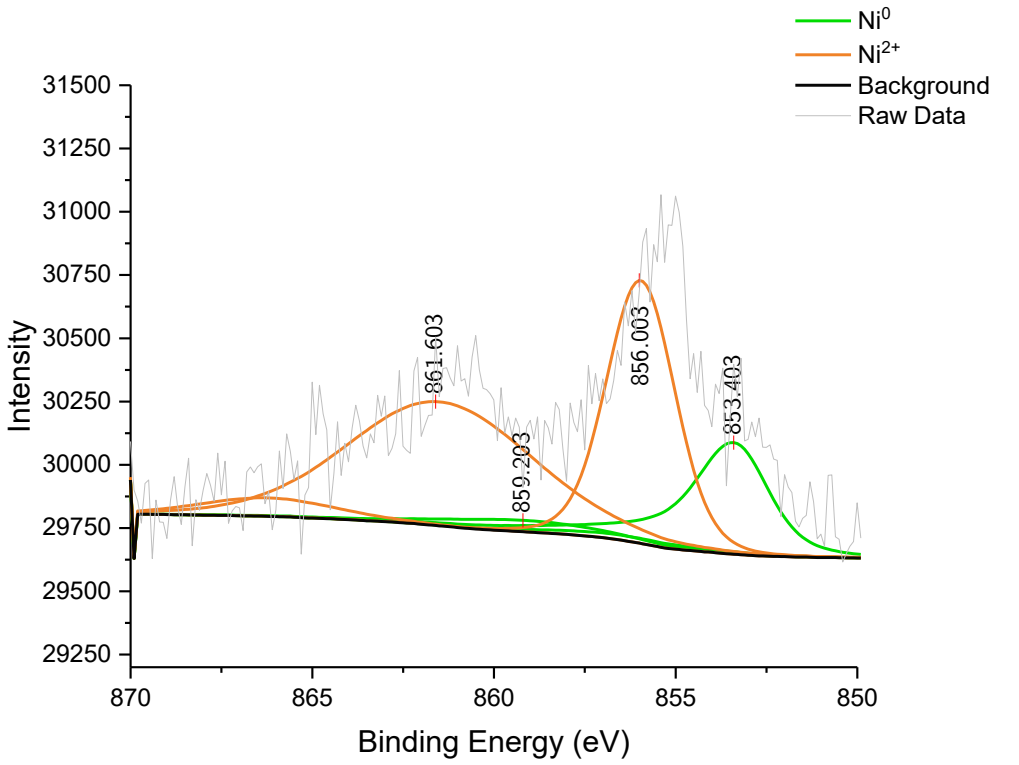

Figure 6-13: XPS narrow scan of the Ni(2p) region of 1%Ni/TiO_2. Ni's characteristic and significant spin-orbit separation of 17.3 eV puts its second Ni($2p_{3/2}$) peaks out of the range of this scan. The binding energy at 856.003 eV is attributed to Ni^{2+}, present predominantly as $Ni(OH)_2$.[23]

The binding of Ni^0 foil is reported to be 852.6 eV, with the shift of 0.8 eV of its Ni($2p_{3/2}$) peak attributed to the binding of Ni particles to the TiO_2 support. The Ni^{2+} binding energy of 856 eV is attributed to the presence of $Ni(OH)_2$ on the catalyst's surface.

Element	XPS Surface Concentration (At%)	
Ni^0	0.1	**Ni^0/Ni^{2+} Ratio** = 1:3.2
Ni^{2+}	0.32	
Ti	16.00	
O	44.54	
C	40.05	

Table 6-3: XPS elemental surface composition of 1%Pd/TiO_2

Ni^{2+} is present as $Ni(OH)_2$ on the surface of this catalyst, based on its calculated binding energy from XPS data. Nickel is predominantly present in this form on the surface, being 3.2 times as abundant than Ni^0. This finding reinforces the statement made in section 6.2.2.1, where it was concluded that the catalyst preparation temperature that was used for the catalysts was insufficient for a complete attachment

of Ni to the support, with the additional finding that the attached Ni had not been reduced to the same extent as Pd on the 1%Pd/TiO_2 catalyst.

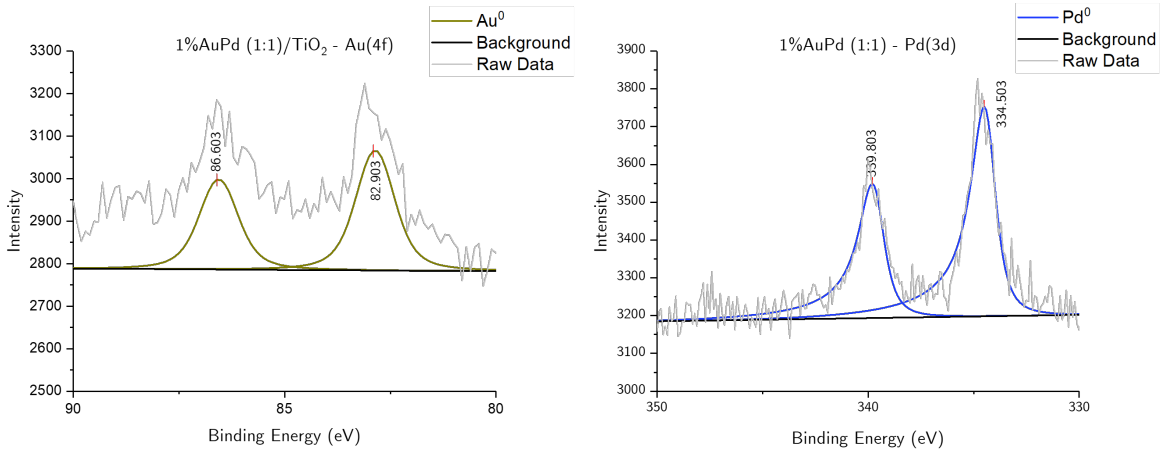

Figure 6-14: XPS narrow scans of the Au(4f) and Pd(3d) regions of 1%AuPd (1:1)/TiO_2.

Figure 6-14 shows the XPS narrow scans of AuPd (1:1)'s Au(4f) and Pd(3d) regions. As was observed with the corresponding Au and Pd monometallic catalysts, the binding energies of Au(4f) and Pd(3d) are shifted due to the interaction between the metals and the TiO_2 support material. Both Au and Pd are present in their fully reduced forms; no contributions arising from Pd^{2+} were observed, as was the case with the monometallic Pd catalyst.

Element	XPS Surface Concentration (At%)	
Au	0.04	**Au/Pd Ratio** = 1:3
Pd	0.12	
Ti	20.99	
O	53.69	
C	22.24	

Table 6-4: XPS elemental surface composition of 1%AuPd (1:1)/TiO_2, along with the ratio of Au/Pd.

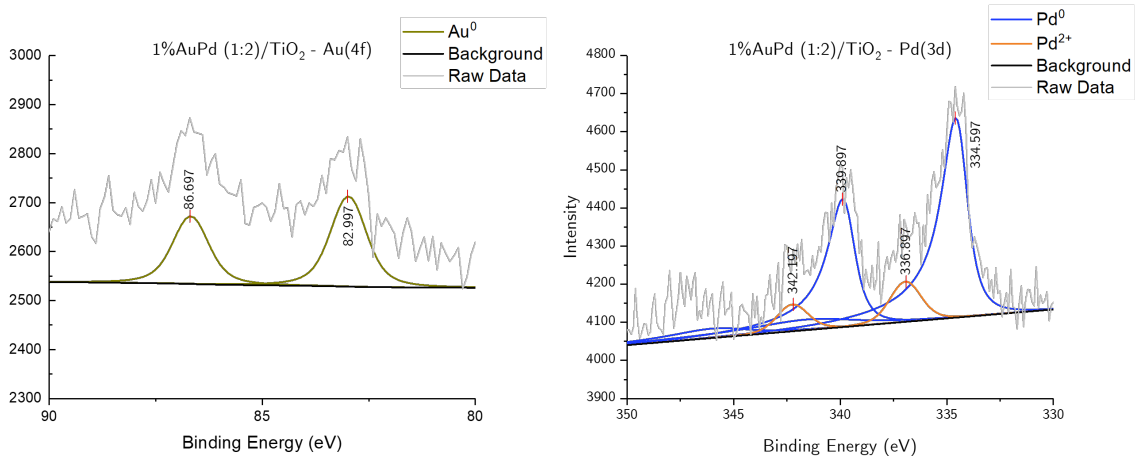

Figure 6-15: XPS narrow scans of the Au(4f) and Pd(3d) regions of 1%AuPd (1:2)/TiO_2.

Figure 6-15 shows the XPS narrow scans of palladium rich AuPd (1:2)'s Au(4f) and Pd(3d) regions. Au($4f_{7/2}$)'s binding energy in this case is 82.997 eV, again shifted from its typical binding energy by ≈ 1 eV due to metal-support interactions. Pd($3d_{5/2}$)'s binding energy is 334.597 eV, shifted from that of Pd foil by 0.403 eV. In this case, a proportion of Pd was present in its oxidized form, as PdO. Table 6-5 gives the elemental composition of the catalyst, along with the ratio of Au/Pd and the ratio of Pd^0/Pd^{2+} within the Pd component.

Element	XPS Surface Concentration (At%)	
Au	0.02	**Au/Pd Ratio** = 1:3 **Pd^0/Pd^{2+} Ratio** = 5:1
Pd^0	0.12	
Pd^{2+}	0.02	
Ti	16.41	
O	44.4	
C	40.04	

Table 6-5: XPS elemental surface composition of 1%AuPd (1:2)/TiO_2, along with the ratio of Au/Pd and Pd^0/Pd^{2+}

Despite the larger proportion of Pd present in this catalyst by molar ratio, the ratio of Au/Pd on the surface remains unchanged from that of AuPd (1:1), at 1:3. The ratio of Pd^0/Pd^{2+} is identical to that of the monometallic Pd/TiO_2 catalyst.

Figure 6-16 shows the XPS narrow scans of gold rich AuPd (2:1)'s Au(4f) and Pd(3d) regions.

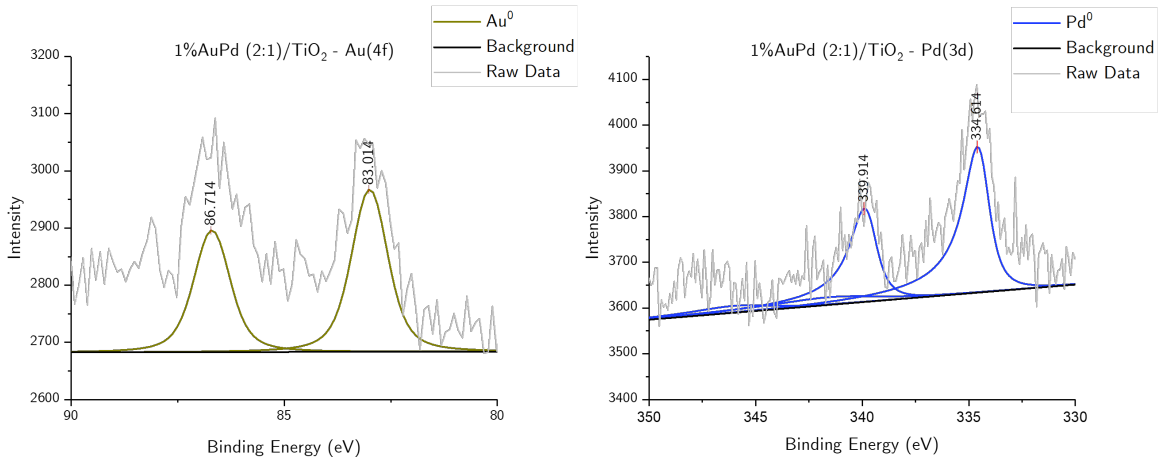

Figure 6-16: XPS narrow scans of the Au(4f) and Pd(3d) regions of 1%AuPd (2:1)/TiO_2

As was the case with AuPd(1:1), both Au and Pd are present in their reduced forms. It appears from the analysis of this data that the incremental addition of Au to an AuPd catalyst stabilises the Pd, preventing its oxidation to PdO on the surface.

Element	XPS Surface Concentration (At%)	
Au	0.03	**Au/Pd Ratio** = 1:3
Pd	0.09	
Ti	18.34	
O	48.64	
C	32.9	

Table 6-6: XPS elemental surface composition of 1%AuPd (2:1)/TiO_2, along with the ratio of Au/Pd.

As is the case with the two other AuPd catalysts with varying molar ratios of Au/Pd, the surface Au/Pd ratio of this gold-rich catalyst is 1:3. Despite XPS being a surface sensitive technique, it is not purely so. The sampling of most elements analysed by XPS will be of the first several nanometres, which at the scale of a typical nanoparticle, represents a significant quantity of its bulk. Therefore, it is not feasible to determine whether the AuPd catalysts prepared at varying Au/Pd ratios display core-shell structures, or are homogeneously alloyed, though it can be concluded from this data that within the uppermost layers of AuPd particles, the ratio of Au/Pd remains Pd-rich, despite varying the abundance of Au.

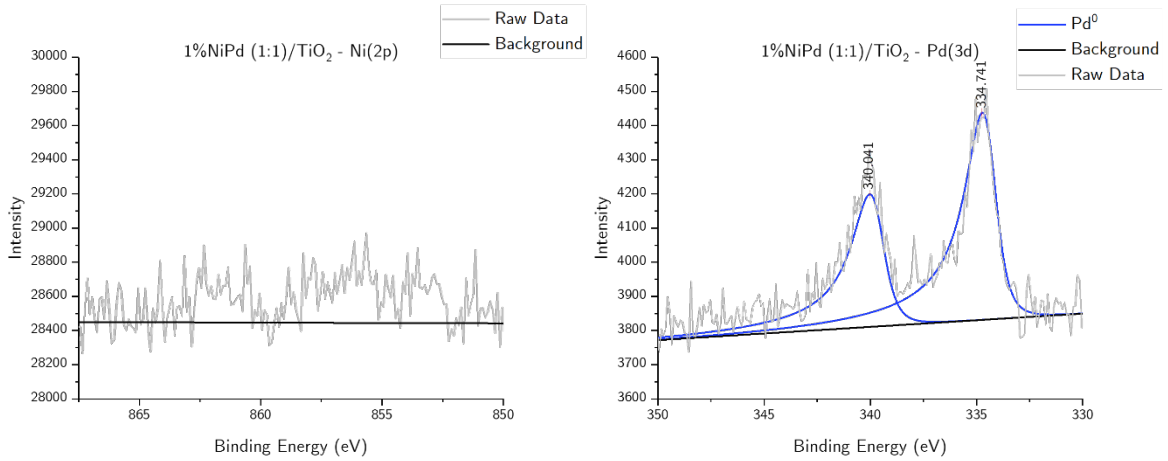

Figure 6-17: XPS narrow scans of the Ni(2p) and Pd(3d) regions of 1%NiPd (1:1)/TiO_2

Element	XPS Surface Concentration (At%)	
Ni	0.13	**Ni/Pd Ratio** = 1:1.15
Pd	0.15	
Ti	16.17	
O	46.95	
C	37.59	

Table 6-7: XPS elemental surface composition of 1%NiPd (1:1)/TiO_2, along with the ratio of Ni/Pd

Figure 6-17 shows the XPS narrow scans of NiPd (1:1)'s Ni(2p) and Pd(3d) regions. In the case of NiPd (1:1), the binding energy of Ni($2p_{3/2}$) or its satellite peaks could not be deconvoluted from the background reading. Pd($3d_{5/2}$)'s binding energy of 334.741 eV is a 0.26 eV shift from its expected value of 335 eV. This is a smaller shift than was observed in the case of all AuPd catalysts. It was suspected that this may indicate a weaker metal-support interaction in this catalyst; however, the size of the nanoparticles also has an effect on the binding energy of their corresponding metal. Zhou *et al.* reported a Pd binding energy shift of 0.21 eV as the size of analysed Pd particles decreased from 40 nm to 9 nm.[24] The binding energy of Pd is dependent on the properties of its surrounding matrix.[25] This makes any conclusive reason for the differences in its binding energy between NiPd and AuPd catalysts difficult to establish, however, the upward shift may indicate that NiPd (1:1) particles are smaller than their AuPd (1:1) counterpart. The practically equal Ni/Pd ratio indicates that the two metals are alloyed homogeneously on their surface layers.

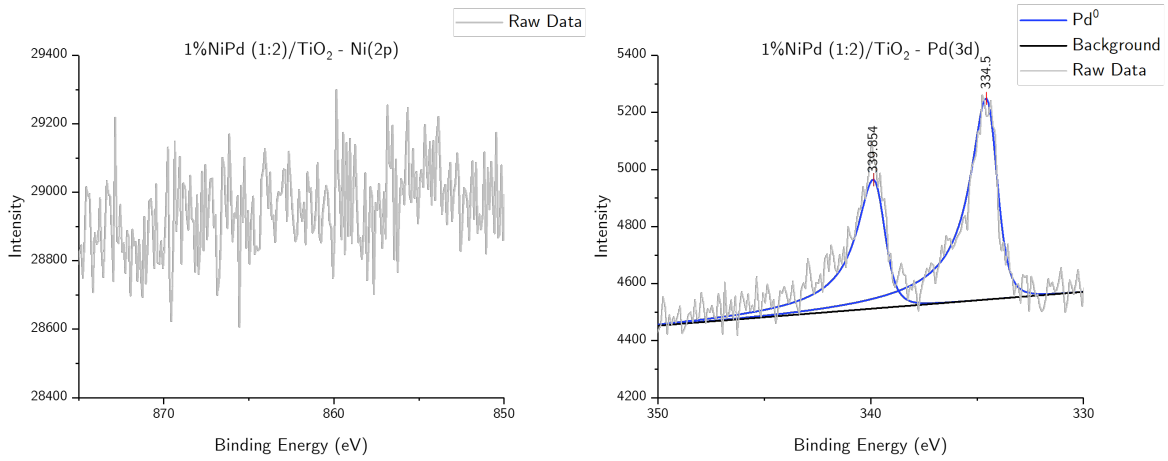

Figure 6-18: XPS narrow scans of the Ni(2p) and Pd(3d) regions of 1%NiPd (1:2)/TiO_2

Element	XPS Surface Concentration (At%)
Ni	
Pd	0.12
Ti	13.51
O	41.87
C	44.49

Table 6-8: XPS elemental surface composition of 1%NiPd (1:2)/TiO_2

Figure 6-18 shows the XPS narrow scans of NiPd (1:2)'s Ni(2p) and Pd(3d) regions. As with NiPd (1:1), the binding energy of Ni($2p_{3/2}$) or its satellite peaks could not be deconvoluted from the background reading. This catalyst was expected to have the lowest amount of Ni by molar ratio (0.1 wt.%) however its actual Ni content, as determined by MP-AES was even lower than expected, at just 0.02 wt.%, which may explain the difficulty in deconvoluting its peaks in this instance. Pd($3d_{5/2}$)'s binding energy is 334.554 eV, placing its shift from Pd foil (335 eV) at 0.45 eV, in line with those seen in the AuPd series of catalysts and that of the monometallic Pd catalyst. It appears that the less pronounced Ni/Pd interactions taking place in the absence of any significant quantity of Ni gives this catalyst the traits of its monometallic counterpart. This is reinforced by elemental surface composition data, which did not show any amount of Ni detected on the catalyst's surface.

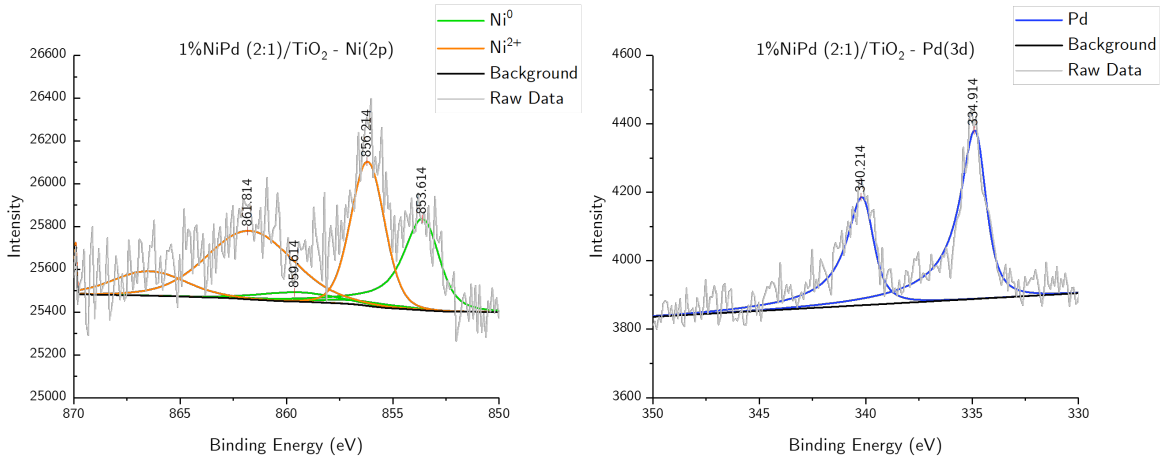

Figure 6-19: XPS narrow scans of the Ni(2p) and Pd(3d) regions of 1%NiPd (2:1)/TiO_2

Figure 6-19 shows the XPS narrow scans of NiPd (2:1)'s Ni(2p) and Pd(3d) regions. In contrast to NiPd (1:1) and NiPd (1:2), nickel rich NiPd (2:1) had characteristic Ni peaks which could be detected and deconvoluted.

Element	XPS Surface Concentration (At%)	
Ni^0	0.09	**Ni/Pd Ratio** = 3:1 **Ni^0/Ni^{2+} Ratio** = 1:2.3
Ni^{2+}	0.21	
Pd	0.10	
Ti	14.60	
O	43.32	
C	41.70	

Table 6-9: XPS elemental surface composition of 1%NiPd (1:1)/TiO_2, along with the ratio of Ni/Pd and ratio of Ni^0/Ni^{2+}

In contrast to AuPd catalysts, the ratio of Ni/Pd in nickel-rich NiPd (2:1) indicates that the particles are nickel-rich at their surfaces rather than Pd rich. Also here is further evidence that Ni was not fully reduced by the catalyst synthesis procedure, with Ni^{2+} being 2.3 times as abundant as metallic Ni^0. This NiPd catalyst was the least active for H_2O_2 synthesis, indicating that a higher concentration of nickel in an NiPd catalyst is detrimental to catalyst activity, perhaps due to its disproportionate concentration on the surface of the metal particles hindering the available Pd sites.

6.2.2.4: Scanning Electron Microscopy

Scanning electron microscopy, along with energy dispersive X-ray spectroscopy (EDX) was performed on two monometallic catalysts (Au/TiO_2 and Pd/TiO_2) and a bimetallic catalyst ($AuPd\ (1:1)/TiO_2$) in order to gain an understanding of surface morphology and particle size characteristics. In the case of the bimetallic catalyst, the relative composition of nanoparticles at two particle sizes of a relatively smaller and larger size (20nm and 40nm).

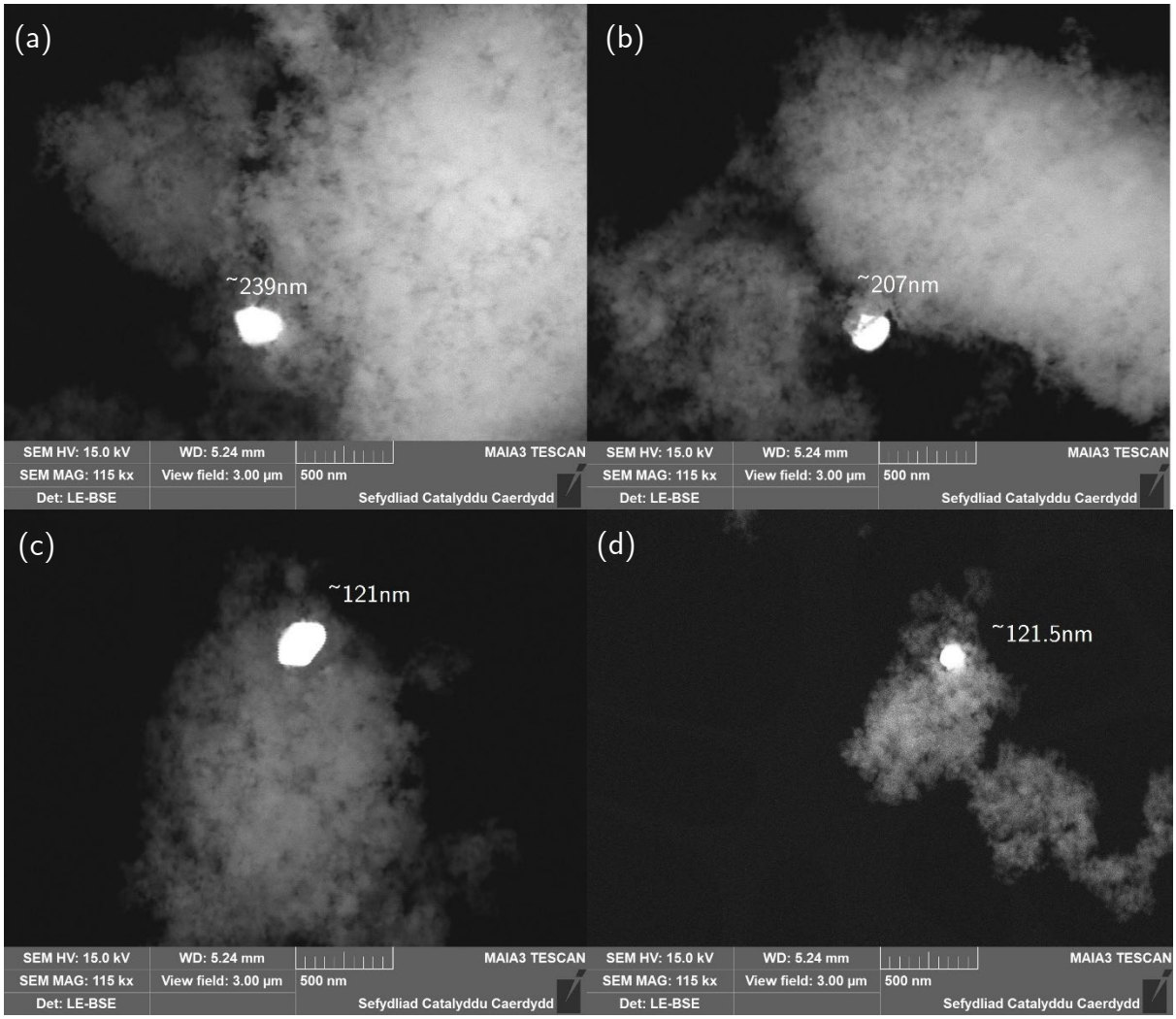

Figure 6-20: Representative FEG-SEM BSE images of 1%Au/TiO_2 (preparation temperature: 150 °C, preparation time: 10 minutes). Imaging parameters and the scale is shown in the information window below each image. All images were captured at 115kX magnification.

Images of 1%Au/TiO_2 in Figure 6-20 show large, poorly-dispersed particles, ranging from approximately 121 nm to 239 nm that, even at their smallest observed size, are larger than what is considered a 'nano' particle.[26] This phenomenon may be due to the

sintering of initially deposited smaller particles during the synthesis or in the time between synthesis and imaging. Smaller nanoparticles in the size ranges that are relevant for catalysis were not observed. These may be present, however due to the limitations of the resolution of the SEM, are not visible. A particle size distribution analysis, similar to that conducted for selected Ru/C catalysts using the TEM, would establish whether the Au is present exclusively as these 'meso' particles, or whether there is also a significant distribution of nanoparticles of various sizes. Even if this were to be the case, further investigations would be required to eliminate the formation of such large gold particles for Au/TiO_2 catalysts using the polyol synthesis technique. In future investigations, the activity of Au catalysts prepared by this synthesis technique could be compared to other supported Au catalyst types, using a reaction where such types are known to be active, such as the oxidation of carbon monoxide.[27]

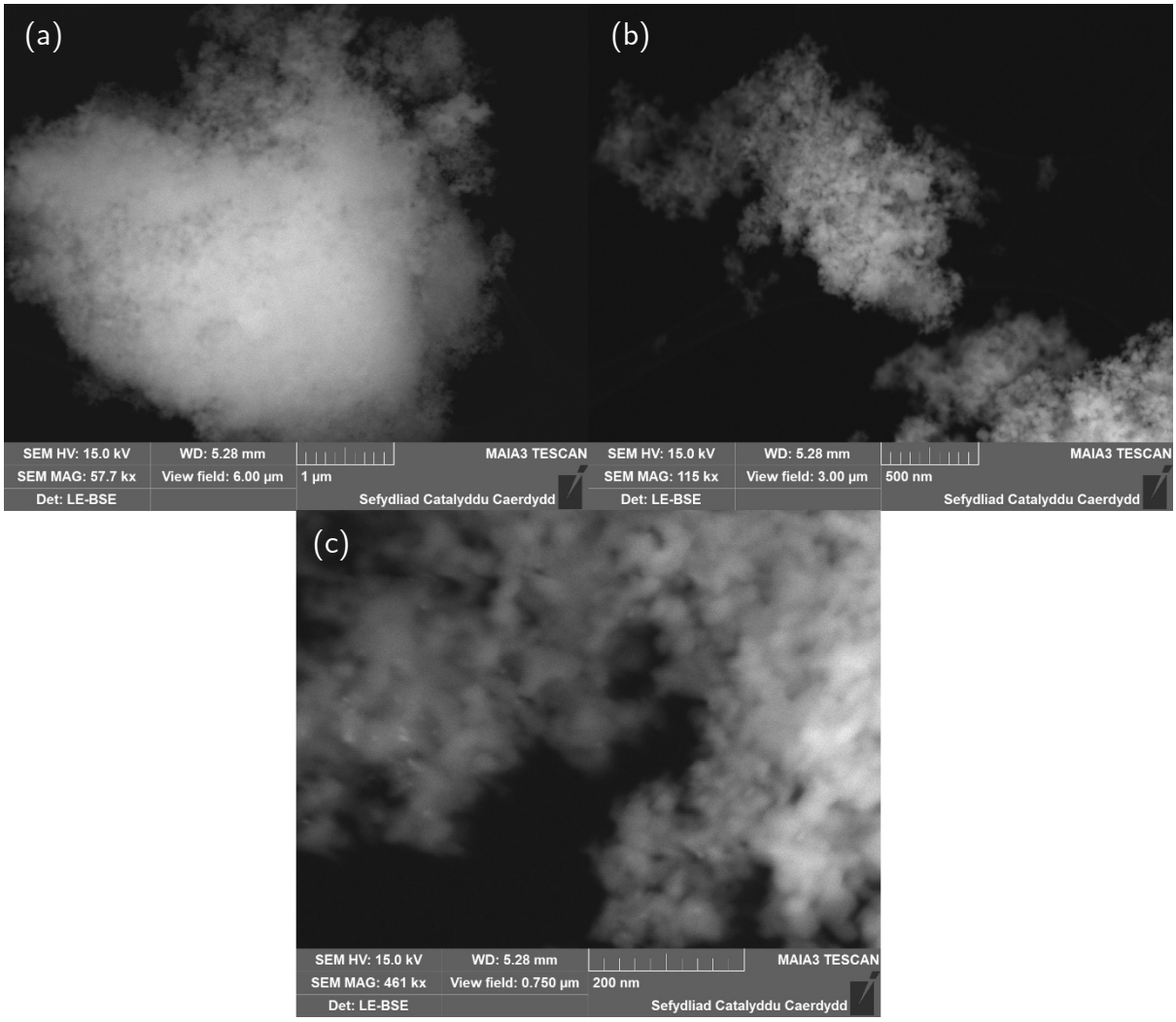

Figure 6-21: Representative FEG-SEM BSE images of 1%Pd/TiO_2 (preparation temperature: 150 °C, preparation time: 10 minutes). Imaging parameters and the scale is shown in the information window below each image. Images (a) and (b) were taken at 57.7kX and 115kX, respectively, and show no Pd particles. Image (c) was taken at 461kX and shows a small cluster of evenly distributed Pd particles. This image suffers from wobble due to adjacent construction that was taking place at the time.

In contrast to 1%Au/TiO_2, images of 1%Pd/TiO_2 at lower magnifications show an absence of large particles. It is of note that the quality of the image obtained at the highest magnification level could not be improved due to significant ground works that were taking place for the construction of a nearby building, which caused the images to suffer from distortion. Even so, it shows much smaller, evenly distributed nanoparticles. As was mentioned for 1%Au/TiO_2, further analysis using a higher-resolution imaging technique would provide useful information on the particle size distribution of Pd nanoparticles on the surface of this catalyst.

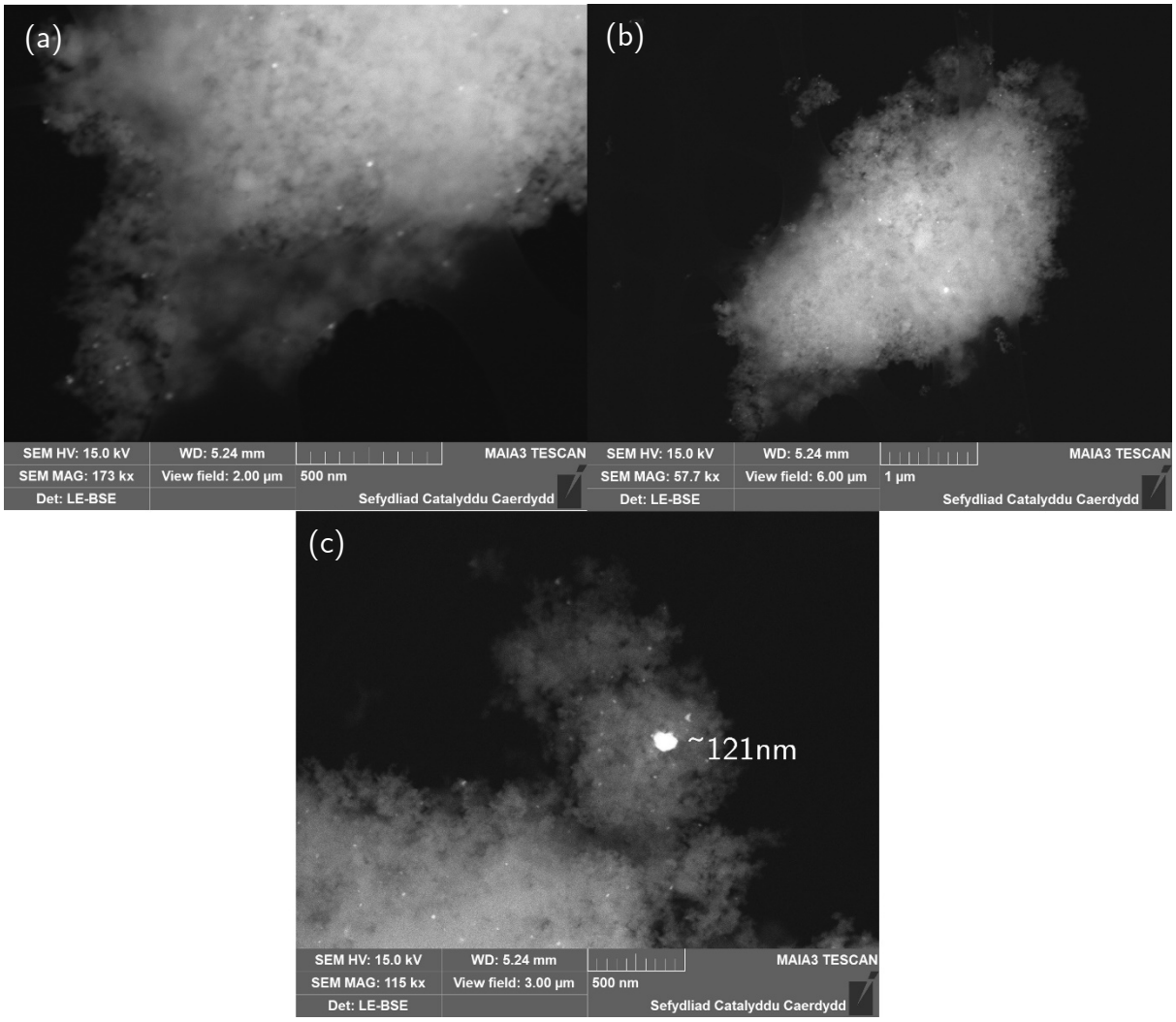

Figure 6-22: Representative FEG-SEM BSE images of 1%AuPd(1:1)/TiO_2 (preparation temperature: 150 °C, preparation time: 10 minutes). Imaging parameters and the scale is shown in the information window below each image. Image (c) shows the presence of a very large particle, whose composition is unknown.

Images of 1%AuPd(1:1)/TiO_2 show nanoparticles that appear to be evenly distributed, and of a variable size. Image (c) in Figure 6-22 shows the presence of a very large particle (~ 121 nm) which is of a similar size to those seen in images of 1%Au/TiO_2. The exact composition of this particle is not known, as it was not analysed using EDX, however it is likely to be Au-based, as particles of that size were not observed when imaging 1%Pd/TiO_2. It is notable that the presence of Pd appears to limit the number of larger particles that were observed and promotes the formation of smaller, more evenly distributed particles overall. In order to gain an understanding of the elemental composition of a representative sample of these particles, EDX was performed on two

comparably smaller particles (diameter ≈ 20 nm) and two larger particles (diameter ≈ 40 nm). The result of this analysis is shown in Figure 6-23.

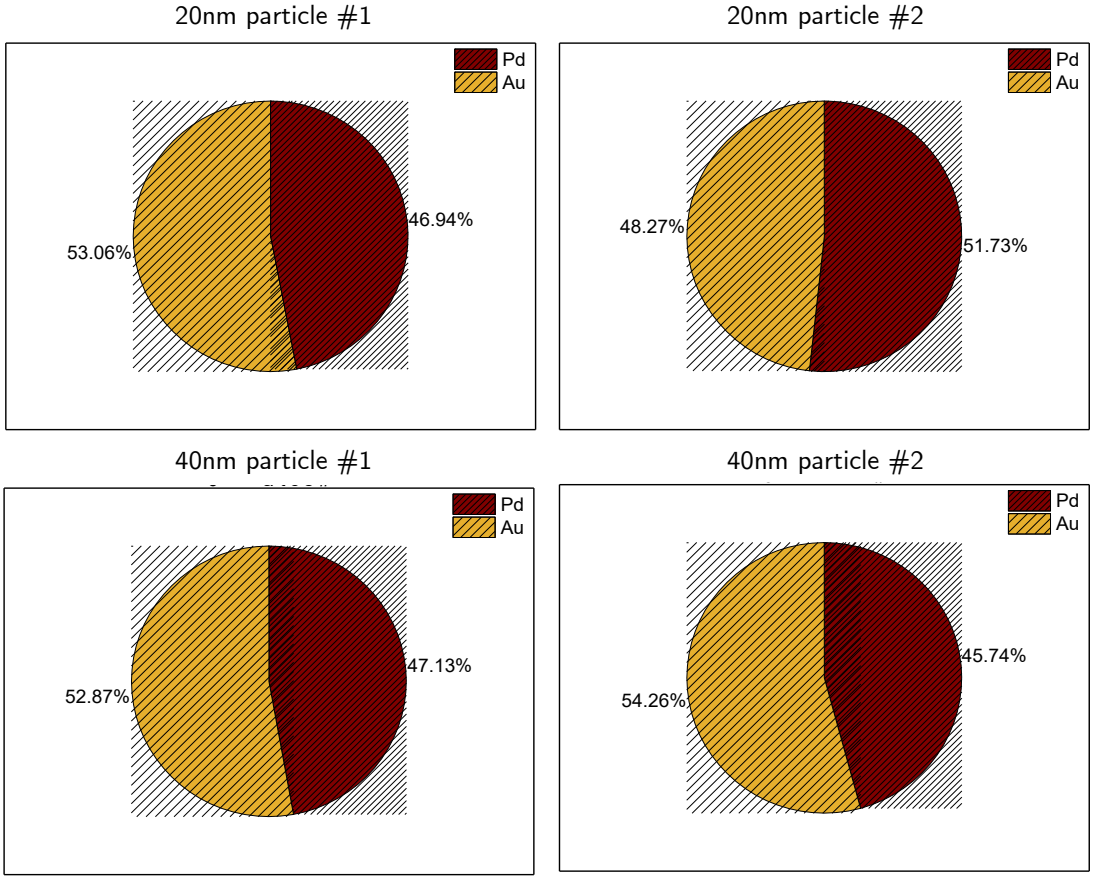

Figure 6-23: EDX analysis of two representative particles of 1%AuPd(1:1)/TiO_2 at a smaller size (20 nm) and a larger size (40 nm). Percentages are given as At.%.

The results are inconclusive as to whether the composition of nanoparticles within 1%AuPd(1:1)/TiO_2 varies with particle size. The ratio of Au:Pd across all sampled particles is generally in agreement with the intended ratio of 1:1. Both 40 nm particles being more Au rich could indicate that particles become more Au rich as they increase in size, however this cannot be conclusively stated due to the small sample size. Smaller particles being more palladium-rich is supported by the findings of previous literature on size-dependent compositional variation in supported AuPd nanoparticles.[28] Analysis with a greater sample size and across a wider range of particle sizes would conclusively determine if there is a size-dependent effect to particle composition across the range of catalysts that were synthesised for this chapter.

6.3: Conclusions and Future Works

In this chapter, the microwave-assisted polyol method that was used for the synthesis of Ru/C catalysts in chapter 4 was also used to the synthesis of a series of 1 wt.% x/TiO_2 (x = Au, Pd, Ni, AuPd, NiPd) for the direct synthesis of hydrogen peroxide. As well as alloying palladium with gold, nickel was investigated as an alternative, low-cost replacement. The 1 wt.% NiPd (1:1) catalyst produced 77 mol_{H2O2} kg_{cat} h^{-1}, performing admirably against the most active AuPd catalyst of the series, which produced 85 mol_{H2O2} kg_{cat} h^{-1}. In the case of the monometallic Au/TiO_2 and Ni/TiO_2 catalysts, which are inactive for the direct synthesis of H_2O_2, an alternative testing regime should be used in order to establish their catalytic activities in relation to comparable catalysts synthesised by more conventional means.

A wider range of synthesis variables should be investigated for solvothermally prepared catalysts for the direct synthesis of H_2O_2. In particular, increasing the synthesis temperature in order to improve the attachment of nickel to the TiO_2 support in the case of Ni/TiO_2 and the NiPd series of catalysts. It was found that not only did nickel have an incomplete attachment to the support material in all instances, but it also leached a significant amount into reaction solutions, and it is suspected that increasing the temperature of the catalyst synthesis would resolve this issue.

Characterisation of the catalysts by X-Ray photoelectron spectroscopy revealed that a stabilising effect occurs when Pd is alloyed to another metal, either Au or Ni, so long as the second metal is present in a sufficient quantity. In the case of AuPd catalysts, the surface of each nanoparticle remained Pd rich despite varying the Au:Pd ratio to be Au rich. In the case of NiPd catalysts, the surface layers of the nanoparticles were more homogeneous in their Ni:Pd ratio in the case of the NiPd (1:1) and NiPd (1:2) catalysts, particularly in the case of nickel rich NiPd (2:1).

6.4: References

1 A. McKillop and D. Kemp, *Tetrahedron*, 1995, **51**, 6145–6166.

2 J. M. Campos-Martin, G. Blanco-Brieva and J. L. G. Fierro, *Angew. Chemie - Int. Ed.*, 2006, **45**, 6962–6984.

3 T. Richards, J. H. Harrhy, R. J. Lewis, A. G. R. Howe, G. M. Suldecki, A. Folli, D. J. Morgan, T. E. Davies, E. J. Loveridge, D. A. Crole, J. K. Edwards, P. Gaskin, C. J. Kiely, Q. He, D. M. Murphy, J. Y. Maillard, S. J. Freakley and G. J. Hutchings, *Nat. Catal.*, 2021, **4**, 575–586.

4 S. Maity and M. Eswaramoorthy, *J. Mater. Chem. A*, 2016, **4**, 3233–3237.

5 V. R. Choudhary, C. Samanta and A. G. Gaikwad, *Chem. Commun.*, 2004, **0**, 2054–2056.

6 J. K. Edwards, B. Solsona, E. N. N, A. F. Carley, A. A. Herzing, C. J. Kiely and G. J. Hutchings, *Science*, 2009, **323**, 1037–1041.

7 J. Pritchard, L. Kesavan, M. Piccinini, Q. He, R. Tiruvalam, N. Dimitratos, J. A. Lopez-Sanchez, A. F. Carley, J. K. Edwards, C. J. Kiely and G. J. Hutchings, *Langmuir*, 2010, **26**, 16568–16577.

8 E. N. Ntainjua, J. K. Edwards, A. F. Carley, J. A. Lopez-Sanchez, J. A. Moulijn, A. A. Herzing, C. J. Kiely and G. J. Hutchings, *Green Chem.*, 2008, **10**, 1162–1169.

9 J. K. Edwards, B. Solsona, E. N. N, A. F. Carley, A. A. Herzing, C. J. Kiely and G. J. Hutchings, *Science (80-.).*, 2009, **323**, 1037–1041.

10 J. K. Edwards, A. F. Carley, A. A. Herzing, C. J. Kiely and G. J. Hutchings, *Faraday Discuss.*, 2008, **138**, 225–239.

11 R. J. Lewis, K. Ueura, Y. Fukuta, S. J. Freakley, L. Kang, R. Wang, Q. He, J. K. Edwards, D. J. Morgan, Y. Yamamoto and G. J. Hutchings, *ChemCatChem*, 2019, **11**, 1673–1680.

12 A. G. R. Howe, P. J. Miedziak, D. J. Morgan, Q. He, P. Strasser and J. K. Edwards, *Faraday Discuss.*, 2018, **208**, 409–426.

13 A. G. R. Howe, Cardiff University, 2018.

14 J. Aguilhon, C. Boissière, O. Durupthy, C. Thomazeau and C. Sanchez, *Nickel nanoparticles with controlled morphologies application in selective hydrogenation catalysis*, Elsevier Masson SAS, 2010, vol. 176.

15 M. Sankar, Q. He, M. Morad, J. Pritchard, S. J. Freakley, J. K. Edwards, S. H. Taylor, D. J. Morgan, A. F. Carley, D. W. Knight, C. J. Kiely and G. J. Hutchings, *ACS Nano*, 2012, **6**, 6600–6613.

16 N. Agarwal, L. Thomas, A. Nasrallah, M. A. Sainna, S. J. Freakley, J. K. Edwards, C. R. A. Catlow, G. J. Hutchings, S. H. Taylor and D. J. Willock, *Catal. Today*, 2021, **381**, 76–86.

17 S. Kanungo, L. van Haandel, E. J. M. Hensen, J. C. Schouten and M. F. Neira d'Angelo, *J. Catal.*, 2019, **370**, 200–209.

18 J. Brehm, R. J. Lewis, D. J. Morgan, T. E. Davies and G. J. Hutchings, *Catal. Letters*, 2021, **152**, 254–262 DOI:10.1007/s10562-021-03632-6.

19 M. Sankar, Q. He, M. Morad, J. Pritchard, S. J. Freakley, J. K. Edwards, S. H. Taylor, D. J. Morgan, A. F. Carley, D. W. Knight, C. J. Kiely and G. J. Hutchings, *ACS Nano*, 2012, **6**, 6600–6613.

20 N.-D. Jaji, M. B. H. Othman, H. L. Lee, M. H. Hussin and D. Hui, *Nanotechnol. Rev.*, 2021, **10**, 318–329.

21 J. K. Edwards, B. E. Solsona, P. Landon, A. F. Carley, A. Herzing, C. J. Kiely and G. J. Hutchings, *J. Catal.*, 2005, **236**, 69–79.

22 A. G. R. Howe, R. Maunder, D. J. Morgan and J. K. Edwards, *Catalysts*, 2019, **9**, 9, 748.

23 Thermo Fisher Scientific, XPS Interpretation of Nickel, https://www.jp.xpssimplified.com/elements/nickel.php, (accessed 5 January 2022).

24 W. P. Zhou, A. Lewera, R. Larsen, R. I. Masel, P. S. Bagus and A. Wieckowski, *J. Phys. Chem. B*, 2006, **110**, 13393–13398.

25 K. Noack, H. Zbinden and R. Schlögl, *Catal. Letters*, 1990, **4**, 145–156.

26 G. L. Hornyak, J. J. Moore, H. F. Tibbals and J. Dutta, *Fundamentals of Nanotechnology*, CRC Press, Boca Raton, 2018.

27 J. H. Carter, S. Althahban, E. Nowicka, S. J. Freakley, D. J. Morgan, P. M. Shah, S. Golunski, C. J. Kiely and G. J. Hutchings, *ACS Catal.*, 2016, **6**, 6623–6633.

28 P. Centomo, P. Canton, C. Burato, C. Meneghini and M. Zecca, *Appl. Sci.*, 2019, **9**, 15. DOI:10.3390/app9152959.

7: Conclusions

The first results chapter of this study (Chapter 4) reports on the investigations into whether a novel source of a biomass-like material (RNF) derived from recycled nappies could be inserted into a typical biomass conversion process.

Firstly, thermogravimetric analysis of the RNF was carried out to determine which materials were present in the greatest quantity. Here, it was discovered that cellulose was the most abundant component by weight, making up ≈ 40 wt.% of the material. This was a promising result; cellulose being present at that abundance is comparable to the abundance of cellulose in a typical source of lignocellulosic biomass. When inserted into a cellulose hydrolysis reaction along with a solid acid catalyst, a greater yield of glucose was produced (4.5%) than from Avicel PH-101 (2.7%), a type of microcrystalline cellulose that is commonly used as a reference material in biomass conversion studies. To attempt to increase the yield of glucose from the RNF without an associated increase in humin formation, two cellulose pre-treatment methods were employed: ball-milling and phosphoric acid regeneration. These were found to have a minimal effect; XRD analysis of both materials pre- and post-treatments found that no appreciable reduction in the crystallinity of RNF's cellulose was achieved with either technique. Furthermore, there was evidence that treatment with phosphoric acid encourages the formation of a more thermodynamically stable polymorph of cellulose. Future work in this area should include a more detailed characterisation of cellulose's properties, with particular focus on the influence that different cellulose polymorphs have on its propensity to be hydrolysed, as it could not be determined if the presence of cellulose II was a significant factor, detrimental or otherwise. Work should also focus on determining the influence that the other components within the RNF may be having on the cellulose hydrolysis reaction. It was assumed that they would not play a significant role, however as mentioned in chapter 4, section 4.2, sodium polyacrylate's thermal decomposition generates reactive compounds.

The second results chapter (Chapter 5) shifts focus to the design of 1 wt.% Ru/C and Ru/TiO_2 catalysts for a one-pot cellulose hydrolysis/hydrogenation and levulinic acid hydrogenation. A novel catalyst synthesis method was used, involving a microwave-assisted solvothermal deposition of the Ru onto the support material.

An initial investigation into the suitability of RNF for the one-pot cellulose hydrolysis/hydrogenation reaction found that a minimal amount of sorbitol is produced (0.2 % yield) when compared to Avicel (32.7 % yield). This was found to be due to, in part, the presence of residual $CaCl_2$ within the RNF as received from NappiCycle. The incremental addition of $CaCl_2$ to a glucose hydrogenation reaction with a representative Ru/C catalyst reduced the yield of sorbitol from 50.4 % to 1.9%. Therefore, future work in this area should aim to either investigate whether it is feasible to remove this residual $CaCl_2$, and whether doing so improves the yield of sorbitol from RNF. Failing this, catalyst design methodology should focus on whether modifying the Ru/C catalysts can increase their suitability for use with RNF.

Catalyst screening reactions were carried out that investigated the effects of catalyst synthesis parameters on the Ru/C catalyst's performance for glucose hydrogenation. Many highly active catalysts were synthesised for this reaction, and it was found that the choice of carbon support had the greatest influence on catalytic activity, along with the choice of ruthenium precursor. The carbon support was found to influence the rate of sorbitol yield when added as a dopant alongside a glucose hydrogenation with a Ru/TiO_2 catalyst; therefore, future work should focus on a wider range of carbon support material types, along with the influence of modifying its surface functional groups. As many of the most active catalysts were synthesised at the lowest synthesis temperature and time, the parameters for catalyst synthesis parameters should be widened to determine if activity can be increased further with yet lower synthesis temperatures and shorter synthesis times. This is also the case with the Ru/TiO_2 catalysts when tested for levulinic acid hydrogenation. TEM analysis of a limited range of Ru/C catalysts determined that whilst the average Ru particle size remains relatively unchanged as the synthesis time is increased, the distribution of particle sizes

broadens. This indicates that a degree of particle size control is possible using the microwave-assisted solvothermal technique.

The final results chapter (Chapter 6) shifts focus to the direct synthesis of hydrogen peroxide from its constituent gaseous elements: hydrogen and oxygen, using a series of mono- and bimetallic 1 wt.% x/TiO_2 (x = Au, Pd, Ni, AuPd, NiPd) catalysts synthesised by the microwave-assisted solvothermal method.

The effect of varying the ratio of metals in the bimetallic catalysts was also investigated. It was found in the case of both the AuPd and the NiPd catalysts that a 1:1 ratio of both metals produced the most active catalyst. The 1 wt.% NiPd (1:1) catalyst produced 77 mol_{H2O2} kg_{cat} h^{-1}, and the most active AuPd (1:1) catalyst of the series produced 85 mol_{H2O2} kg_{cat} h^{-1}, however in the case of Ni-containing catalysts, there was an inadequate attachment of Ni to the catalyst, resulting in lower metal loading than what was nominally expected, and a significant amount of leaching. It was suspected that this was, in part, due to the synthesis temperature of Ni-based catalysts being too low for a complete attachment, therefore future work therefore should investigate a wider range of synthesis variables, particularly the synthesis temperature to attempt to improve the attachment of nickel to the support. XRD analysis of the catalysts indicated that despite varying the ratio of metals, a stabilising effect occurs when Pd is alloyed so long as the second metal is present in a sufficient quantity, and in the case of the AuPd catalysts, the particles remain Pd-rich even if it is not the dominant alloying metal by molar ratio. To determine the precise distribution of each metal within the bimetallic series' nanoparticles in future work, a more detailed analysis should be undertaken with a high-resolution microscopy technique coupled with elemental analysis, such as STEM-EDX.

Appendices

Appendix A: NappiCycle's Process Flow Diagram

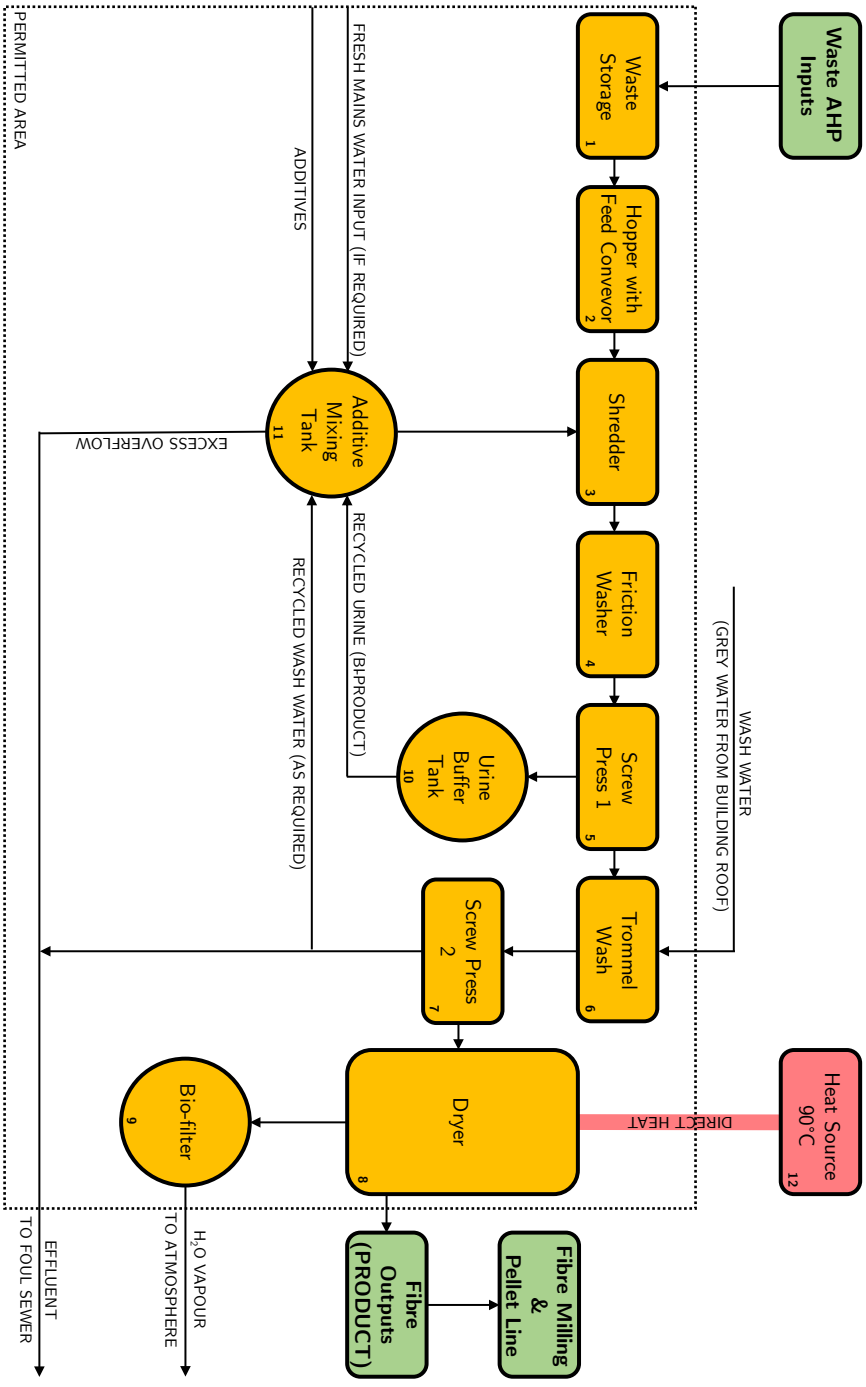

Note that there is an attempt to re-cycle wastewater through step 10, however wastewater discharge takes place in steps 9 and 11.

Appendix B: Complete Table of Ru/C Weight Loadings

Support	***Precursor***	***Synthesis Time - Temperature*** *(°C - min)*	***Expected Ru Loading*** *(wt.%)*	***Actual Ru Loading*** *(wt.%)*
Vulcan XC72R	$RuCl_3$	150-5	1	1
		150-10		1
		150-15		1
		175-5		1
		175-10		1
		175-15		1
		200-5		1
		200-10		1
		200-15		1
	$Ru(acac)_3$	150-5		0.93
		150-10		0.97
		150-15		1
		175-5		1
		175-10		1
		175-15		1
		200-5		1
		200-10		1
		200-15		1
Vulcan Black Pearls 2000	$RuCl_3$	150-5		0.93
		150-10		0.73
		150-15		0.37
		175-5		1
		175-10		1
		175-15		1
		200-5		1
		200-10		1
		200-15		1
	$Ru(acac)_3$	150-5		0.85
		150-10		0.79
		150-15		0.77
		175-5		0.94
		175-10		0.97
		175-15		0.97
		200-5		1
		200-10		1
		200-15		1